Acceptance Criteria for Ultrasonic Impact Treatment of Highway Steel Bridges

by

Rana Tehrani Yekta

A thesis
presented to the University of Waterloo
in fulfillment of the
thesis requirement for the degree of
Master of Applied Science
in
Civil Engineering

Waterloo, Ontario, Canada, 2012

Author's Declaration

I hereby declare that I am the sole author of this thesis. This is a true copy of the thesis, including any required final revisions, as accepted by my examiners. I understand that my thesis may be made electronically available to the public.

Abstract

The need for rehabilitation of bridges has become a critical challenge due to aging and an increase in traffic loads. Many of these bridges are exceeding their design fatigue life. Since many of these bridges are structurally deficient, they need to be rehabilitated or replaced by a new bridge. The most susceptible and weak parts of steel bridges to cracks and fatigue are the welds, due to the presence of high stress concentrations, tensile residual stresses, and imperfections as a result of the welding process. Inspection and repair of welds are difficult and elimination of welded details is not possible in steel bridge construction. Ultrasonic impact treatment (UIT) is a promising and innovative post-weld treatment (PWT) method for improving the fatigue performance of existing welded steel and steel-concrete composite structures such as highway bridges. The fatigue resistance of treated joints is enhanced by improving the geometry of the weld toe, and introducing compressive residual stresses. However, a lack of tools for quality assurance has slowed UIT's adoption by bridge authorities.

The current study was undertaken to examine the fatigue performance of structural steel welds subjected to UIT at various levels, including intentional under-treatment and over-treatment, and to relate the fatigue performance of the treated welds to geometric and metallurgical properties measured to control the treatment quality. The last objective was to use the laboratory results to develop acceptance criteria for the quality control of UIT in bridge applications.

Fatigue tests of non-load carrying fillet welded attachments were conducted on properly treated, under-treated, and over-treated weld toes. Statistical analyses of the fatigue life data were performed and crack growth was monitored using the alternating current potential drop (ACPD) method. Measurement of local properties (such as weld toe geometry, local hardness, and residual stresses) and examination of the weld toe microstructure were also performed on the untreated and treated welds. The effects of weld toe geometry on the local stresses in the untreated and treated welds were also investigated using elastic finite element analysis (FEA) to obtain the stress concentration factor (SCF) for the different treatment cases and to examine the changes in the SCF for the different weld toe geometries.

Based on the statistical analysis performed in this research, the results illustrated that UIT significantly improved the fatigue lives of weld details regardless of the investigated level of

treatment quality. The fatigue lives of welded details under constant amplitude (CA) loading and constant amplitude loading with under-loads (CA-UL) were increased up to 30 and 27 times respectively. On average, the fatigue life of the treated weld details was slightly lower under CA-UL than under CA loading. Treatment quality had little impact on the mean of the S-N curves. However, it did impact the design (95% survival probability) S-N curves, with the curve associated with a proper treatment slightly higher than the curves for poor or unknown treatment quality. Local near-surface microhardness and compressive residual stresses were greatest for the over-treated welded details, followed by the properly treated and then the under-treated welded details. Increasing the treatment speed resulted in a greater reduction in the surface microhardness and compressive residual stresses than decreasing the treatment intensity.

Finite element analyses showed that changes in weld toe geometry due to UIT can cause a decrease in the SCF near the surface of the treated weld toe. The SCF was the lowest for the properly treated steel specimens and slightly higher for the under-treated specimens. For the over-treated specimens, the SCFs were nearly as high as for the untreated weld. The SCF increases as the thickness of the flange increased up to 19 mm. With further flange thickness increase to 38 mm, the SCF did not change substantially.

The work presented herein demonstrated that indent depth measurements from the base metal side, commonly used for quality control, may not identify over-treatment on their own. Indent depth measurements from both the weld and the base metal sides, obtained by measurement of weld toe impressions, offer a good alternative means for identifying over-treatment. However, for identifying under-treatment, indent depth measurements should be used in conjunction with visual inspection for traces of the original weld toe.

Acknowledgements

I would like to express my deep gratitude to Dr. Scott Walbridge, my research supervisor, for his patient guidance, enthusiastic encouragement and useful critiques of this research work. Without his support and contributions, I would have not been able to finish this amazing journey.

Along with my supervisor, I would like to express my sincerest appreciation to the readers of my thesis, Dr. Timothy Topper and Dr. Monica Emelko for all their insightful comments.

My grateful thanks are also extended to the structures lab technicians Doug Morton, Rob Sluban and specially Richard Morrison for their great assistance with the technical issues in the lab.

The Ministry of Transportation of Ontario (MTO) is gratefully acknowledged for providing financial support for this research.

Sam Abston at Applied Ultrasonics is gratefully acknowledged for providing technical input and specimen treatment.

I am particularly grateful for the assistance given by Kasra Ghahremani. I very much appreciated his help and guidance. I valued his advice and experience that he shared with me over the past two years.

Special thanks to my undergraduate research assistant, Iris Chang, my officemates and my kind friends who made this journey memorable for me.

I would like to thank the most amazing friend in the world, Sogol Roohparvarzadeh, for making these two years the happiest and the most enjoyable years of my life. Thanks for being the best friend I needed and for always being there for me.

Last but not least, I would like to thank the most important people in my life: my parents and my brother. My parents for their unconditional love, for believing in me, for all the sacrifices they made and for all the great opportunities they provided to see me grow and to become successful. Thanks to my brother, Erfan Tehrani Yekta, for his continuous love and care.

Dedicated to my lovely parents,

Hengameh and Mohammad

"You only live once, but if you work it right, once is enough."

Mae West

TABLE OF CONTENTS

List of Figures

List of Tables

1 Introduction

1.1 Background and Motivation

In North America, the need for rehabilitation of bridges has been increasing as these structures age. With consistent and routine maintenance, the bridges in Canada are expected to have a service life of 50 to 100 years. However, the maintenance of these bridges is becoming harder as the demand and traffic volume increases (Zoubir Louni, 2007). These factors combined with a lack of funding for maintenance and the severity of the Canadian climate (e.g. freeze-thaw cycles and heavy road salt use) have significantly affected the aging and deterioration of structures (Zoubir Louni, 2007). Aside from this deterioration, many of these structures are exceeding their design fatigue life (Kulak & Smith, 1993). According to the National Research Council Canada (NRCC) over 40% of the bridges in Canada are more than 40 years old. The cost of upgrade and maintenance of existing bridges in Canada has been estimated to be $66 billion (Council of the Federation, 2005). In Ontario, 70% of the bridges in the province were constructed between 1950 and 1980 (The Office of the Auditor General of Ontario, 2009). Because many of these bridges are structurally deficient, they need to be rehabilitated or replaced. A significant percentage of the cost of maintaining these structures is due to deterioration of welded steel and steel-concrete bridges caused by fatigue (Fisher, 1984). The welded parts of these bridges are particularly susceptible to fatigue (Kuhn et al., 2008).

Approximately 80-90% of failures in steel structures are related to fatigue and fracture. Many of these failures are the result of poor detailing (Albrecht, Artley-Dean, & Bergman, 1982). Survey results from 142 bridges with cracks in twenty U.S. states and the province of Ontario, Canada found that at least 60 of these bridges had fatigue cracks (Fisher, 1984). In one survey 448 steel structure damage cases were reported, 45.1% of the reported cases were building failures, 16.1% of the cases were railway bridges, and 8.7% were road bridges (Kuhn et al., 2008). 38.3% of these bridge failures could be attributed to fatigue problems.

There are a number of possible approaches for dealing with fatigue problems in bridges, including: increased inspection frequency, load restrictions, member reinforcement, and member replacement. In certain situations, drilling a hole at the crack tip or "softening" the critical fatigue detail so that it attracts less load are also possibilities. Another possibility is the use of post-weld

treatments (PWTs). These treatments can improve the fatigue performance of weld details that experience crack growth from the toe of the weld (Roy & Fisher, 2006). PWTs can be divided into two main categories: geometry improvement methods and residual stress-based methods. Hammer peening, needle peening and shot peening, as well as Ultrasonic impact treatment (UIT), are residual stress-based methods. With these treatment methods, the objective is to eliminate tensile stresses and to introduce compressive residual stresses by plastically deforming the weld toe, in order to slow or stop the propagation of fatigue cracks.

The Ministry of Transportation of Ontario (MTO) has been seeking ways to improve the fatigue performance of its bridges and address fatigue problems. Ultrasonic impact treatment, which is a recently developed PWT method, represents a promising way to improve the fatigue performance of steel bridges by replacing tensile residual stresses with beneficial compressive residual stresses. The effectiveness of UIT is well documented through research by (Haagensen, Statnikov, & Lopez-Martinez, 1998), (Vilhauer, Bennett, Matamoros, & Rolfe, 2012) and (Nyborg, Moffatt, Cavaco, & Nyborg, 2006). However, there are a few challenges related to this treatment method that have slowed down its adoption by bridge authorities such as MTO. The most important challenge is the lack of suitable quality control procedures for accepting or rejecting the treatment once the work is completed. The effects on fatigue life of under-treatment and over-treatment are also uncertain.

1.2 Objectives

The objectives of the current thesis are as follows:

1. to examine the fatigue performance of structural steel welds subjected to UIT at various levels, including intentional under-treatment and over-treatment,
2. to relate the fatigue performance of the treated welds to geometric and metallurgical properties that can be measured to control the treatment quality, and
3. to use the results of the research conducted to achieve Objectives 1) and 2) to develop acceptance criteria for quality control of UIT in bridge applications.

1.3 Scope

Forty two non-load carrying cruciform welded joints were fatigue tested in the University of Waterloo Structures Laboratory using a Material Testing System (MTS) 810 fatigue testing machine with a load capacity of 100 kN. The research was limited to the investigation of a single weld detail, specifically a non-load carrying fillet welded attachment, fabricated from CSA G40.21 350W steel, which is used commonly in Canadian steel bridges (Walker, Van Berkel, & Walbridge, 2008). This weld detail falls under Detail Category 'C' according to the Canadian Highway Bridge Design Code, CAN/CSA S6-06 (Canadian Standards Association (CSA), 2006). The fatigue tests were conducted under two loading conditions (constant amplitude with and without under loads) with frequencies not exceeding 23 Hz.

The post-weld treatment method that was the focus of this research study was ultrasonic impact treatment (UIT). This treatment method was evaluated through a variety of methods, including: fatigue testing, a statistical analysis of the fatigue life data, crack growth monitoring using the alternating current potential drop (ACPD) method, measurement of local properties (such as weld toe geometry, local hardness, and residual stresses), and an examination of the weld toe microstructure for untreated and treated welds. The effects of weld toe geometry on the local stresses in the untreated and treated welds were also investigated using elastic finite element analysis (FEA). All of the work presented in this thesis was performed at the University of Waterloo, except for the residual stress measurements, which were performed by an external laboratory specializing in laser x-ray diffraction (Proto Manufacturing).

1.4 Organization of the Thesis

Chapter 2 of this thesis provides an introduction and a literature review of key concepts, including: the role of cracks and discontinuities in the fatigue process, the fatigue behaviour of cyclically loaded structures, fatigue design, and post-weld treatments for improving fatigue performance, with a focus on ultrasonic impact treatment (UIT).

Chapter 3 describes the test procedures and measurement methods used in this research. It includes a description of the specimen geometry, the testing procedures, and the test matrix that was used in this research, as well as the procedures used for measuring weld toe geometry, micro-hardness, and residual stresses, in order to assess the treatment quality.

Chapter 4 presents the fatigue test results, along with the crack growth curves obtained using the ACPD method. Various weld toe property measurements are also presented in this chapter, including weld toe geometry, microhardness, and residual stress measurements.

Chapter 5 summarizes the analytical work conducted for this research project. It begins with a statistical analysis of the stress-life data from the fatigue tests followed by t-test analyses to understand whether there is a significant difference between the treatments. A study is then presented investigating the effects of weld toe geometry on the local stresses in untreated and treated welds using elastic finite element analysis (FEA). Stress concentration factors (SCF) for each loading condition are determined.

Chapter 6 presents the conclusions of this research project. It also provides recommendations for the quality control of UIT in bridge applications, based on the presented research, as well as a number of recommendations for future research in this area.

2 Literature Review

2.1 Introduction

In this chapter, the role of cracks and discontinuities in the fatigue process is explained, as well as the fatigue behaviour of cyclically loaded structures. Various methods for fatigue design are then discussed, including the classification, hot-spot stress, and fracture mechanics methods. Following this, post-weld treatment methods are explained with a focus on ultrasonic impact treatment (UIT), which was the treatment method used in this research. The quality control section is last and focuses on different methods to assure the treatment is applied properly.

2.2 Cracks and Discontinuities

Cracks and discontinuities have a major role in the fatigue process (Stephens, Fatemi, Stephens, & Fuchs, 2001). Discontinuities may exist as a result of the fabrication process and cracks can initiate in structures even before they are put into service as a result of transportation (Kulak & Smith, 1993). Every time a load is applied to a structure that has a crack, the crack may grow. Pre-existing crack-like defects or "discontinuities" are typically present in welded structures due to the presence of: undercuts, porosity, lack of fusion, and partial penetration (Kulak & Smith, 1993). These common flaw types are shown in Figure 2.1.

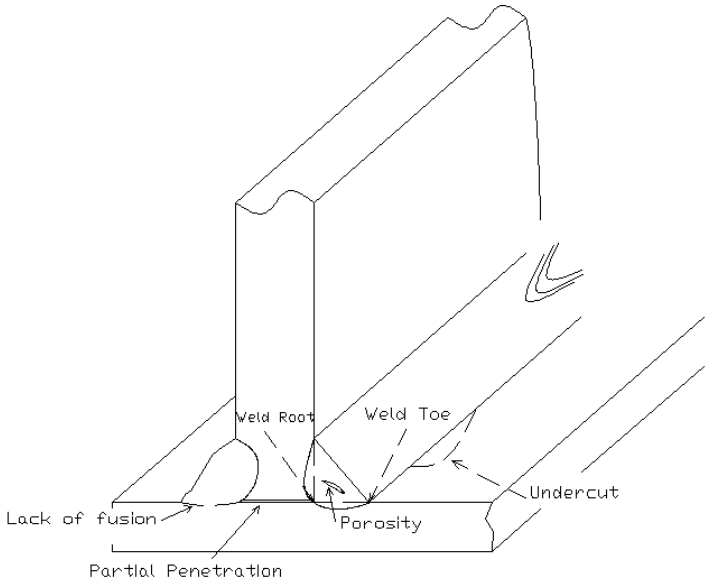

Figure 2.1: Common flaw types (Kulak & Smith, 1993)

These flaws occur during the fabrication and welding of steel structures and reduce the fatigue life significantly compared to the detail without any welding (Kulak & Smith, 1993). All welded structures subjected to cyclic loading, such as bridges, are susceptible to fatigue cracking (Kulak & Smith, 1993). Taking fatigue into account in the design of these structures is critical for ensuring that they reach their design service lives (Ghahremani, 2010).

Welds are weak spots in structures because of their brittle fracture and fatigue strength (Stephens et al., 2001). This weakness can be due to flaws, such as: slag inclusions, lack of fusion, and undercuts, and may eventually lead to failures (Vilhauer et al., 2012). Fatigue cracks tend to occur at welded joints where stress concentrations are high due to the sudden change in joint geometry in the vicinity of the welds (Kirkhope, Bell, Caron, Basu, & Ma, 1999) and high tensile residual stresses, which are also present due to the welding process (Roy & Fisher, 2005). Cover plates, connection plates, transverse and longitudinal stiffeners, and web to flange connections are examples of joint geometries that require welding and hence are susceptible to fatigue problems (Vilhauer et al., 2012).

Tensile residual stresses have a negative effect on fatigue performance. The tensile residual stresses present after the welding process modify the mean stress experienced by a welded joint under fatigue loading (Maddox, 2000). These stresses are present at vicinity of the weld toe due to contraction of the weld metal upon solidification (Kulak & Smith, 1993). These stresses keep the crack tip open. Compressive residual stresses have the reverse effect, keeping the crack tip closed under cyclic loading and thus increasing the fatigue life.

There are different methods available to prevent fatigue cracking or to slow crack propagation. These include (Ghahremani, 2010 & Kulak & Smith, 1993):

- reducing the applied stress concentration and dynamic magnification,
- reducing the number of load cycles applied to the structure,
- changing the local geometry,
- removing crack like defects at the weld toe, and
- removing harmful tensile stresses and introducing beneficial compressive ones.

The fatigue life of a component can be divided into two distinct phases crack initiation and crack growth (Welding Technology Institute of Australia, 2006) (see Figure 2.2).

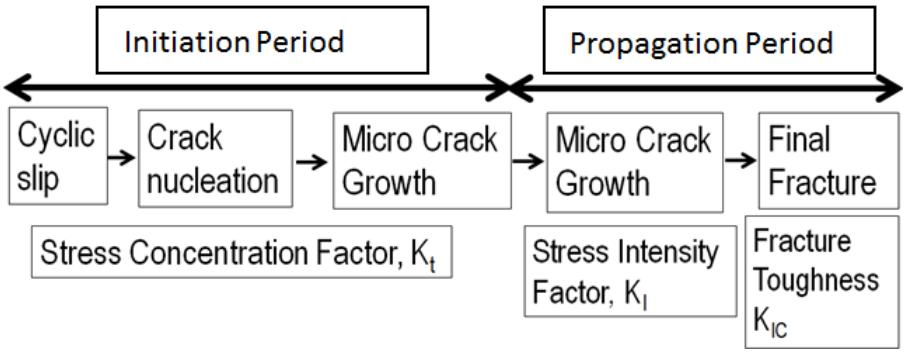

Figure 2.2: Crack initiation and propagation (Welding Technology Institute of Australia, 2006)

On a microscopic scale there are imperfections in metal, which are known as dislocations (Welding Technology Institute of Australia, 2006). Cyclic loading of the material causes these dislocations to move, which is the first phase of the initiation period. Cyclic slip occurs within the grains at an atomic scale. The resulting slip bands introduce local stress concentrations, which eventually lead to crack initiation. Crack propagation under cyclic loading starts after the crack initiation stage. As shown in Figure 2.2, at the end of the crack initiation process, micro-cracks have formed, which will lead to the next stage of macro-crack growth. Propagation continues until the final fracture occurs, which is when the remaining cross section cannot carry the load (Welding Technology Institute of Australia, 2006).

Figure 2.3 shows the process of fatigue through crack initiation all the way to final fracture (Albrecht et al., 1982). The plate in this figure is loaded axially. The direction of the crack is perpendicular to the direction of maximum tensile stress. This figure provides a graphical explanation of the two phase process. After crack initiation, fatigue striations are apparent and the brittle cleavage starts after that. The crack initiation stage can be observed using non-destructive techniques (Albrecht et al., 1982). The final fracture occurs at a 45° angle.

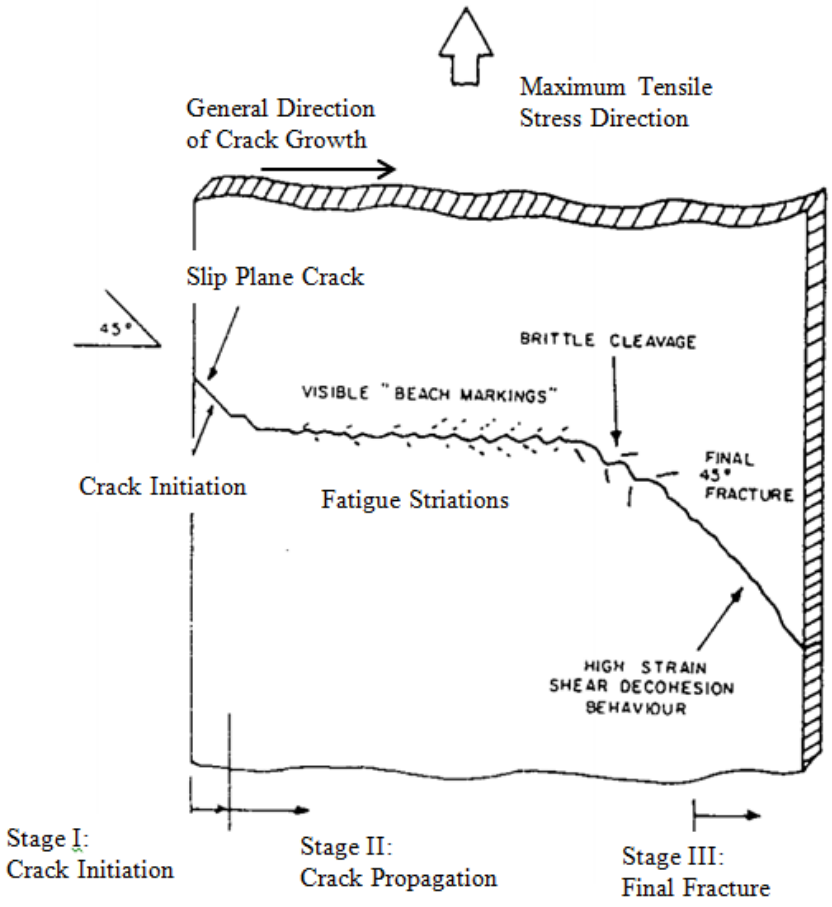

Figure 2.3: Different stages of crack growth (Albrecht et al., 1982) (not to scale)

At low strain amplitudes, 90% of the crack life occurs in the initiation stage (Bannantine, Comer, & Handrock, 1990). However, if the strain amplitude is high, the majority of the life occurs in the propagation period. Fracture occurs when the stress intensity factor (SIF), K_I, increases beyond the critical value, $K_{IC,}$ which is referred to as fracture toughness (brittle fracture) or the remaining material is not able to carry the applied stress (ductile fracture) (Kulak & Smith, 1993). The fracture toughness depends on different factors such as the thickness of the plate, temperature, material properties, and the rate of loading (Kulak & Smith, 1993). Welded structures tend to have little or no crack initiation phase, as there are usually pre-existing cracks or crack-like defects in the component as a result of the welding process (Welding Technology Institute of Australia, 2006). In welded components, fatigue cracks can originate from either the weld toe or the weld root (see Figure 2.1). However, the root of the weld is not accessible for improvements, and hence the best way to increase the fatigue resistance of the welded component is to focus on the weld toe of details such as the stiffeners (Roy & Fisher, 2006).

2.3 Fatigue Behaviour of Cyclically Loaded Structures

The problem of metal fatigue was first identified in 1840s as a result of repeated cyclic loading in the railway industry, where it was noticed that the axles failed repeatedly at the shoulders (Stephens et al., 2001). Wohler, a German engineer, performed tests under repeated loading and used S-N curves (Stephens et al., 2001) to prove that the most important factor in fatigue failure is the stress amplitude (Schutz, 1996). During World War II, the brittle fracture of welded tankers and American "Liberty ships" resulted in more attention being given to efforts to improve our understanding of residual stresses, defects, and fatigue (Stephens et al., 2001).

Fatigue can be defined as: *"the formation of a crack or cracks as a result of the repeated application of loads, each of which is insufficient, by itself, to cause normal static failure"* (Gurney, 1971). An alternative definition is: "*the initiation and propagation of microscopic cracks into macro cracks by the repeated application of stresses"* (Kulak & Smith, 1993). Fatigue failure occurs when a crack grows to a point where the remaining material can no longer support the imposed loads. Thus, a sudden fracture occurs. Fatigue cracks form on planes of maximum shear and grow on planes of maximum tensile stress (Stephens et al., 2001). Failure involves the interaction of load, time, and the environment (Stephens et al., 2001). High stress ranges, poor weld quality, the presence of stress concentrations, corrosion damage, incorrect fabrication procedures (Kulak & Smith, 1993), and dynamic loading have a significant influence on the long term performance of welded steel structures (Roy & Fisher, 2005).

When designing a component, it should be considered whether the life is going to be finite or infinite (Schutz, 1996). At very low stress ranges, infinite fatigue lives are possible. Service loads and stresses applied on a component play a major role in the fatigue design of that component (Schutz, 1996). It must be noted that a welded component's fatigue life generally does not increase with an increase in the material's strength (Maddox, 2000). A constant amplitude cyclic loading history is illustrated in Figure 2.4.

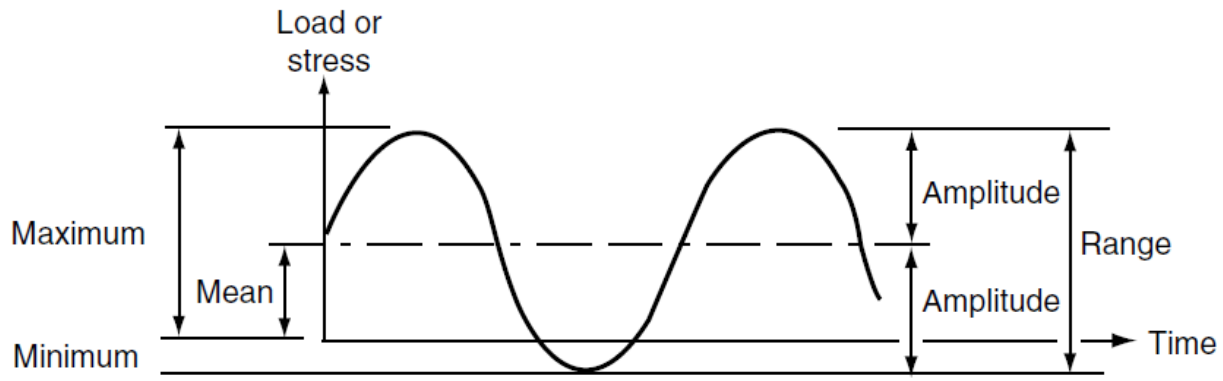

Figure 2.4: Typical constant amplitude cyclic loading history (Pineault, Belassel, & Brauss, 2002)

The maximum and minimum stresses are shown in this figure (Pineault et al., 2002). As defined in this figure, the maximum and minimum stress levels, the stress range, and the number of applied cycles are the parameters that influence the severity of the repeated fluctuations of stresses (Welding Technology Institute of Australia, 2006). Equation 2.1 and 2.2 provide mathematical definitions for the stress range ($\Delta\sigma$) and stress ratio (R) respectively.

$$\Delta\sigma = \sigma_{max} - \sigma_{min} \quad 2.1$$

$$R = \frac{\sigma_{min}}{\sigma_{max}} \quad 2.2$$

σ_{max} and σ_{min} are the maximum and minimum nominal stresses respectively. Crack growth rates tend to increase as the value of the stress ratio, R, becomes more positive (Bannantine et al., 1990). When $R > 0$, no significant stress ratio influence is observed on the crack growth rate (Bannantine et al., 1990). The stress cycles are caused by live loads and not by the dead load that is always present in the member (Kulak & Smith, 1993).

Stress-life or S-N curves (sometimes called Wohler curves) are used to understand metal fatigue. These curves are most useful for cases where the applied stress is within the elastic range of the material (Bannantine et al., 1990). S-N diagrams show the applied stress range versus the number of cycles to failure, N_f, and are used to show the fatigue tolerance of metal materials and components by describing the number of cycles they can tolerate before failure (Welding Technology Institute of Australia, 2006). A log-log scale is typically used for these curves because data plotted in this way tend to fall on a straight line (Welding Technology Institute of Australia, 2006). Figure 2.5 shows a typical S-N curve.

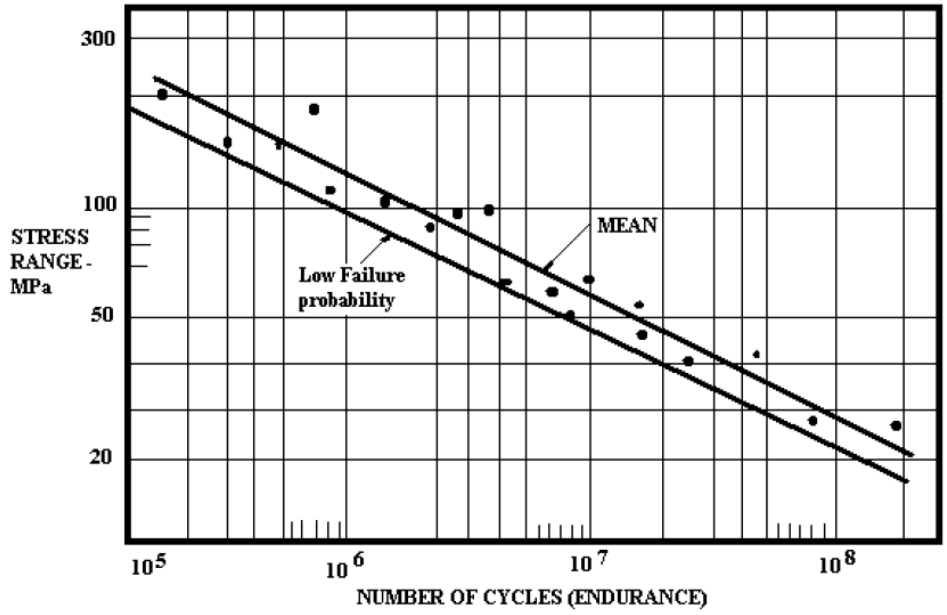

Figure 2.5: S-N curve on a log-log scale (Welding Technology Institute of Australia, 2006)

To produce an S-N curve, many tests need to be performed, due to the high degree of scatter in the results (Welding Technology Institute of Australia, 2006). Small cycles do not contribute much to fatigue damage (Kulak & Smith, 1993). A constant amplitude fatigue limit (CAFL) can be defined for many materials, as illustrated in Figure 2.6.

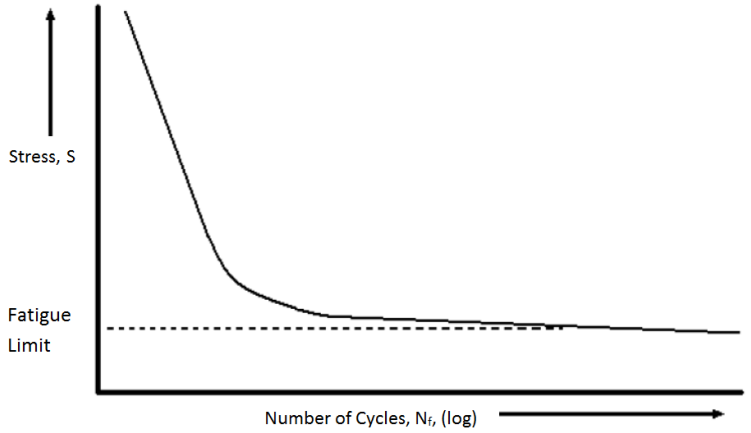

Figure 2.6: Constant amplitude fatigue limit (Welding Technology Institute of Australia, 2006)

As shown in this figure, fatigue life decreases as the stress range increases (Stephens et al., 2001). It is also shown that failures do not occur below the fatigue limit (Stephens et al., 2001). It should be noted that in welded structures with high tensile residual stresses, the applied stress

range is more important than the maximum stress (Stephens et al., 2001) even if the applied load is compressive (Maddox, 2000). All welded structures that are subjected to cyclic loading are at risk of fatigue cracking and thus this has to be taken into account while designing such structures (Stephens et al., 2001). The fatigue data plotted as an S-N curve in the finite life domain can be represented with a straight line, defined by Equation 2.3 (Ye & Moan, 2008):

$$logN = log\,A - mlogS \qquad 2.3$$

where N is the number of cycles, S is the stress range, A is a constant defining the vertical position of the line and m is a constant defining the slope. Given this equation, the fatigue strength of a component can be determined by calculating the number of cycles to cause failure at a given stress range (Ye & Moan, 2008). The number of cycles to fatigue failure of all components depends not just on the material, but also the component geometry. To account for this, S-N curves can be established for different geometries or "detail categories" in order to enable fatigue design. Figure 2.7 shows the S-N curve for typical welded components.

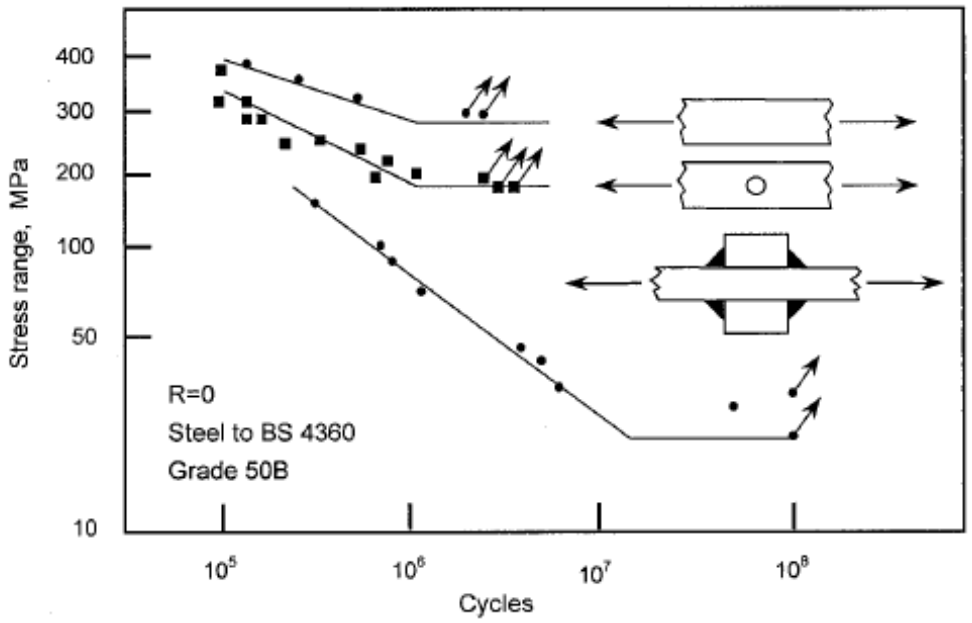

Figure 2.7: S-N curve for as-welded components (Maddox, 2000)

Cyclic stresses are applied to each of the components. In this figure, the top, the middle and the bottom curves are for un-notched, notched, and welded components respectively. Based on this figure, it can be concluded that the parameters influencing the fatigue performance of a

component are the detail category of the component (which determines the S-N curve position), the stress range applied, and the number of cycles of loading (Kulak & Smith, 1993).

The plastic strain can be correlated with the total number of cycles of components to failure, in the low cycle domain (Pineault et al., 2002). Oppositely, elastic strain dominates the material behavior in the high-life range. Several cracks tend to occur in separate highly stressed areas if the component has a short fatigue life. A crack spreads from a single origin if a component has a long fatigue life (Pineault et al., 2002). The low cycle domain is usually deformed by fatigue lives between 10^4 to 10^5 cycles to failure. In this domain, a 5-10% change in the stress range can produce a 50% change in component life. Thus, errors made in stress range estimation will have a significant effect on fatigue life of the component (Pineault et al., 2002).

If a crack is visible, the structure is usually assumed to have reached the end of its fatigue life (Kulak & Smith, 1993). Corrosion damage, fabrication-induced discontinuities, and large eccentricities can contribute to failure of a structure as well. During a visual inspection, if a crack is present in a steel member, there is a high probability that with a more careful examination additional cracks will be found (Kulak & Smith, 1993). Hence, it is very important to inspect a fatigued structure and if any cracks are found, immediate actions need to be taken (Kulak & Smith, 1993).

2.4 Residual Stresses, Size, and Corrosion Effects

The detail category, applied stress range, number of applied cycles, and residual stresses can play an important role in determining the fatigue performance of a structural component (Roy & Fisher, 2005). When steel structures are fabricated and welded, residual stresses are introduced due to welding which have significant effects on the initiation and propagation of fatigue cracks (Kulak & Smith, 1993). Figure 2.8 illustrates a typical pattern of the residual stress in a welded plate (Kulak & Smith, 1993). As the weld cools down, it tries to contract. However, the plate and the weld still need to maintain length compatibility (Kulak & Smith, 1993). For this reason, the weld material is restrained by the plate during the cooling and contraction period, which puts the welded area and parts of the plate in tension while the rest of the plate is put in compression (Kulak & Smith, 1993). These stresses, which are present without any external forces (i.e. they are self-equilibrating), are called residual stresses.

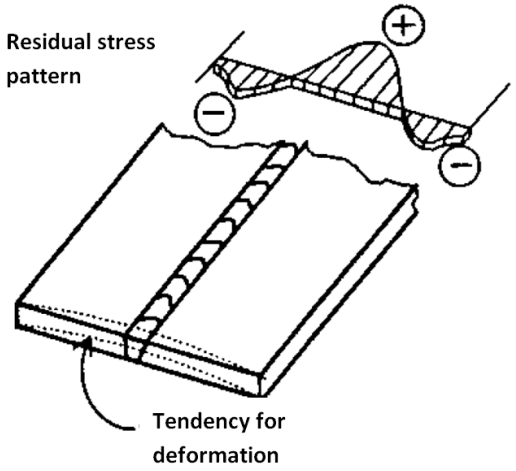

Figure 2.8: Residual stress pattern in a welded plate (Kulak & Smith, 1993)

The distribution and pattern of the residual stresses resulting from the welding process usually depend on factors such as the steel strength, the geometry of the connected components, the size of the weld, and the welding process employed. The magnitude of the tensile residual stress can be as high as the yield strength of the material (Kulak & Smith, 1993).

It has been shown that as the thickness of the plate increases, the fatigue resistance decreases (Kulak & Smith, 1993). This may be due to a number of factors, including: the higher stress concentration associated with a weld toe in a larger plate, the higher probability of having larger flaws in thicker plates, and the presence of higher residual stresses due to the welding process in thicker plates (Kulak & Smith, 1993). In order to increase the fatigue life for thick plates (>25 mm), a lower fatigue detail category may be chosen (Kulak & Smith, 1993). Over time, environmental effects can play a major role in the fatigue life of welded structures. For instance, corrosion due to high humidity and a salt-laden atmosphere can reduce the cross section and produce a notch effect or in other words high stress concentrations at the locations of corrosion pits (Kulak & Smith, 1993). Corrosion can significantly influence fatigue crack growth. As the stress range passes the endurance limit, cracks grow much faster in the presence of corrosive material (Kulak & Smith, 1993). It must be noted that effects of corrosion on fatigue life and crack growth are very time dependent (Kulak & Smith, 1993).

2.5 Fatigue Design

The presence of fatigue has to be considered during the design stage (Maddox, 2000). There are a number of different methods that can be used for the fatigue design of the bridges (Walbridge, 2005). The most commonly used methods are: the classification method, the hot-spot stress method, and the fracture mechanics method, which are described briefly below (Ghahremani, 2010).

2.5.1 Classification Method

The classification method is a relatively simple approach, which has been widely be used by engineers. This method is based on stress versus fatigue life or S-N curves. These curves can be defined to represent a certain survival probability for fatigue design (Walbridge, 2005). A 95% or 97.7% survival probability are typically assumed (the latter limit corresponds with two standard deviations below the mean fatigue life). The number of cycles to failure can be estimated from these curves based on the stress range (Ghahremani, 2010). This approach is highly dependent on the availability of test results for specimens similar to the fatigue detail of interest (Maddox, 2000). Different "detail categories" characterize the susceptibility of a welded part to fatigue failure (Vilhauer et al., 2012). In the Canadian and American bridge codes, eight categories are defined in the order of increasing severity: A, B, B', C, C', D, E, and E' (Vilhauer et al., 2012). The S-N curves for these categories are plotted in Figure 2.9.

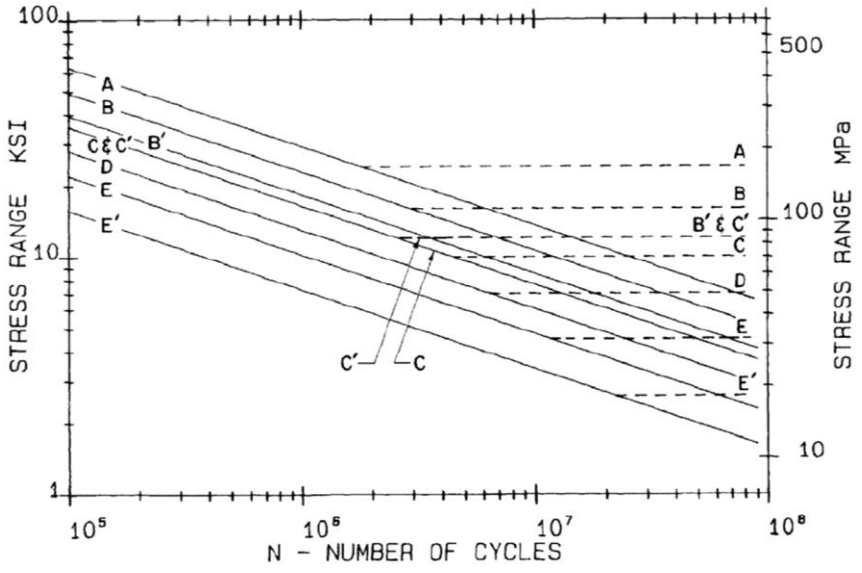

Figure 2.9: Fatigue design S-N curves (AASHTO, 2008)

The horizontal and vertical axes represent the number of cycles and the stress range respectively. The slope of the log-log curve is usually m = 3.0 for steel (Kulak & Smith, 1993). In order to use the classification method, the engineer determines the stress range and the number of stress cycles. These values are then compared to the design curve for the detail category (Walbridge, 2005). If the point falls above the line, the design is safe, otherwise redesign is required.

In equation form, the design verification includes two parts: in the first the fatigue resistance is computed based on the assumption that the fatigue life is finite and m = 3.0. In the second, the fatigue resistance is computed based on the CAFL, assuming that the fatigue life is infinite (Vilhauer et al., 2012). The resulting fatigue resistance is taken as (AASHTO, 2008):

$$\Delta F_n = (\frac{A}{N})^{\frac{1}{3}} \geq \frac{1}{2}(\Delta F)_{TH} \quad 2.4$$

Where ΔF_n is the fatigue resistance, A is a constant and N is the number of cycles to failure and ΔF_{TH} is the CAFL. This equation implies that when the stress range is half of the fatigue threshold, the component will have an infinite fatigue life (Vilhauer et al., 2012). This factor accounts for the possibility that the weld may experience a small number of high stress cycles during its lifetime, which are caused by trucks heavier than the design truck. In the design codes, it is accepted that the tensile residual stresses are present at the same level as the yield strength and for this reason the fatigue life is not dependent on the stress ratio. Rather it is mainly influenced by the stress range (Maddox, 2000). The material tensile strength is not considered, as it is seen to have little or no influence on fatigue life (Maddox, 2000). A disadvantage of the classification method is that it cannot be used for the design of fatigue details that have not been previously tested. Rather, it can only be used for the design details that are considered in the design code (Walbridge, 2005). Another disadvantage of this method is that no information about the crack growth rate can be gathered from it (Walbridge, 2005).

2.5.2 Hot-Spot Stress Method

A “hot-spot” refers to the location in a fatigue-prone connection where a crack is likely to initiate. The hot-spot stress method for fatigue design can be used for unusual welded joint geometries that are not considered in the design code (Ghahremani, 2010). The hot-spot stress is the theoretical stress at the crack location including the global geometry effects, but not the additional stress concentration due to the local weld profile (Walbridge, 2005). The hot-spot

stress method defines the fatigue strength of a range of welded joints using far fewer curves than the classification method (Maddox, 2000). According to this method, the hot-spot stress range and the number of cycles to failure are calculated. Similar to the classification method, these values are compared to a design S-N curve, which is a single curve for all geometries, with the exception that a size-effect correction factor may be applied (Walbridge, 2005). Unlike the classification method, this method can be used to estimate the fatigue lives of welded joints with complex and unusual geometries. In order to determine the hot-spot stress range, a coarse finite element analysis (FEA) or an instrumented prototype can be used. The S-N curve used in the hot-spot stress method can be applied for all structural details because the stress concentration due to the global geometry is used to calculate the hot-spot stress and the local geometry effects are considered in the establishment of the hot-spot stress S-N curve (Ghahremani, 2010). One disadvantage of the hot-spot stress method is that this method can only be used for the fatigue design of weld toes and not weld roots (Walbridge, 2005). Like the classification method, another disadvantage of the hot-spot stress method is that it does not provide any information about the size of the crack and its growth (Ghahremani, 2010).

2.5.3 Fracture Mechanics Method

Linear elastic fracture mechanics (LEFM) is a tool that can be used to predict the crack propagation phase of the fatigue life, including crack growth rates and crack sizes at various stages during the service life of a cyclically loaded component (Walbridge, 2005). LEFM relates the stresses at the crack tip to the stresses applied to the structure (Bannantine et al., 1990). LEFM is used to evaluate pipelines, automotive parts, spacecraft, and robotic structures (Kulak & Smith, 1993). In the evaluation of welded structures using LEFM, it is assumed that the component has a crack or crack-like discontinuity at the beginning of the fatigue life. For welded structures such as bridges, this is a reasonable assumption (Walbridge, 2005).

A fatigue failure is assumed to have occurred when the crack has grown to a critical depth, a_{cr} (Kulak & Smith, 1993). A critical crack depth for fracture can be calculated given the fracture toughness of the material (Kulak & Smith, 1993). The yield strength of the material can be used to calculate the critical crack depth associated with ductile fracture. The lower of the two critical crack depths will determine the fracture mode. Figure 2.10 shows a crack in a wide plate. The crack opens up a distance that is shown by the letter d after a stress is applied.

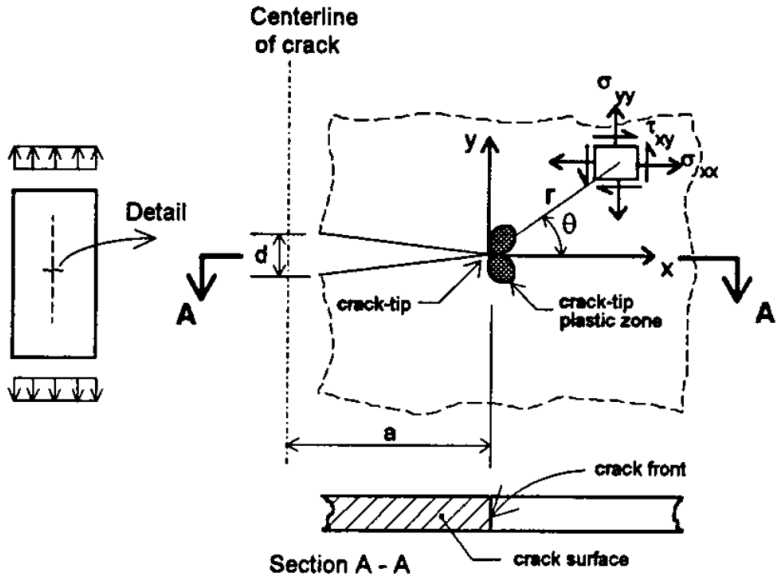

Figure 2.10: A crack in a wide plate (Kulak & Smith, 1993)

If plasticity is ignored, the stress field in the y-direction near the crack zone can be described by Equation 2.5 (Kulak & Smith, 1993). This equation can be used when the crack length, a, is larger than r which is the distance from the crack tip (Kulak & Smith, 1993).

$$\sigma_{yy} = \frac{\sigma\sqrt{\pi a}}{\sqrt{2\pi r}} \qquad 2.5$$

As *r* approaches zero in the above equation, the stress increases to infinity (Kulak & Smith, 1993). Plasticity occurs when the stresses exceed the yield stress; hence a plastic zone is created near the crack tip (Bannantine et al., 1990). The numerator of this equation is called K_I which is the stress intensity factor (SIF). Thus:

$$K_I = \sigma\sqrt{\pi a} \qquad 2.6$$

The SIF is a measure of the magnitude of the stresses near the crack tip (Bannantine et al., 1990). It must be noted that the σ in this equation is the remote stress applied to the component and not the stress at the crack tip. The stress intensity factor can be thought of as a measure of the crack driving force. If two cracks with different stress levels and crack lengths have the same *K* value, then they tend to behave similarly (Walbridge, 2005). Even though there is plasticity occurring at the crack tip, LEFM can still be used if the plastic zone at the crack tip is less than 2% of the plate thickness and the crack length except in some rare cases (Kulak & Smith, 1993).

Equation 2.6 is only applicable to a through crack in a uniformly loaded, infinitely wide plate. A more general equation is shown in Equation 2.7 (Kulak & Smith, 1993):

$$K_I = WY\sigma\sqrt{\pi a} \tag{2.7}$$

where *W* is a correction factor to account for non-uniform stresses that are caused by stress gradients and stress concentrations. *Y* is a correction factor that is used to account for the true shape of the crack and the presence of a free surface or plate edge (Walbridge, 2005), (Kulak & Smith, 1993). Knowing the applied stress range, Equation 2.7 can be modified to calculate the stress intensity factor range under cyclic loading (Kulak & Smith, 1993):

$$\Delta K_I = K_{max} - K_{min} = WY\Delta\sigma\sqrt{\pi a} \tag{2.8}$$

The stress intensity factor range can be related to the crack-growth rate (Kulak & Smith, 1993) using the Paris-Erdogan crack growth equation (Equation 2.9):

$$\frac{da}{dN} = C\Delta K^m \tag{2.9}$$

where *da/dN* is the derivative of the crack length versus the number of cycles, *a* is the crack length, *N* is the number of cycles, *C* and m are material constants obtained from a regression analysis. Regression analysis is used in statistics to investigate the relationships of variables on each other (Schneider & Maddox, 2003). In order to obtain the fatigue life, Equation 2.9 is integrated over the crack depth range from an initial crack length (a_0) to the critical crack length (a_{cr}) (Walbridge, 2005):

$$Nc = \int_{a_0}^{a_{cr}} \frac{da}{C\Delta K^m} \tag{2.10}$$

The Paris-Erdogan equation is valid for modelling stable fatigue crack growth. For very low SIF ranges, it tends to over-estimate crack growth rates, and for SIF ranges approaching the fracture toughness of the material, it under-estimates the crack growth rate (see Figure 2.11). The horizontal and vertical axes in Figure 2.11 represent the stress intensity factor range and the crack growth rate respectively.

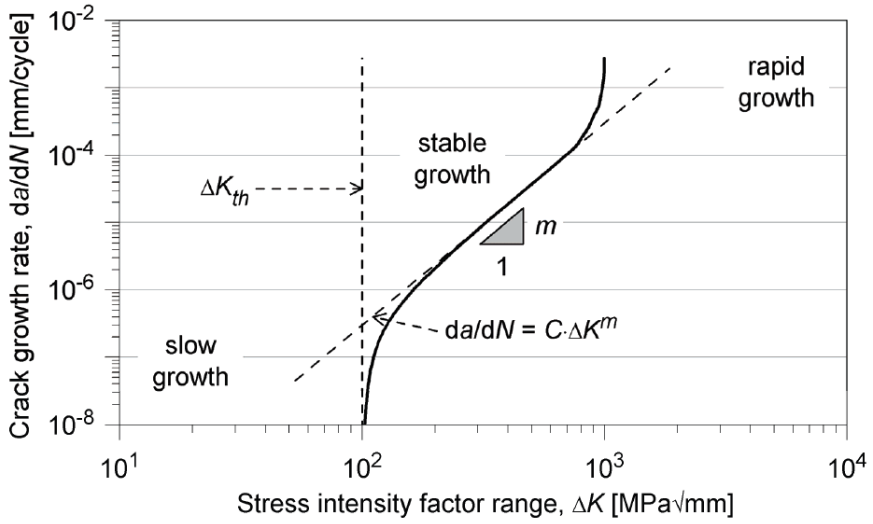

Figure 2.11: Three phases of fatigue crack growth bridges (Walbridge, 2005)

This figure shows that at very low crack growth rates, the true crack growth rate curve is almost vertical, which indicates the presence of a crack growth threshold, ΔK_{th} (Kulak & Smith, 1993). This is the slow growth phase. In this phase, the fatigue threshold is dependent on the stress ratio, *R*, which is defined by Equation 2.2. The other two factors that affect the threshold value are the frequency of loading and the environment (Bannantine et al., 1990). No failures will result as long as all loading cycles for a component has a value of ΔK that is lower than ΔK_{th}; however, this requires that very low stress levels are maintained, which often is not economic (Bannantine et al., 1990). At higher ΔK levels, the ΔK vs. *da/dN* curve is linear (Kulak & Smith, 1993). Crack growth in many structures is associated with the stable growth phase (Bannantine et al., 1990). The slope of the linear portion at the ΔK vs. *da/dN* usually falls between 10^{-6} and 10^{-3} mm/cycle (Bannantine et al., 1990). The region has a constant slope and is called the stable growth phase and is the only region where Equation 2.10 is accurate. In the rapid growth phase, the slope becomes almost vertical again as the fracture toughness of the material is approached (Kulak & Smith, 1993). This phase can be ignored in crack growth analysis, because it does not significantly affect the predicted crack propagation life (Bannantine et al., 1990). As mentioned earlier, residual stresses are often present due to welding. Since the distributions of the residual and applied stresses are different, the value of SIF for the residual stresses is calculated separately and then added to the SIF value for the applied stresses in order to calculate the total SIF associated with a given applied load level (Kulak & Smith, 1993).

2.6 Variable Amplitude Loading

In real structures, the stress ranges needed for use in any of the fatigue design methods described in the preceding sections can be difficult to determine, because the actual stress ranges experienced by these structures vary in amplitude. In order to determine whether a structure is safe or not under variable amplitude (VA) loading, Miner's rule is commonly used (Maddox, 2000). This rule is described by the following equation:

$$\sum \frac{n_i}{Ni} < 1 \qquad 2.11$$

where n_i is the number of stress cycles at a stress range i and N_i is the number of cycles causing failure at stress range i. If the left-hand side of Equation 2.11 is less than one, the structure is assumed to be safe; however, when the equation equals or exceeds one, failure is assumed to have occurred (Kulak & Smith, 1993). Using Miner's rule, the root-mean-cube (RMC) stress method can be used to correlate VA fatigue lives with constant amplitude (CA) fatigue lives (Ghahremani, 2010) by defining an equivalent stress range:

$$\sigma_{eq} = (\sum \gamma_i \sigma_i^3)^{1/3} \qquad 2.12$$

where σ_{eq} is the stress range for the VA loading, σi is the stress range for stress block i, and γ_i is the ratio of the number of cycles at stress block i to the total number cycles applied (Ghahremani, 2010). Along with Miner's rule, a stress cycle counting method such as the rainflow cycle counting method is needed to convert the variable amplitude stress history into a histogram of stress blocks with varying stress ranges (Kulak & Smith, 1993).

2.7 Finite Element Theory

In the 1940s, analytical methods were widely applied to solve the problems in structural mechanics (Tinsley Oden, 1990). Due to the increasing complexity of component shapes, analytical methods became less feasible and numerical methods were developed (Tinsley Oden, 1990). The development of the finite element method can be traced back to the work by Hrennikoff and Courant (Tinsley Oden, 1990). In 1973, Strang and Fix provided a rigorous mathematical foundation for the finite element method. Today, this method is applied across the boundaries of applied mathematics, physics, and engineering. By now, it has become the most significant numerical approach to solve complex geometrical problems (Tinsley Oden, 1990).

The practical implementation of the finite element method can be summarized into three steps: pre-processing, solution, and post-processing (Roensch, 2008). In the pre-processing step, the analyst will develop a finite element mesh to divide the subject geometry into subdomains for mathematical analysis, and apply material properties and boundary conditions (Roensch, 2008). In the solution step, the analyst will derive the governing matrix equations for the model and solve for the primary quantities. In the last step, the analyst validates the solution, examines the values of primary quantities, and derives and examines additional quantities (Roensch, 2008).The use of the finite element method is widespread. It has a variety of applications, such as solid mechanics, fluids, and heat transfer (Roensch, 2008).

Finite element analysis has been used, for example, to study fatigue crack closure for center-cracked plates, single-edge-cracked plates, and single-edge cracked plates with plane stresses (McClung, 1994). Also, the NASA aeronautics research board developed a common generic software program that uses the finite element method for engineers to model and analyze different aerospace structures including any kind of spacecraft and aircraft (Rugg, 2008).

The finite element method can be applied to various problems of fluids mechanics. Practically all situations of flow require a two or three dimensional treatment. The finite element method allows a fully unstructured and arbitrary domain subdivision to be used to approximate a problem (Zienkiewicz & Taylor, 2005). The finite element method can also be used to analyze two- and three- dimensional elasticity problems, as well as plane strain and plane stress problems (Pepper & Heinrich, 2006). High stressed areas, low stressed areas and stress gradients can be obtained from the finite element method. High stressed areas are the areas with highest tensile stress that are vulnerable to yielding or cracking (Pineault et al., 2002). As the most commonly used numerical method in structural mechanics, the finite element method has its advantages and disadvantages. Firstly, the finite element method can handle all kinds of geometry problems. Secondly, this analysis method is much more economical (Desai & Abel, 1971). There are hundreds of commercial programs available (Dechaumphai & Phongthanapanich, 2009). The programs allow the analyst to test the same model under various environments with different boundary conditions, nodal and element loads, and different time or frequency dependent loadings (Desai & Abel, 1971). Lastly, the user can improve a design without actually producing a prototype (Dechaumphai & Phongthanapanich, 2009). Along with these advantages; however,

the finite element method also has its limitations (Desai & Abel, 1971). The most significant disadvantage of the method is that it can only provide an approximate solution. Other disadvantages include the software and user training costs (Dechaumphai & Phongthanapanich, 2009).

2.8 Post-Weld Treatment Methods

Any action taken after welding to improve the fatigue performance of the weld can be referred to as a post-weld treatment (PWT) (Ghahremani, 2010). Such treatments are generally applied to the weld toe, in the area where the weld meets the base metal (AASHTO, 2008). PWTs can be divided into two categories: geometry improvement and residual stress-based methods.

Geometry improvement methods are used to improve the weld profile and to remove crack-like defects (<1 mm). Grinding and Tungsten Inert Gas (TIG) dressing are two examples of geometry improvement methods (Smith & Hirt, 1985). Improving the weld profile by increasing the toe radius will help to reduce the stress concentration, while removing crack-like defects will help to reduce the initial crack depth or fully eliminate it (Walbridge, 2005).

Residual stress-based methods are used to remove harmful tensile residual stresses and to introduce compressive residual stresses near the weld toe (Walker et al., 2008). Needle peening, hammer peening, shot peening, and ultrasonic impact treatment (UIT) are examples of residual stress-based methods. The objective of residual stress-based methods is to introduce permanent plastic deformation where the crack is located. This plastic deformation forces the crack tip to stay closed during cyclic loading and slows down the propagation (Ghahremani, 2010).

2.8.1 Grinding Methods

Grinding is a geometry improvement method that is used to remove the defects and discontinuities at the weld surface. By removing these defects a new crack initiation period is introduced for the fatigue life of the structure (Ye & Moan, 2008). Grinding methods also aim to reduce the stress concentration at the weld toe. Due to the reliability of weld toe grinding, it has become a popular PWT method (Ye & Moan, 2008). The grinding tools that can be used are disk and burr grinders (Walbridge, 2005). Figure 2.12 shows an electric grinder and burrs with different sizes to match the plate thickness.

Figure 2.12: Grinder and burrs (Haagensen & Maddox, 2001)

The diameters of these burrs are usually between 10-25 mm for plate thicknesses that vary between 10 to 50 mm in thickness. The final groove should be 0.25% of the total thickness of the component (Haagensen & Maddox, 2001). Grinding methods are very effective, reliable, and use readily available tools. Disk grinding uses a rotating disk, rather than a burr, and is faster and cheaper but less effective than burr grinding (Walbridge, 2005).

2.8.2 Dressing Methods

Dressing methods are also geometry improvement methods and include tungsten inert gas (TIG) and plasma dressing (Walbridge, 2005). Similar to grinding, the objective is to remove the crack-like defects. With dressing methods, the weld toe is re-melted. In both methods, the weld toe is melted by a welding torch. However, twice the amount of heat input is used for plasma dressing than for TIG dressing. This will result in a faster treatment. On the other hand, the plasma dressing tool is not as mobile and readily available as TIG dressing which can remove cracks as deep as 6 mm, according to (Smith & Hirt, 1985). Dressing methods in general can be highly effective for improving fatigue performance but they do require a high level of skill and proper cleaning of the weld.

2.8.3 Peening Methods

Peening methods are residual stress-based treatment methods (Walbridge, 2005). Peening is a cold working procedure that deforms the weld toe plastically through high velocity impacts (Roy & Fisher, 2006). Needle and hammer peening are examples of peening methods. Needle or hammer peening result in an upward shift in the S-N curve, increasing the fatigue strength by a factor of 1.3-1.6 for stress ranges up to 100 MPa (Ghahremani, 2010). Peening creates compressive residual stresses at the surface that are balanced by tensile residual stresses below the surface. Cracks can be slowed down or fully stopped if the magnitude of the compressive

residual stresses is sufficiently high. Peening treatments can cover large areas. They are particularly effective when used with high strength steel (Kirkhope et al., 1999).

Hammer peening is done with four passes of 6-18mm diameter rods at a treatment speed of 25 mm/s for the best results. If done correctly, after the peening, the weld should have a smooth surface with a groove depth of approximately 0.5 mm (Walbridge, 2005). Figure 2.13 shows a pneumatic riveting gun that can be used for hammer peening (Haagensen & Maddox, 2001).

Figure 2.13: Pnuematic riveting gun used for hammer peening (Haagensen & Maddox, 2001)

Typically a pneumatic or hydraulic hammer is used; however, riveting guns have been used due to their lighter weight and reduced vibration (Haagensen & Maddox, 2001). A small diameter tip is preferred for hammer peening to increase the likelihood that the base of the weld toe will be impacted by the peening tool (Haagensen & Maddox, 2001). When peening, the operator must hold the tool firmly and keep the tool tip in contact with the weld toe (Haagensen & Maddox, 2001). The operator should also hold the hammer at about $45^{o} – 80^{o}$ with respect to the plate surface and $75^{o} – 90^{o}$ with respect to the travelling direction as shown in Figure 2.14.

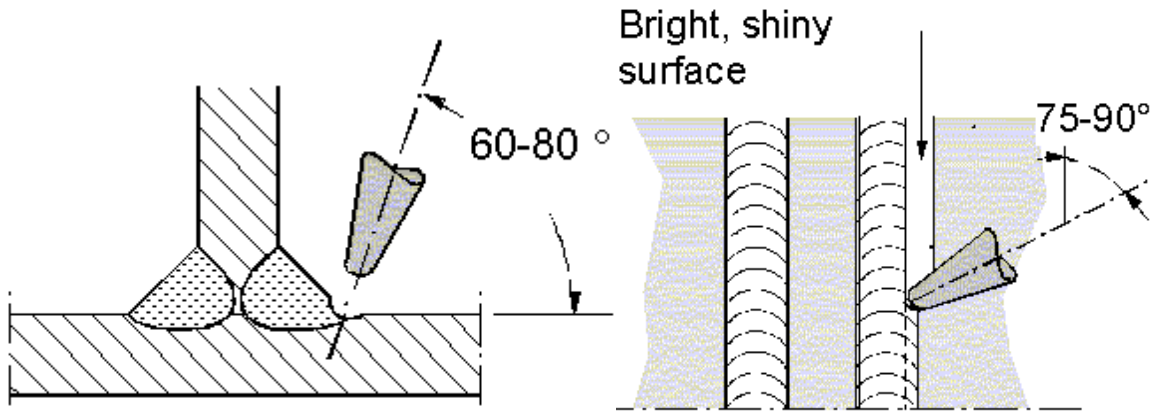

Figure 2.14: Hammer peening operation (Haagensen & Maddox, 2001)

Needle peening works the same a hammer peening except that a standard needle gun for removing slag after welding is used. In needle peening, 10-15 rods of 2-3 mm in diameter are used (Walbridge, 2005). The smaller the diameter of the peening rods, the greater the possibility of removing the original weld toe (AASHTO, 2008). If the treatment is done correctly, the welding surface should be left with overlapping indentations on the surface (Walbridge, 2005). Figure 2.15 shows a typical needle peening tool in the top figure. The bottom figure shows the tip of the needle bundle (Haagensen & Maddox, 2001).

Figure 2.15: Needle peening equipment (left) and the tip (right) (Haagensen & Maddox, 2001)

If peening is applied correctly, it is considered to be a very effective and reliable method for increasing the fatigue life of welded structures (Walbridge, 2005). On the other hand, hammer and needle peening are both very noisy and are difficult for a tool operator to do for long periods of time, due to the heavy vibration of the treatment tool.

2.8.3.1 Ultrasonic Impact Treatment

Ultrasonic impact treatment (UIT), also known as ultrasonic peening, is a relatively new weld treatment method that enhances and increases the fatigue lives of the treated parts by replacing tensile residual stresses with beneficial compressive residual stresses and by reducing the stress concentration in the critical region by improving the weld toe geometry (Roy & Fisher, 2005) & (Lihavainen & Marquis, 2000). The UIT process is very similar to the conventional needle and hammer peening, with additional improvement of the weld toe geometry and the surface microstructure due to its effects (Haagensen et al., 1998). Since the primary mechanism leading to a fatigue life increase is the effect of UIT on residual stresses, UIT falls under the category of residual stress-based improvement methods.

There are some differences between UIT and conventional peening methods. In contrast with needle peening, for example, where a pneumatic tool is used to impact the weld toe at a frequency of 25-100 Hz, UIT uses four 3 mm diameter rods to impact the welds (Applied Ultrasonics, 2006). These rods vibrate at an ultrasonic frequency of 27,000 Hz (Tilly, Jackson, & Maddox, 2010). A significant advantage of UIT over the conventional methods from an occupational health and safety perspective is that it is a much quieter device (Tilly et al., 2010). The vibrations felt by the equipment operator (which can be considerable for hammer or needle peening) are also significantly less, which makes it possible for much larger areas to be treated and allows the operator to use it for longer periods of time before getting tired.

The first UIT specifications were developed in 1996 and were further tested and studied at NSTC laboratory in Severodvinsk, Russia and at the E.O. Paton Electric Welding Institute in Kiev, Ukraine (Statnikov, 1999). Since then, UIT had been developed by Applied Ultrasonics® in Birmingham, Alabama, USA. Over the years, the design and technical issues were addressed and improved (Statnikov, 1999). Figure 2.16 shows the UIT tool and the description of each part. Ultrasonic oscillations are shown in the figure. UIT technology converts these ultrasonic oscillations of the transducer to ultrasonic impact pulses that are shown in the figure. The impact pulses locally and plastically deform the weld toe up to 1.5 mm and induce compressive residual stresses down to a depth of 3-5 mm according to (Statnikov, 1999).

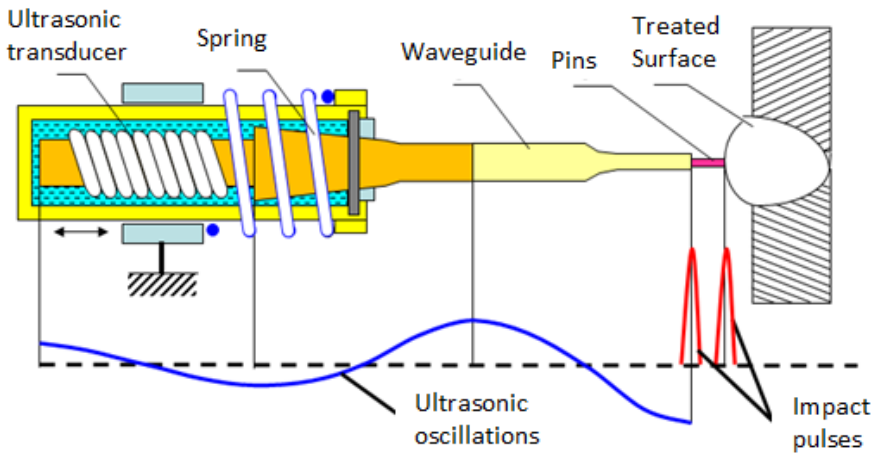

Figure 2.16: UIT mechanism (Statnikov, 1999)

Various research groups have reported fatigue performance improvements due to UIT. It is reported that the fatigue lives of treated specimens have improved by 50-200% by (Haagensen et al., 1998). Results have shown that UIT has the potential to increases the fatigue life by a factor of up to 25 and more (Vilhauer et al., 2012). UIT has been used on a CN Railway Bridge in Port Hope, Ontario during 2001. Based on the monitoring of the treated welds, excellent results have been obtained (Roy & Fisher, 2006).

The treatment included the UIT of stiffener welds and web-to-flange welds. Researchers at Lehigh University conducted many large-scale fatigue tests using UIT and they confirmed that the fatigue life increased without changing the slope of the S-N curve (Roy & Fisher, 2006). Based on this study, it was found that both the stress range and the minimum stress have significant contributions on the degree of improvement (Roy & Fisher, 2006).

The UIT equipment consists of an ultrasonic transducer, a power unit; a hand-held tool with striking needles, an electronic control box, and a wave guide (see Figure 2.17).

Figure 2.17: Ultrasonic impact treatment equipment

This equipment is easier to use than the traditional peening equipment because it provides a comfortable work environment with a minimum vibration and noise (Roy & Fisher, 2006). Various heads are available for the hand tool to treat different details (Roy & Fisher, 2005). In situations where the weld toe is located at a tight corner, a head that has one 5 mm diameter pin can be used. The control box has different settings for the level of output power range where the intensity of the treatment can be chosen. The oscillation amplitude of the indenters which is usually from 30-40 microns on the electronic display of the control box must be constantly monitored to make sure the operation is done properly (Roy & Fisher, 2005). For a proper treatment the pins impact the weld toe at different angles (Applied Ultrasonics, 2006). Figure 2.18 shows that the pins first impact the weld toe at a 45° angle while the tool is moving parallel to in the direction of the weld toe.

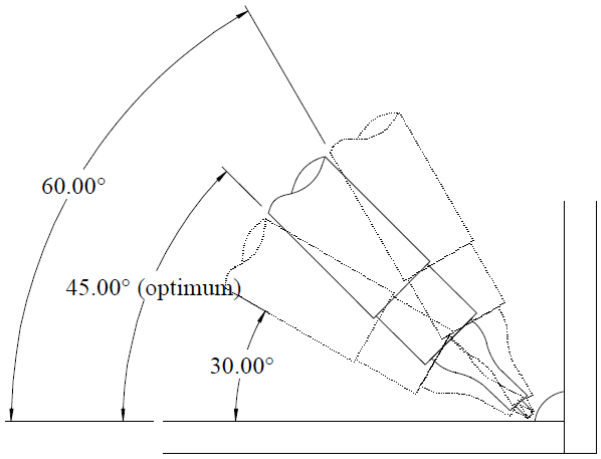

Figure 2.18. Impacted angles for proper treatment (Applied Ultrasonics, 2006)

The tool can be moved between a 30° and a 60° angle (Applied Ultrasonics, 2006). The self-weight of the hand-held tool is sufficient and extra force is not needed while holding the tool (AASHTO, 2008). This way a desired shiny groove with an appropriate depth can be obtained. The appearance of the groove that is formed by the impacting energy of the pins (AASHTO, 2008) can be used as a criterion for quality assurance. Additional passes might damage the weld toe by deepening the groove (Applied Ultrasonics, 2006) and causing material to flake off. After the treatment is done, the radius of the groove should be approximately the same as the radius of the impacted pin. Otherwise, the weld toe has not been treated properly, which will result in the appearance of dark lines on the weld toe (Applied Ultrasonics, 2006). The treatment speed for a properly treated weld is usually 30-60 cm/min. To get optimum results, all pins should be in contact the weld toe (Applied Ultrasonics, 2006).

Figure 2.19 shows two simples cases of under-treated welds (Applied Ultrasonics, 2006). The weld on the left has a line of untreated material along the intersection of the weld and base metal and the weld on the right has a start-stop gap in the treatment.

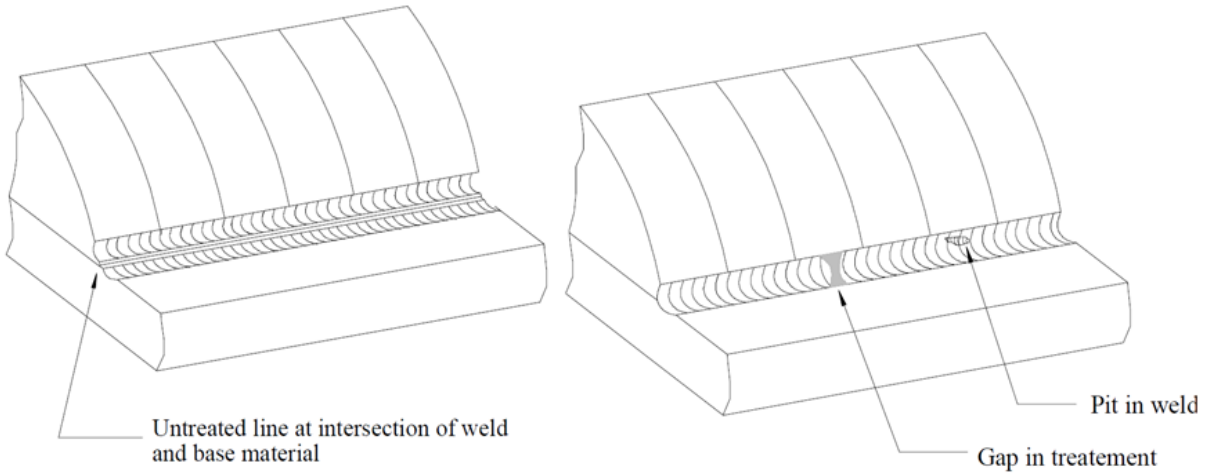

Figure 2.19: Under-treated welds (AASHTO, 2008)

Heat treatment and hot dipped galvanizing should not be performed after UIT. The reason is that UIT introduces beneficial compressive residual stresses and performing these other treatments will relieve these stresses (AASHTO, 2008). If significant dead loads are present on the structure, it is recommended to subject the structure to the dead loads first (e.g. erect the structure with the welds untreated) and then perform the treatment on-site (AASHTO, 2008).

2.9 Quality Control

Achieving high weld quality is critical for ensuring the fatigue performance of as-received welds. Quality control is also important for ensuring that post-weld treatments are carried out in a way that achieves the desired objectives, in terms of increasing fatigue performance.

2.9.1 Quality Control of As-Received (Untreated) Bridge Welds

NCHRP Project 10-31 defines acceptance criteria for as-received (untreated) bridge welds (Crosley & Ripling, 1990). This report distinguishes between harmful cracks that will cause failure in the welds as well as harmless cracks that will not contribute to the failure (Crosley & Ripling, 1990). According to (Haagensen & Maddox, 2001), quality control should include visual inspection, weld toe radius measurement, angle and groove depth measurements. Visual inspection of welds is very important. In addition to visual inspection, various other non-destructive inspection methods can be used. These methods include dye-penetrant testing using products such as SPOTCHECK® (see Figure 2.20) and Zyglo penetrants. Radiographic and magnetic particle inspection can also be used to detect cracks (Crosley & Ripling, 1990).

Figure 2.20: SPOTCHECK® sprays (Ghahremani, 2010)

The average weld toe angle for untreated welds was approximately 40° (Ghahremani, 2010). The average radius for untreated and treated specimens was 0.65 mm (Ghahremani, 2010). In another study, the average weld toe radius and weld toe angle for as-received welds were found to be 0.2 mm and 39° respectively (Lopez-Martinez & Korsgren, 1993). Lopez-Martinez and Korsgren (1993) also performed a study to compare how well the shape of the replica of a weld toe will represent the local and actual shape of the weld toe (1993). The study included three welds and

seven replicas. The results show that if the welds are cleaned, the shape of the replica will give a good representation of the shape of the weld toe allowing the measurement of the weld toe angle and the weld toe radius (Lopez-Martinez & Korsgren, 1993).

2.9.2 Quality Control of Post-Weld Treatments

2.9.2.1 Visual Inspection

Welds are checked by an inspector to confirm that the UIT has been done correctly (Tilly et al., 2010). Although, visual inspection of the treated weld toe is an important component of quality control, it is not possible to only depend on the visual inspection (AASHTO, 2008). Visual inspection can be much more effective with the use of a 10X magnifying glass to check the uniformity and consistency of the treatment (AASHTO, 2008). Figure 2.21 shows an as-received (untreated) weld and a similar weld treated by UIT (Applied Ultrasonics, 2006).

Figure 2.21: Untreated weld toe (left) and Treated weld toe (right) (Applied Ultrasonics, 2006)

This figure shows correctly and incorrectly treated weld toes.

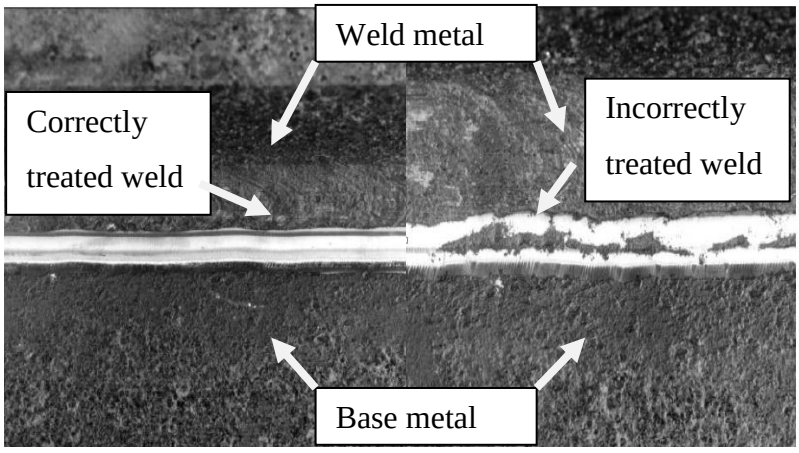

Figure 2.22: Correctly and incorrectly treated welds (Haagensen & Maddox, 2001)

According to (Tilly et al., 2010) some factors that need to be considered when visually inspecting to ensure the quality of UIT are as follows:

- The groove resulting from the plastic deformation along the toe of a weld treated by UIT should be visible, continuous, and metallic-looking.
- The groove should be centered on the weld toe.
- The groove should be uniformly smooth and homogeneous along the weld toe.
- Any evidence of cracks, visible lines, digging, or undercut should be avoided.
- There should not be any trace of the original weld toe after the treatment.
- The groove is typically 3-5 mm wide and the groove depth varies from 0.3 – 0.6 mm.

For hammer peening an indent depth of 0.5 mm is desired (see Figure 2.14) and a minimum groove depth of 0.3 mm is recommended by (Haagensen & Maddox, 2001).

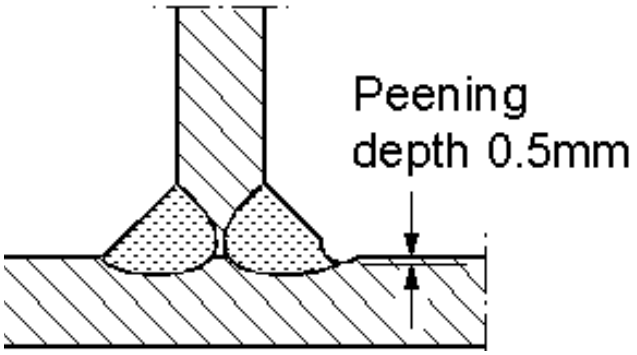

Figure 2.23: Hammer peening operation and peening depth (Haagensen & Maddox, 2001)

In addition, the groove surface must be smooth, with no individual indentations visible as shown in Figure 2.14 (left). In Figure 2.14 (right), an unacceptable hammer peened weld is shown, with individual indentations visible, as a result of insufficient coverage.

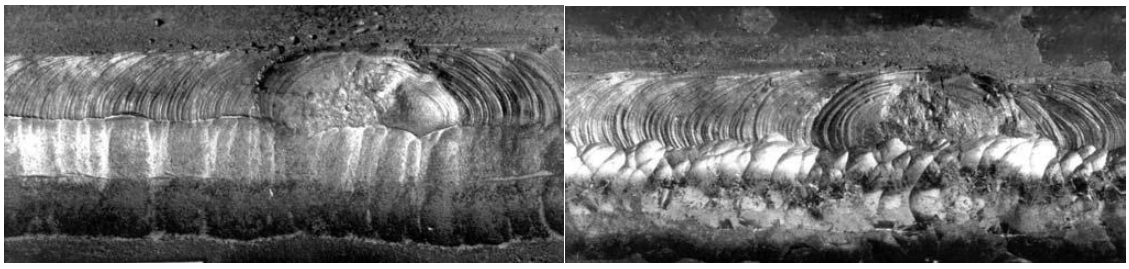

Figure 2.24: Acceptable (left) and unacceptable (right) hammer peened weld toe (Haagensen & Maddox, 2001)

2.9.2.2 Weld Toe Geometry and Radius Measurement

Overall, it is not possible to perform a quality control on a weld by solely doing a visual inspection (AASHTO, 2004). Another possible inspection method involves taking impressions of the weld toe and measuring the weld toe radius and indent depth. Haagensen & Maddox (2001) recommend the use of the silicon rubber used by the dentists to take impressions of the weld toe and use them to perform weld toe geometry measurements for the quality control of grinding treatments. Figure 2.25 shows the toe geometry of a weld treated by grinding.

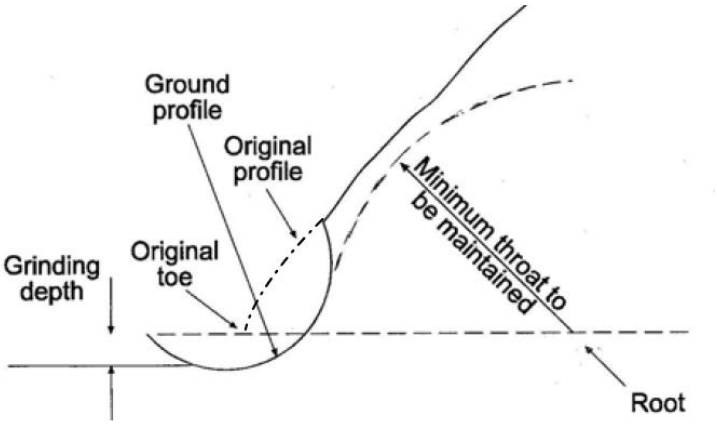

Figure 2.25: Weld toe geometry after grinding (Haagensen & Maddox, 2001)

Figure 2.26 shows a radius and groove depth measurement after UIT (Roy & Fisher, 2005).

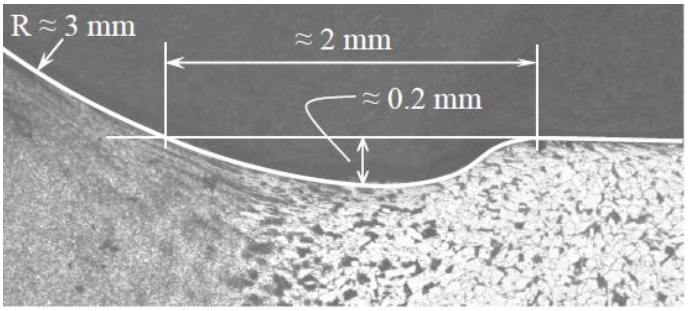

Figure 2.26: Radius and groove depth measurements (Roy & Fisher, 2005)

To measure the indent depth, a picture of the weld toe is taken using a microscope. A straight line is drawn and extended from the base metal. Then, the maximum perpendicular distance from that straight line to the bottom of the weld toe is taken as the indent depth. As shown in this figure, (Roy & Fisher, 2005) found an indent depth of 0.2 mm and a weld toe radius of 3 mm to be typical for weld toes treated by UIT. AASHTO recommends a depth of 0.25-0.5 mm for the

quality control of weld toes treated by UIT (AASHTO, 2004). In order to measure grinding or indent depth after treatment, a depth gauge can be used (Haagensen & Maddox, 2001). Figure 2.27 shows a standard weld inspector's depth gauge that can be used to measure grinding or indent depth. This device is referred to as a 'go- no go' type of gauge because the weld toe either passes the requirement or does not.

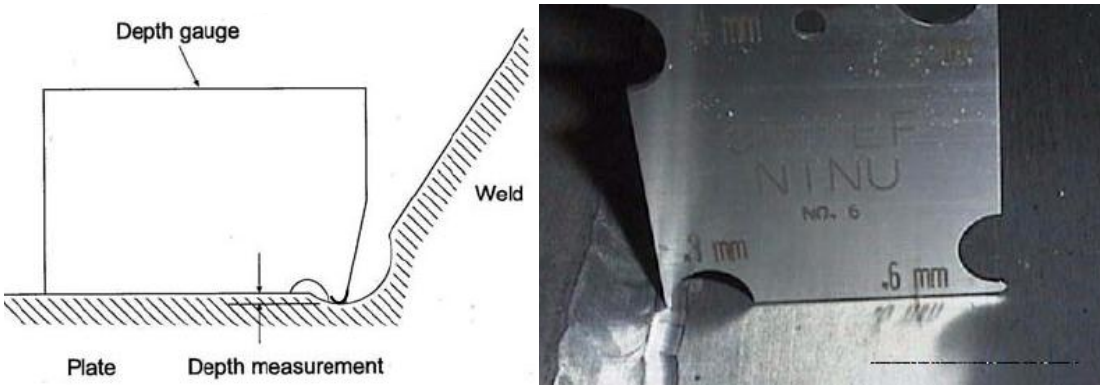

Figure 2.27: Depth gauge measurement device (Haagensen & Maddox, 2001)

2.9.2.3 Controlling Treatment Inputs

Typically, the travel speed of the tool is kept between 50 and 100 mm/min per pass (Haagensen & Maddox, 2001). At this treatment speed, the required number of passes required is usually around four times to reach the desired groove depth for hammer peening (Haagensen & Maddox, 2001) and to cover all of the areas that are missed as a result of the vibration of the hammer. The hammer tip diameter is a factor that influences the indentation surface (Haagensen & Maddox, 2001). If the hammer tip has a small diameter, the weld toe line will be indented and disappear after the treatment (Haagensen & Maddox, 2001). If the hammer tip has a larger diameter (more than 12 mm), the hammer tip will deform the weld or parent metal instead of the weld toe itself (Haagensen & Maddox, 2001). This is a problem due to the diminished compressive residual stresses introduced in this case (Haagensen & Maddox, 2001). The tool for UIT should be positioned on the specimen in a way that the weld and base metal will get treated equally (AASHTO, 2004). In order to achieve this, the UIT tool must be rocked back and forth while positioned at the center of the weld toe (AASHTO, 2004). The angle that the tool must be held varies from 40°-80° with respect to the base metal (AASHTO, 2004). According to AASHTO, the treatment speed shall be 0.3 to 1.5 m/min (AASHTO, 2004). The final groove width is equal to or greater than 3 mm, as recommended for properly treated welds (Applied Ultrasonics, 2006).

3 Test Procedures and Measurements

3.1 Introduction

This chapter focuses on the test procedures and measurements. Section 3.2 describes the specimen geometry and the fabrication process. Section 3.3 and 3.4 give a detailed description of the loading and the type of treatment used in this research. Section 3.5 discusses the test matrix in detail. Section 3.6 focuses on the ACPD instrumentation that was used to measure the crack growth and to identify the crack initiation and propagation. Weld toe geometry measurements were made to evaluate the weld shape, the angle, and the indent caused by UIT, which were thought to be possible measures of treatment quality. Section 3.7 explains the procedures used to make these measurements. Microhardness measurements were performed to get a better understanding of the effect of UIT on the microstructure of the material. The procedures used to make the microhardness measurements are described in Section 3.8. Residual stress measurements are discussed in Section 3.9. The purpose of these measurements was to characterize the residual stresses introduced by UIT in the vicinity of the weld toe.

3.2 Specimen Details

The small-scale fatigue specimens used in this study are representative of welded connections on bridges that are prone to fatigue (Klippstein & Schilling, 1989). Specifically, the specimen geometry was chosen to be a representative of the bottom tension flange of a girder at the location where a web stiffener is attached. The stiffener in this case is a non-load carrying transverse attachment (Ghahremani, 2010). This geometry falls under Detail Category 'C' according the CAN/CSA S6-06 (Canadian Standards Association (CSA), 2006).

The specimens were fabricated from 300 mm wide plates of CSA grade 350W steel with a thickness of 9.5 mm (3/8"). The transverse stiffeners were welded to the plates with four identical fillet welds using the flux-cored arc welding (FCAW) process. Following the welding, the 300 mm wide stiffened plates were saw cut into 50 mm wide strips. The ends were discarded to ensure that there were not any weld starts or stops within the specimen widths. The dimensions of the initial rectangular specimen geometry are shown in Figure 3.1.

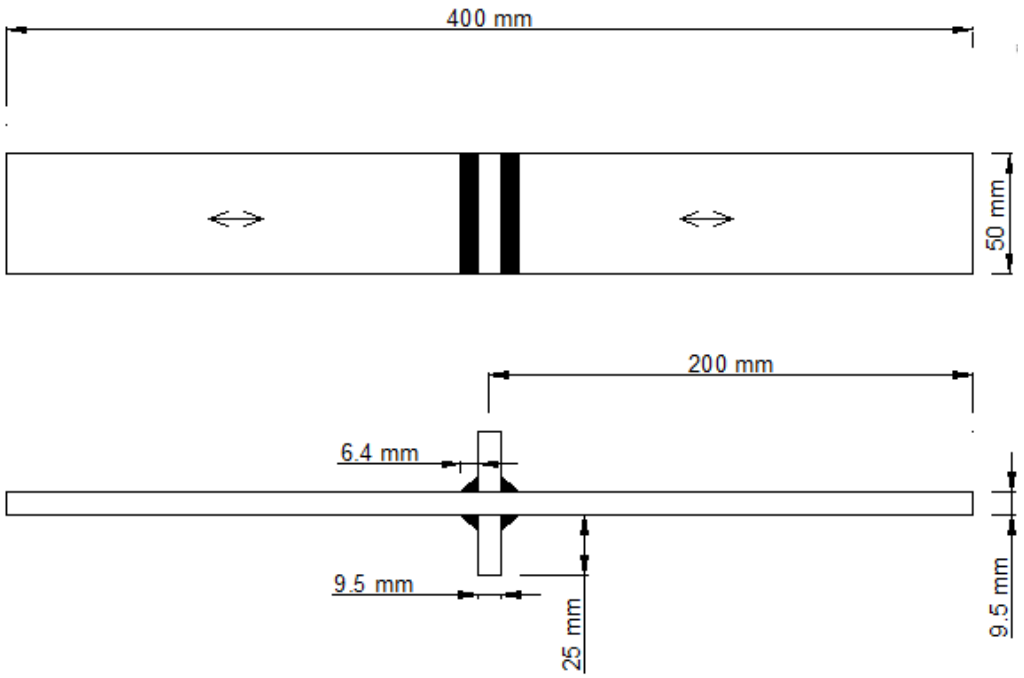

Figure 3.1: Initial transverse stiffener specimen geometry

The 400 mm long horizontal piece in this figure represents the flange of a girder and the vertical part represents a stiffener. The horizontal part of the test specimen is 400 mm long, 50 mm wide and 9.5 mm thick, whereas the two transverse stiffeners are 9.5 by 25 mm. The arrows on the figure show the rolling direction, which is the direction of the grain orientation. After fabrication, the specimens were treated by UIT using procedures and settings specified by the tool manufacturer, modified as specified in the test matrix presented in Table 3.3. Following the treatment, the specimens were "dog-boned" using a computer numerical control (CNC) cutting machine.

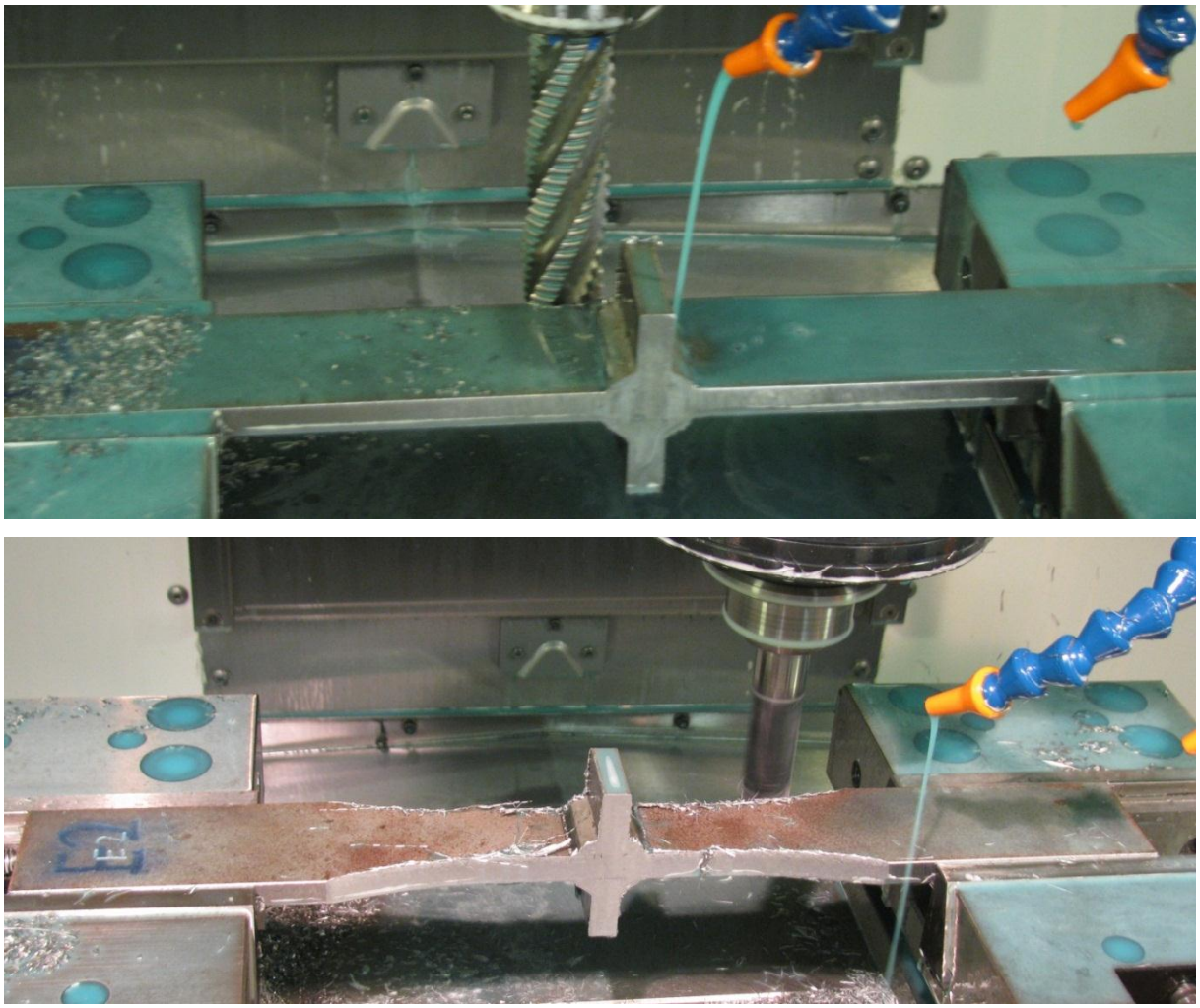

Figure 3.2: Rectangular (top) and dog-boned specimen in the CNC machine

One reason for dog-boning the specimens is that during a previous test series, post-weld treatment by needle peening was so effective in some cases that cracks initiated in the gripped ends of the specimens rather than the weld toe (Ghahremani, 2010). A second reason is that this ensured that there were no UIT starts or stops in the tested specimen width. The geometry of the dog-boned specimen is shown in Figure 3.3.

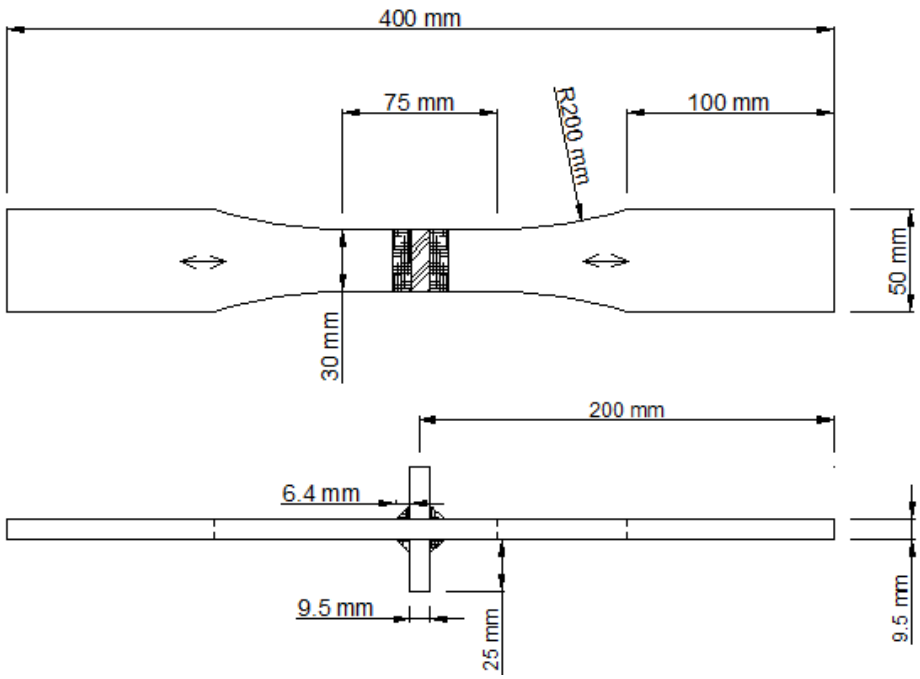

Figure 3.3: Transverse specimen geometry after dog-boning

As seen in this figure, the specimen width was reduced from 50 mm to 30 mm. The final geometry conforms to that of (ASTM E-8, 2004)). After dog-boning the specimens, their dimensions were measured. The mean width and thickness for each group are presented below in Table 3.1.

Table 3.1: Mean specimen dimension measurements

	Average Width	**Percentage Error**	**Average Dog-Boned Width**	**Percentage Error**	**Average Thickness**	**Percentage Error**
Group A	50.16	0.32%	30.06	0.20%	9.57	0.74%
Group B	49.8	0.40%	29.92	0.27%	9.59	0.95%
Group C	49.74	0.52%	29.95	0.17%	9.73	2.42%
Group D	50.03	0.06%	29.89	0.37%	9.68	1.89%
Group E	49.44	1.12%	30	0.00%	9.65	1.58%
Group F	47.05	5.90%	29.94	0.20%	9.68	1.89%
Group G	47.15	5.70%	29.99	0.03%	9.66	1.68%
Average	49.05	1.90%	29.96	0.13%	9.65	1.58%

The last row in this table shows the average for the dimensions of each group. The percentage error, which is the (estimated value-actual value)/actual value, is calculated in the column next to

each dimension measurement. Overall, the percentage errors are smaller than 3% except for the average width of Group F and G.

3.3 Loading

Two stress history types were investigated in this study: constant amplitude (CA) and constant amplitude with periodic under-load cycles (CA-UL). Figure 3.4 shows samples of each history type, where CA loading is shown on the left and CA-UL is on the right side.

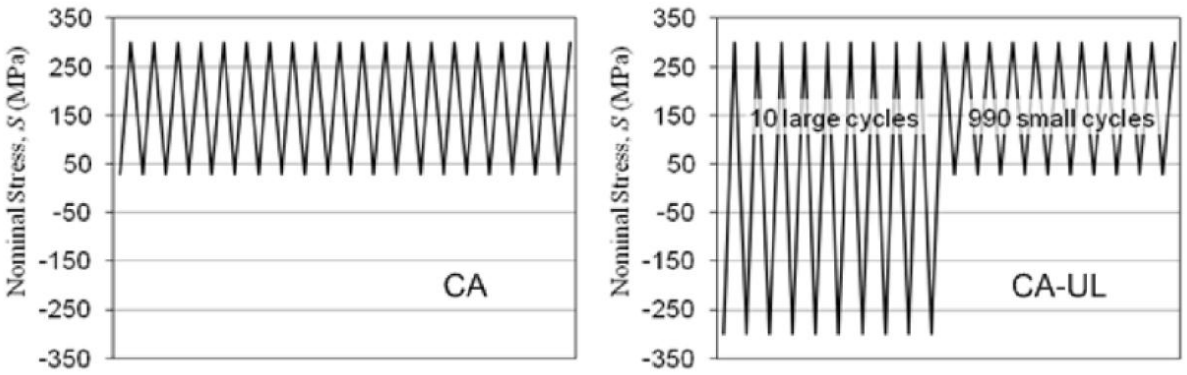

Figure 3.4: CA and CA-UL fatigue loading histories

Even though real stress histories tend to vary in amplitude, CA loading tests are commonly used to characterize the fatigue performance of welds. Compressive under-load cycles are known to be particularly severe for welds improved using residual stress-based post-weld treatments such as UIT. Thus, the two history types were chosen to represent best and worst case scenarios for the cyclic loading histories that actual bridge welds are likely to see while in service.

For each specimen the cycling was continued until fatigue cracks were fully developed or N exceeded $5 \cdot 10^6$ cycles, in which case the specimen was considered to be a "run-out". For the CA loading, specimens were tested at stress ranges of 200, 225, and 250 MPa with loading frequencies not exceeding 23 Hz. A stress ratio of R = 0.1 was used for all of the tests. For the CA-UL loading, 1000 cycle blocks were repeated until specimen failure or $N = 3 \cdot 10^6$ cycles was reached. Of these 1000 cycles, ten were compressive under-load cycles with stress ranges of 440, 500, and 556 MPa and a stress ratio of R = -1. The compressive under loads can have the effect of relaxing the compressive residual stresses due to the peening treatment and reducing the crack opening stress level (Ghahremani & Walbridge, 2011). The other 990 cycles had stress ranges of

200, 225, and 250 MPa and a stress ratio of R = 0.1, which is the same as the CA loading history. For plotting the test data for the CA-UL loading, an equivalent stress range was calculated using Miner's sum (Equation 2.11) and an assumed S-N curve slope of m = 3.

3.4 Weld Treatment

The specimens were treated using an ultrasonic impact treatment (UIT). A company specializing in UIT, Applied Ultrasonics performed the treatment, in accordance with their own recommended procedures (Applied Ultrasonics, 2006). Figure 3.5 shows a specimen before and after treatment.

Figure 3.5: Weld toe of A1 (left) and F6 (right)

As seen in this figure, the treated Specimen F6 has a shiny and think groove that was achieved through the proper application of UIT. The treatment was constantly monitored by a 10X magnifying glass to make sure a shiny and uniform groove was achieved.

In order to study the effects of treatment quality on fatigue performance, treatment quality had to be one of the main parameters varied in the experimental program. In the current study, treatment quality was varied intentionally. Under-, over-, and properly treated specimens were tested. The under-treated specimens were tested to determine whether a fatigue life increase still occurs if the magnitude of the compressive residual stresses is reduced. The over-treated specimens were tested to determine whether over treating results in damage to the weld. Of these two scenarios, bridge owners are generally more concerned about over-treatment, since this problem tends to be a less easy one to correct than under-treatment. The treatments were performed either manually or using a robot. The robot was programmed to perform the treatment at various settings to simulate under-, over-, and proper treatment. Although UIT is performed manually on actual bridges, it was thought that the use of the robot for simulating the various levels of treatment quality would lead to reduced scatter in the experimental results. Table 3.2 shows the treatment specifications for the robotically applied UIT (Applied Ultrasonics, 2006). Proper treatment is assumed to correspond with a treatment speed of 10 mm/s, a power level of

9, and amplitude of approximately 27-29 μm. The power level is a number established by the tool maker, which is directly related to the amplitude. As seen in this table, two kinds of under-treatment were considered: under-treatment by reducing the amplitude (from 27-29 μm down to 18 μm) and by increasing the treatment speed (from 10 to 20 mm/s). Over-treatment was simulated by reducing the treatment speed from 10 mm/s to 1 mm/s. This results in a large increase in the number of impacts of the UIT pins per mm of weld. In all cases, the treatment was carried out in four "passes" of the UIT tool along the weld toe at 45º, 30º, 60º, and 45º.

Table 3.2: Treatment specification

Group	**Treatment**	**Speed (mm/s)**	**Power Level**	**Amplitude (μm)**	**Volts**
B	Under-treated with reduced amplitude	10	4	18	50.7~51.8
C	Under-treated with increased speed	20	9	27~29	80.6
D	Over-treated with reduced speed	1	9	27~29	80.6
E	Properly treated	10	9	27~29	80.6

Figure 3.6 shows a specimen after over-treatment using the robot. In the case of the over-treated specimens, a significant flaking of the weld toe material was apparent after the treatment. The flakes of material removed from the weld toe are clearly visible in this figure. The presence of such flakes could be used as a means of quality control. However, it would only be a reliable one if the inspector was present while the treatment was being performed.

Figure 3.6: Over-treated specimen (left), and robot (right)

The tool should be gently rocking back and forth parallel to the direction of the weld through angles of 45º, 30º, 60º, and 45º (Applied Ultrasonics, 2006). This oscillation is recommended to avoid "digging defects" that may result from holding the pins in only one position (Applied Ultrasonics, 2006). The shiny groove that is created at the center of the weld toe is a result of the pins impacting the weld toe (Applied Ultrasonics, 2006). Figure 3.7 shows three weld toes subjected to under-, over-, and proper treatment.

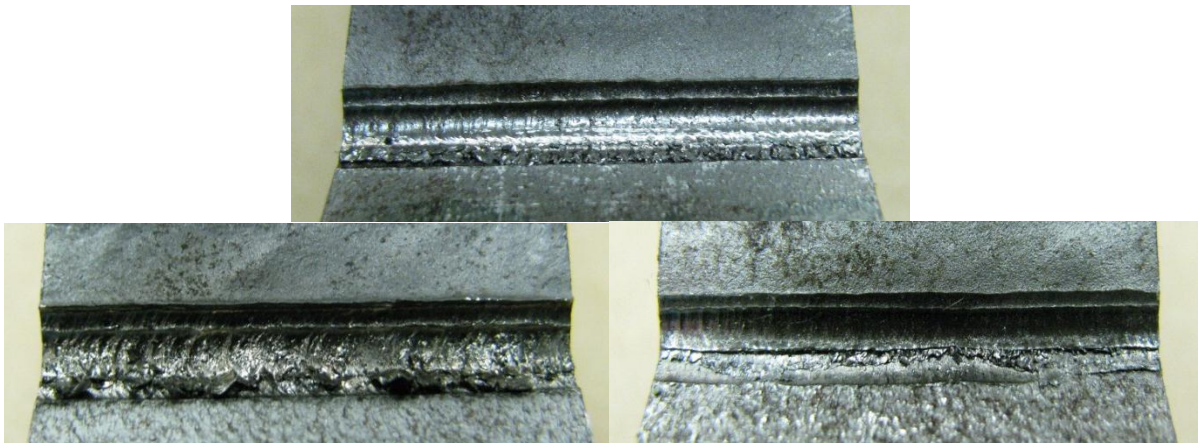

Figure 3.7: Properly treated (Group E, top), over-treated (Group D, left), and under-treated (Group B, right)

The properly treated groove is uniform, smooth, and centred on the weld toe. The over-treated weld toe is rough and flaking. The under-treated weld toe has a visible line at the centre. The width of the groove for the under-treated specimens is less than the diameter of the impact pins (Applied Ultrasonics, 2006).

3.5 Test Matrix

Table 3.3 shows the test matrix used for this experimental program. A limited number of tests were planned due to time and cost constraints. The entire test program for the current study included 42 fatigue specimens divided into seven groups, with six specimens in each group. Each group had different treatment parameters. Treatment timing (before or after pre-cracking) and loading conditions (CA or CA-UL) were also varied, as shown in Table 3.3.

Table 3.3: Test Matrix

					Δσ (Mpa)			
Group	**Treatment**	**Timing**	**Method**	**Loading**	**200**	**225**	**250**	
A	Untreated	N/A	N/A	CA	A1	A2	A3	SPECIMENS
				CA-UL	A4	A5	A6	
B	Under-treated with reduced treatment intensity	Before Cycling	Robotic	CA	B1	B2	B3	
				CA-UL	B4	B5	B6	
C	Under-treated with increased treatment speed	Before Cycling	Robotic	CA	C1	C2	C3	
				CA-UL	C4	C5	C6	
D	Over-treated	Before Cycling	Robotic	CA	D1	D2	D3	
				CA-UL	D4	D5	D6	
E	Properly Treated	Before Cycling	Robotic	CA	E1	E2	E3	
				CA-UL	E4	E5	E6	
F	Properly Treated	Before Cycling	Manual	CA	F1	F2	F3	
				CA-UL	F4	F5	F6	
G	Properly Treated	After cycling to 0.5 mm crack depth	Manual	CA	G1	G2	G3	
				CA-UL	G4	G5	G6	

The specimens were divided in to seven groups from A to G as shown in Table 3.3. Each group has six randomly selected specimens assigned to it. Each specimen is identified by a letter and a number. For example, Group B has six specimens that start from B1 to B6. All of the specimens had their ID number, the type of loading, and the stress range marked on them. Figure 3.8 shows the labelling of Group B.

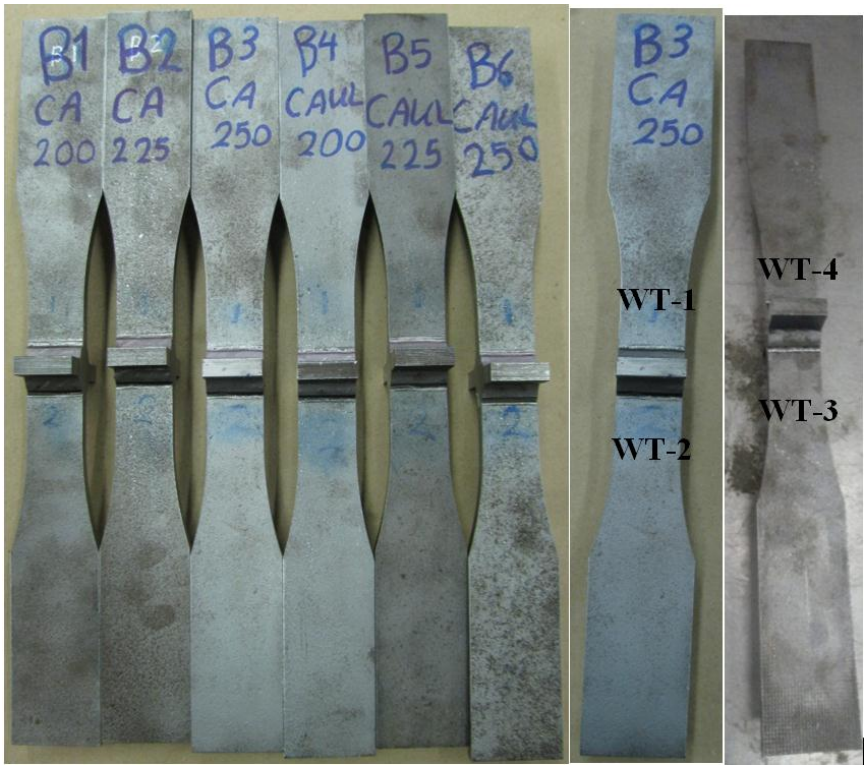

Figure 3.8: Group B specimen (left) and weld toe (right) labelling

The specimens were always inserted in the machine in a way that the side that had the specimen ID marked on it would be on the top right. As shown above, that side was always called WT-1, below that is WT-2, behind WT-2 is WT-3, and above that is WT-4.

Almost all the treatments were applied before the start of the fatigue testing, except for Groups A and G. Group A was not treated at all and was the control group for this study. The Group G specimens were pre-cracked to 0.5 mm and then treated. This was done to observe how the treatment affects already cracked specimens compared to new specimens.

Some specimens were treated manually, so that the effect of robotically versus manually treating the specimens could be determined. All seven groups had the first three specimens tested under CA loading and the last three specimens tested under CA-UL loading. Each group included specimens tested at stress ranges of 200, 225, and 250 MPa.

3.6 Alternating Current Potential Drop Instrumentation

An alternating Current Potential Drop (ACPD) technique was used on all of the specimens (treated and untreated) during the fatigue tests to monitor the crack sizing and crack growth. The theory of ACPD is to produce an alternating current that flows between field probes that are 2 mm apart and then to measure the voltage drop between voltage probes (Costa Borges, 2008). The ACPD system used in this research consisted of a two site ACPD array, TSC ACPD Mk IV instrument, and LIMOS data acquisition software (Lugg, 2008). The LIMOS software shows the crack growth curves and the time when the crack initiated (Lugg, 2008). Each array has four pairs of electrodes where two of them are used for the cross crack measurement (V_c) and the other two are used as reference measurement (V_r) (Lugg, 2008). The V_r and V_c electrode pairs are positioned so that they are 10 mm apart from each other, with 2 mm between electrodes in a pair. Figure 3.9 shows a typical ACPD site array and its dimensions in millimeters (Lugg, 2008). As can be seen in the figure, the ACPD probe has a magnetic field attached to it which allows the probe to simply sit firmly on a ferrous material (Lugg, 2008).

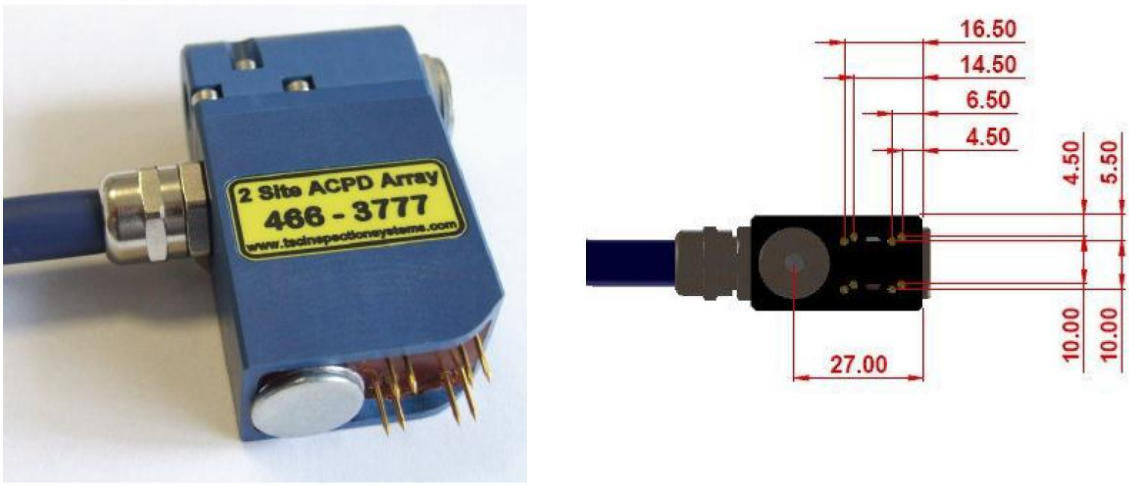

Figure 3.9: ACPD site array and its dimensions (Lugg, 2008)

The voltages from each pair of electrodes (V_r and $V_{c)}$ are used to calculate the depth of the crack. The following equation shows how the crack depth at location i is calculated (Lugg, 2008):

$$di = \frac{\Delta_r}{2}\left(\frac{V_c}{V_r} - \frac{\Delta_c}{\Delta_r}\right) \quad 3.1$$

where di is the crack depth at location i, V_c and V_r are the measured potential difference for the cross-crack and reference probe respectively. Δ_c and Δ_r are the probe spacing for cross-crack and reference probe respectively (Lugg, 2008). The ACPD probes can detect cracks as small as 0.1 mm (Lugg, 2008). The probes measure the surface voltage which is dependent on the current, specimen geometry and the conductivity (Lugg, 2008). Hence, if the spacing and the current are kept constant, the measured voltage difference in only dependent on the metal path between probes (Lugg, 2008).

Before using the ACPD arrays, the specimens were sandblasted to remove mill scale that might interfere with the electrical current. A thin strip of tape was placed on the weld toe before sandblasting to protect it, so that the sand blasting would not influence the test results. Four 2-site ACPD arrays were used for each test. Each ACPD array was connected to a critical weld toe. Figure 3.10 shows the ACPD arrays attached to a fatigue specimen. The ACPD arrays were connected to the TSC ACPD Mk IV data acquisition system and also to a computer to record the data using LIMOS software. The crack depth was recorded every twenty seconds.

Figure 3.10: ACPD probes on the specimen in the machine

Figure 3.11 shows the crack growth curves for a typical specimen, as displayed by the LIMOS software. The data show a straight line at the beginning of the figure and then it starts increasing exponentially until the specimen fractures and then the data smooth out to a straight line again.

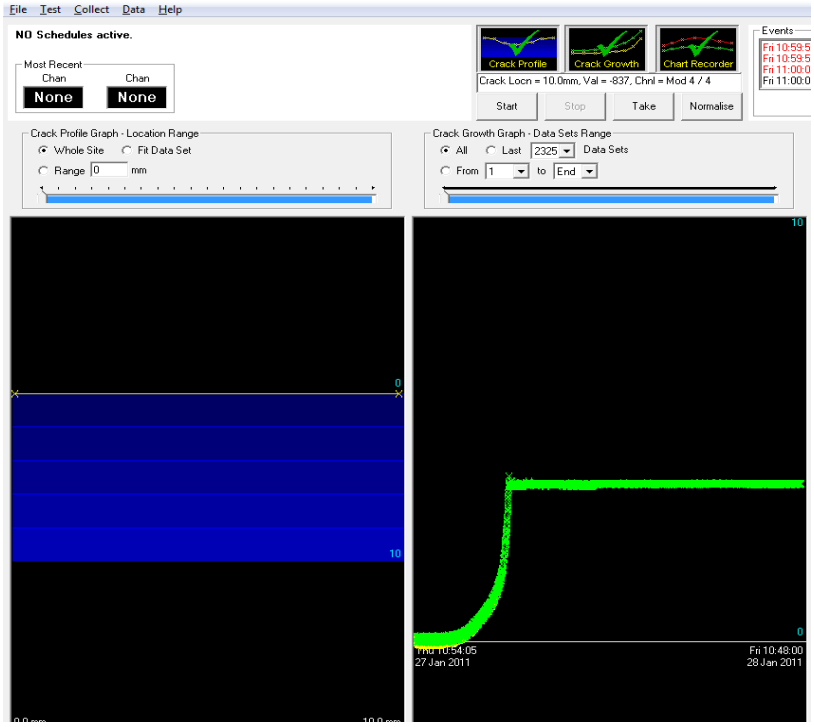

Figure 3.11: Crack growth curves displayed by LIMOS software

3.7 Weld Toe Geometry Measurements

To measure the weld toe geometry, plastic replicas were taken from all four weld toes of each specimen. To obtain the replicas of the weld toes, Extrude® 1 from Kerr Cooperation was used. Extrude® 1 is a vinylpolysiloxane impression material system usually used by dentists to take the impressions of the teeth and is suitable for crowns and bridge impressions. Extrude® 1 has different viscosity levels for different applications which are indicated below:

- Type 3: low consistency – light bodied
- Type 2: medium consistency – medium bodied
- Type 1: high consistency – heavy bodied
- Type 0: very high consistency – putty

The Type 1 viscosity level was used in this research. The complete Extrude® 1 system includes an extruder gun, a cartridge, and a mixing tip (see Figure 3.12).

Figure 3.12: Extrude 1® system components

The cartridge fits into the extruder gun by pulling back the lever at the back of the gun. After that, the mixing tip is attached to the cartridge. By squeezing the trigger on the gun the material starts flowing into the mixing tip. Figure 3.13 shows all the components assembled with some of the impression material flowing in the mixing tip.

Figure 3.13: Extrude1® components assembled

When the impression material is mixed together, it dries in 10 minutes and it can be peeled off easily from the weld toe. Figure 3.14 shows the impression material on the weld toe of a specimen and the side view of it on all four weld toes. Figure 3.17 shows a typical weld toe impression, after it has been peeled off.

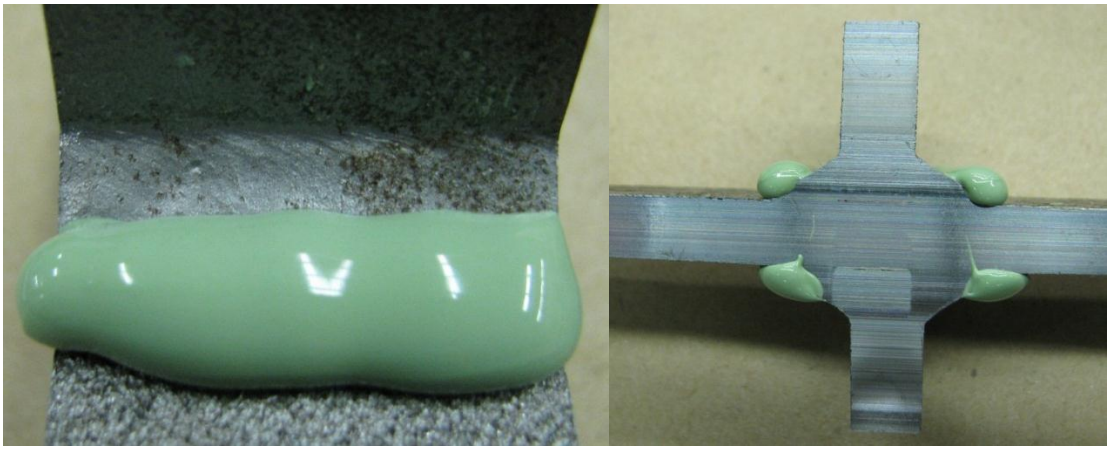

Figure 3.14: Impression on a typical weld toe: top (left) and side view (right)

Figure 3.15: Impression from Specimen C2

The impressions were taken from all four sides of all the specimens. Afterwards, the impression from one weld toe per specimen was randomly chosen, cut, and placed under a low power microscope. Figure 3.16 shows the sliced impressions from Specimen C2. The left image is the impression of the untreated specimen and the right image is the treated impression.

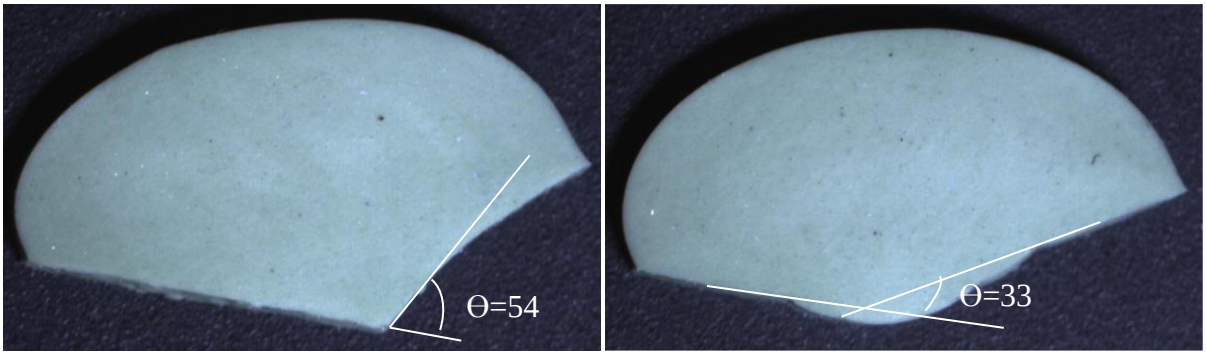

Figure 3.16: Untreated (left) and treated (right) impressions from Specimen C2

As shown in this figure, the differences between these two impressions are that, the treated weld toes have a larger radius than the untreated weld toes and since during treatment the material is pushed away from the weld toe, the measured weld toe angle is larger. The weld toe radius was

measured for the weld toe of the specimens after slicing the impressions and using AutoCAD. Along with the impression measurements, the indent depths were also measured with a weld inspector's pit depth gauge for comparison purposes (see Figure 3.19).

Figure 3.17: Pit depth gauge (G.A.L. Gage Company, 2012)

3.8 Vickers Hardness Test and Microhardness Measurements

Microhardness tests were performed to determine the hardness of the material in the vicinity of the treated weld toe (ASTM E384-10, 2010). The Vickers microhardness test is a type of microhardness measurement that uses a calibrated machine with a diamond indenter of a known geometry. Prior to starting the Vickers test, the desired section was sliced out of the specimen. The specimens were then embedded in a mould using the machine shown in Figure 3.18.

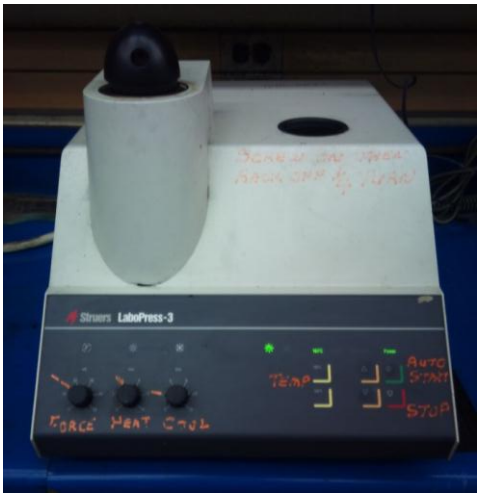

Figure 3.18: Moulding machine

The specimens were then polished using fine grades of emery paper. This process ensured that the surface of the specimen is smooth and defect free and that the indent measurements were accurate (ASTM E384-10, 2010). Figure 3.19 shows a specimen in a mould.

Figure 3.19: Moulded specimen

The specimens were then put in the Vickers microhardness machine where the indentation was applied. According to ASTM E384-10, the specimens should be put in the machine in a way that the surface of the specimens is perpendicular to the axis of the indenter.

Figure 3.20: Vickers microhardness testing machine

A force ranging from 1-1000 grams pushes the diamond indenter into the surface of the material (ASTM E384-10, 2010). For this test it is assumed that after the force is removed, the indentation does not go through elastic recovery and retains the indenter shape (ASTM E384-10,

2010). The Vickers diamond indenter is a "square-based pyramidal-shape" where the face angle is 136° (ASTM E384-10, 2010). The square has two diameters (d_1 & d_2).

Figure 3.21 shows the Vickers indenter with the face angle and the diameter of the square base.

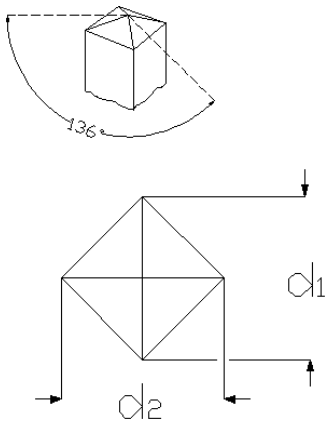

Figure 3.21: Vickers indenter (ASTM E384-10, 2010)

The Vickers indenter creates the same square geometry for different forces applied into the surface of the material (ASTM E384-10, 2010). However the size of the indent decreases as the hardness of the material increases. Microhardness measurements were done for seven specimens (one from each group) to evaluate the effect of UIT on the microstructure of the material at the weld toe. To verify the effective treatment depth, additional weld samples were taken from the specimens to examine the microstructure and perform micro-hardness measurements near the weld surface for each treatment case. ASTM E384-10 procedures were followed for this process. In total seven specimens, one from each group, were chosen for microhardness testing. To be consistent, specimens subjected to the same fatigue loading conditions were tested from each group (CA loading at a stress range of 225 MPa). To measure the size of the indentation, a microscope with a 20X magnification lense was used. Then, as shown in

Figure 3.21, dimensions d_1 and d_2, which are both diagonals of the square indentation, were measured in micrometres. The following equation was then used to calculate the Vickers microhardness.

$$HV = \frac{1854.4F}{d^2} \qquad 3.2$$

where HV is the Vickers Hardness, F is the force applied into the surface in grams, and d is the average of d_1 and d_2. For this test, F was considered to be 200g. The indentations started at the weld toe of the specimen moving 0.1 mm down in the direction of the crack growth. After that, an indentation was perfermed at every 0.2 mm from the previous point (ASTM E384-10, 2010). For all the specimens 11 indentations were made from 0.1 mm at the surface and then every 0.2 mm up to 2.1 mm below the weld toe surface. After the diagonals were measured and HV was calculated, the specimen surface was etched to reveal the microstructure of the treated weld toe. The metal grains and the boundries were revealed by using a 2% Nital solution (ASTM E384-10, 2010). After this, photos were taken using a microscope to record the grains and the grain boundries at the weld toe.

3.9 Residual Stress Measurements

In order to characterize the residual stresses that were created by the treatment, the laser X-ray diffraction (LXRD) method was used. LXRD techniques have been used since 1925 (Pineault et al., 2002). X-ray diffraction is used to measure the residual stress because this method is quantitative and only x-ray diffraction can illustrate the residual stress distribution at different points. This characteristic of the x-ray is due to having high spatial and volumetric resolution. It can also measure the surface and the sub-surface stresses (Proto. Manufacturing Ltd., 2011). This technique can only measure the residual stress in materials with a grain structure. The measured objects can be extremely small or extremely large (Pineault et al., 2002).

In order to measure the residual stress in the subsurface, removing material from the surface is required and can be done by electro-polishing techniques. After successive LXRD measurements and electro-polishing steps, a stress versus depth graph can be plotted based on the measurements (Pineault et al., 2002). LXRD measurement should concentrate on the location of the failure or first cracking area (Pineault et al., 2002). Since the residual stress is released in the direction normal to the cracks, LXRD should evaluate the residual stress in the highest stressed areas before the first crack generated (Pineault et al., 2002).

In X-ray diffraction residual stress measurement, d-spacing is the variable used to measure the distance between crystallographic planes (Pineault et al., 2002). The D-spacing variable will increase or decrease in the direction of stress as the tension stress or compression stress in the material increases or decreases, respectively. The detector in the x-ray measurement equipment

can measure the shift in the XRD peak angular position that is produced if a residual stress is present in the material. Equation 3.3 is used to calculate the d-spacing according to Bragg's law. In Equation 3.3, λ is the x-ray wavelength, n approaches unity and θ is the diffraction angle:

$$n\lambda = 2dsin\theta \tag{3.3}$$

Equation 3.4 gives the strain experienced in the material (Pineault et al., 2002). In Equation 3.4, d_0 is the d-spacing measured in the unstressed condition. d is the d-spacing measured in the stressed condition:

$$\varepsilon = (\mathrm{d} - d_0)/d_0 \tag{3.4}$$

In plane-stress models, the unstressed distance d_0 has to be as accurate to approximately 0.01%, since a 0.1% inaccuracy in d_0 can result in a large error in the stress measurement results (Pineault et al., 2002). In an isotropic, homogeneous, fine-grain material, the $\sin^2\psi$ method, derived from Hooke's law, can also be used to measure the stress in the materials (Pineault et al., 2002). The method employs Equation 3.5:

$$\begin{aligned}\varepsilon_{\phi\psi} = \frac{1}{2}S_2(\sigma_{11}\cos^2\theta + \sigma_{12}\sin 2\phi + \sigma_{22}\sin^2\theta - \sigma_{33})\sin^2\psi - S_1(\sigma_{11}+\sigma_{22}+\sigma_{33}) \\ -S_1(\sigma_{11}+\sigma_{22}+\sigma_{33}) + \frac{1}{2}S_2(\sigma_{13}cos\phi + \sigma_{23}sin\phi)sin2\psi + \frac{1}{2}S_2\sigma_{33}\end{aligned} \tag{3.5}$$

In Equation 3.5, $1/2S_2$ and S_1 are the x-ray elastic constants of the materials. σ_{ij} are the stress tensor components. ϕ is the angle of the direction of strain measurement. ψ is the angle between the bisector of the incident and diffracted component. $\varepsilon_{\psi\theta}$ is the strain in the $\psi\theta$ orientation. Figure 3.22 defined the angles needed in the x-ray diffraction measurements.

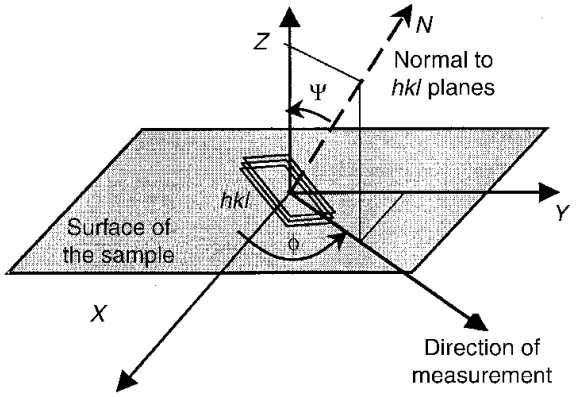

Figure 3.22: Definition of the reference axes and the direction of measurement in XRD residual stress analysis (Pineault et al., 2002)

σ_{ij} can be measured by the D-spacing versus $\sin^2\psi$ graphs and evaluated using different mathematical models and measurement approaches (Pineault et al., 2002).

For the current study, Proto Manufacturing Ltd. was engaged to perform residual stress measurements on six of the fatigue specimens, after they were tested to failure. The measurements were taken on specimens after fatigue testing. The selected specimens were A1, B1, C1, D1, E4 and F1. The weld toe of Specimen E1 was damaged after fracture in the fatigue testing machine. For this reason Specimen E1 was replaced with Specimen E4 because they were both tested at the same equivalent stress level. With the exception of Specimen E4, all of the specimens were tested under CA loading at a stress range of 200 MPa. For this research, one of the stiffeners was removed during this process to provide enough space to perform the measurements. Figure 3.23 shows the specimen with the stiffener removed and the measurement process started.

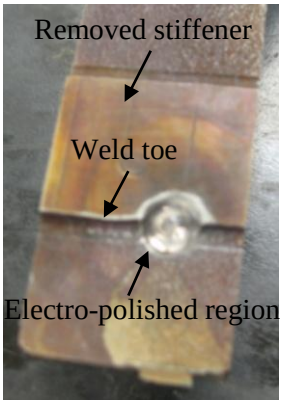

Figure 3.23: Sliced specimen ready for residual stress measurements

Figure 3.24 shows the electrolytic polisher that was used to remove the material from the metal.

Figure 3.24: Electrolytic polisher

Residual stresses were measured at depths of 0 mm, 0.15 mm, 0.3 mm, 0.6 mm, and 1.2 mm below the weld toe surface. Each specimen was electro-polished to the desired depth where the measurements were taken and this process was repeated for all depths. Figure 3.25 shows an LXRD system.

Figure 3.25: LXRD residual stress measurement System (Proto. Manufacturing Ltd., 2011)

The LXRD system has two detectors for stress measurements. They cover both sides of the diffraction cone, doubling the amount of data that can be obtained in a given time. Figure 3.26 shows a specimen in the LXRD system ready to perform a residual stress measurement.

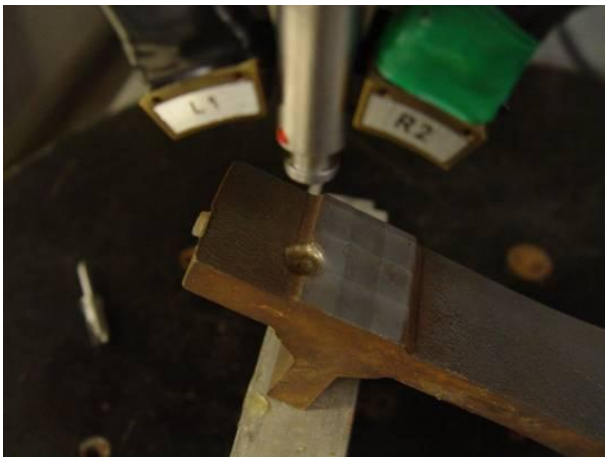

Figure 3.26: A specimen in the LXRD system for residual stress measurement

4 Experimental Results

4.1 Introduction

In this chapter, experimental results are presented in Section 4.2. Fatigue life increase factors are calculated for each group, specimen loading, and treatment case. Also, S-N curves are plotted and used to explain how the different treatment cases and loading conditions affected the results. Section 4.3 presents the results of the crack growth measurements. Section 4.4 presents the weld toe geometry measurements. Section 4.5 presents the microhardness measurements and microstructure images taken from specimens sectioned after fatigue testing. Section 4.6 presents the residual stress measurements.

4.2 S-N Plots and Loading Histograms

As mentioned in Section 2.3 , S-N curves were used to help understand the fatigue behaviour of structural components. Table 4.1 and Table 4.2 show the number of cycles to failure for each tested specimen. The specimens that are in bold are run-outs and did not fail.

Table 4.1: Fatigue lives of Group A, B, C, and D

Specimen ID	**N_f**	**Specimen ID**	**N_f**	**Specimen ID**	**N_f**	**Specimen ID**	**N_f**
A1	248,383	B1	2,099,320	C1	1,537,837	D1	3,436,785
A2	166,821	B2	3,510,188	**C2**	**8,210,202**	D2	1,932,685
A3	105,487	B3	1,773,851	C3	3,031,499	D3	450,647
A4	202,874	**B4**	**3,667,264**	**C4**	**3,564,413**	D4	2,649,012
A5	185,887	B5	4,159,128	**C5**	**4,796,216**	D5	876,309
A6	94,746	B6	816,298	C6	460,835	D6	485,965

Table 4.2: Fatigue lives of Group E, F, and G

Specimen ID	N_f	Specimen ID	N_f	Specimen ID	N_f
E1	3,021,835	**F1**	**7,692,074**	**G1**	**5,598,137**
E2	2,244,137	F2	4,207,209	**G2**	**5,600,000**
E3	2,753,812	F3	1,175,500	G3	2,143,443
E4	**8,873,089**	**F4**	**3,141,363**	G4	397,261
E5	2,064,805	F5	1,938,919	G5	357,136
E6	533,901	F6	561,878	G6	1,495,138

Table 4.3 shows the fatigue life increase factor (treated life / untreated life) of each specimen compared to Group A of the same loading and stress level. The last row in this table shows the average fatigue life increase factor increase for each group.

Table 4.3: Fatigue life increase factor of specimens compared to Group A

Group / Specimen	B	C	D	E	F	G
Specimen 1-CA-200	8.5	6.2	13.8	12.2	>20.1	>20.1
Specimen 2-CA-225	21.0	>30.0	11.6	13.5	25.2	>30.0
Specimen 3-CA-250	17.0	28.7	4.3	26.1	11.1	20.3
Specimen 4-CA-UL-200	>24.6	24.6	13.1	>24.6	>24.6	2.0
Specimen 5-CA-UL-225	22.4	>26.9	4.7	11.1	10.4	1.9
Specimen 6-CA-UL-250	8.6	4.9	5.1	5.6	5.9	15.8
Average:	17	20.2	8.8	15.5	16.3	15.0

Each row shows the increased fatigue life factor for the same loading and stress range but different treatments. The maximum and minimum for each row are shown by underlining or highlighting the factor respectively. It can be seen that Group D (over-treated) has the lowest fatigue life factor and Group B has the highest one. The other groups range from 16-19. As seen in this table, even under-treating the specimens, increases the fatigue life. Note that Section 5.2 presents a more in-depth statistical analysis of these results.

S-N data for all of the specimen groups are presented in the following series of graphs. For all of the graphs, the untreated specimens under CA loading and CA-UL are shown with black and grey hollow symbols respectively. The treated specimens under CA loading and CA-UL are shown with filled black and grey symbols respectively. Figure 4.1 shows the S-N data for Group A and Group F.

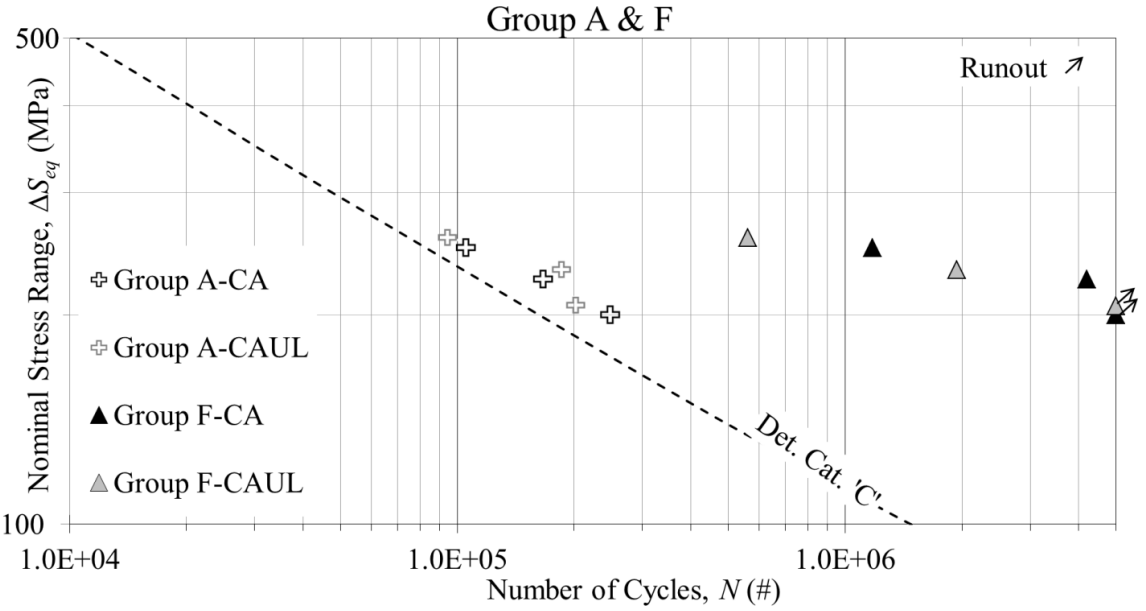

Figure 4.1: S-N curve Group A & F

Because the specimen geometry falls under Detail Category ‘C’, the design curve for this category is also shown in this figure. The Detail Category ‘C’ design curve corresponds to 97.7% survival probability (AASHTO 2008). It can be observed that all of the data points are above this curve. This figure shows a comparison of untreated specimens and properly treated specimens. As illustrated in this figure, the fatigue lives of the untreated specimens are closer to the Detail Category ‘C’ line whereas, the fatigue lives of the Group F specimens are shifted to the right and

hence there is an improvement in fatigue performance as a result of the treatment. Group F had two run-outs that are shown with an arrow on top of the symbol. The improvement in the fatigue lives of all the specimens in Group F is high. The worst case is CA-UL loading with a stress range of 250 MPa. According to Table 4.3, the fatigue lives of specimens in Group F were improved by a factor of 14.7 on average. Figure 4.2 presents the S-N data for Group A, E and F. The difference between this figure and the previous one is that Group E data, which are properly treated using a robot, are included. As seen in this figure, the results from Group E and F fall on top of each other, which mean there is not much difference between the data of these groups.

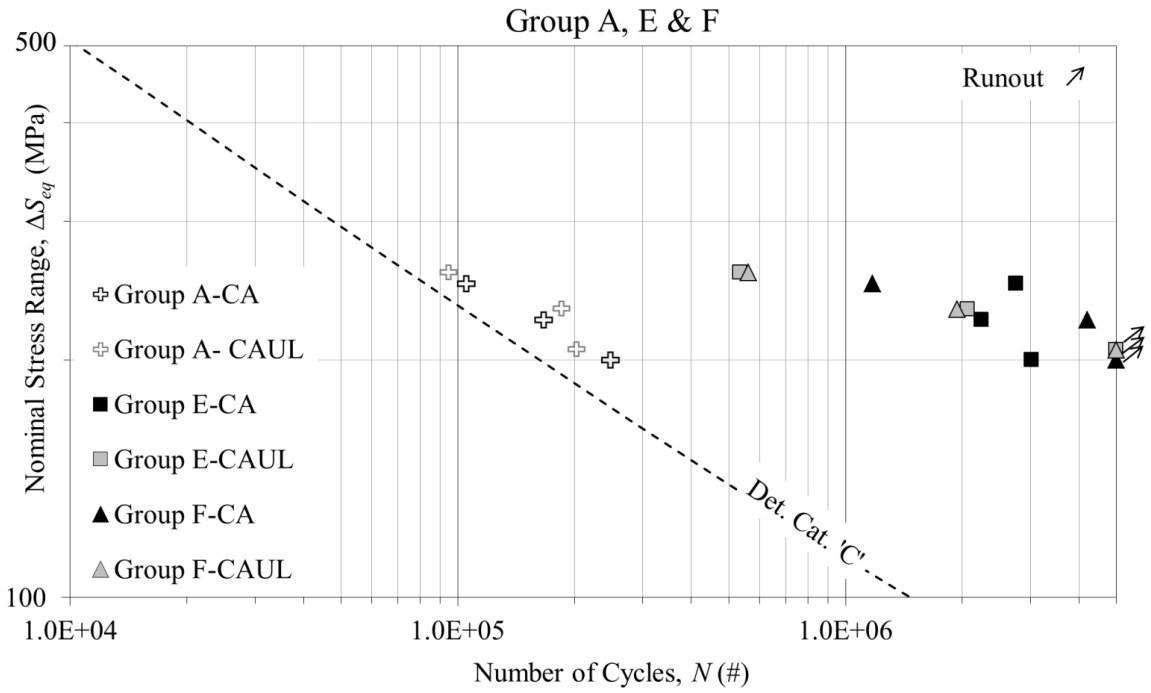

Figure 4.2: S-N curve Group A, E & F

The fatigue lives for Group E have improved by a factor of 15.5 compared to Group A. Hence, both treatment cases result in a similar performance and increase in fatigue life. Figure 4.3 shows the S-N data for Group A, F and G. Specimens in Group G were properly treated (manually) after pre-cracked to 0.5 mm.

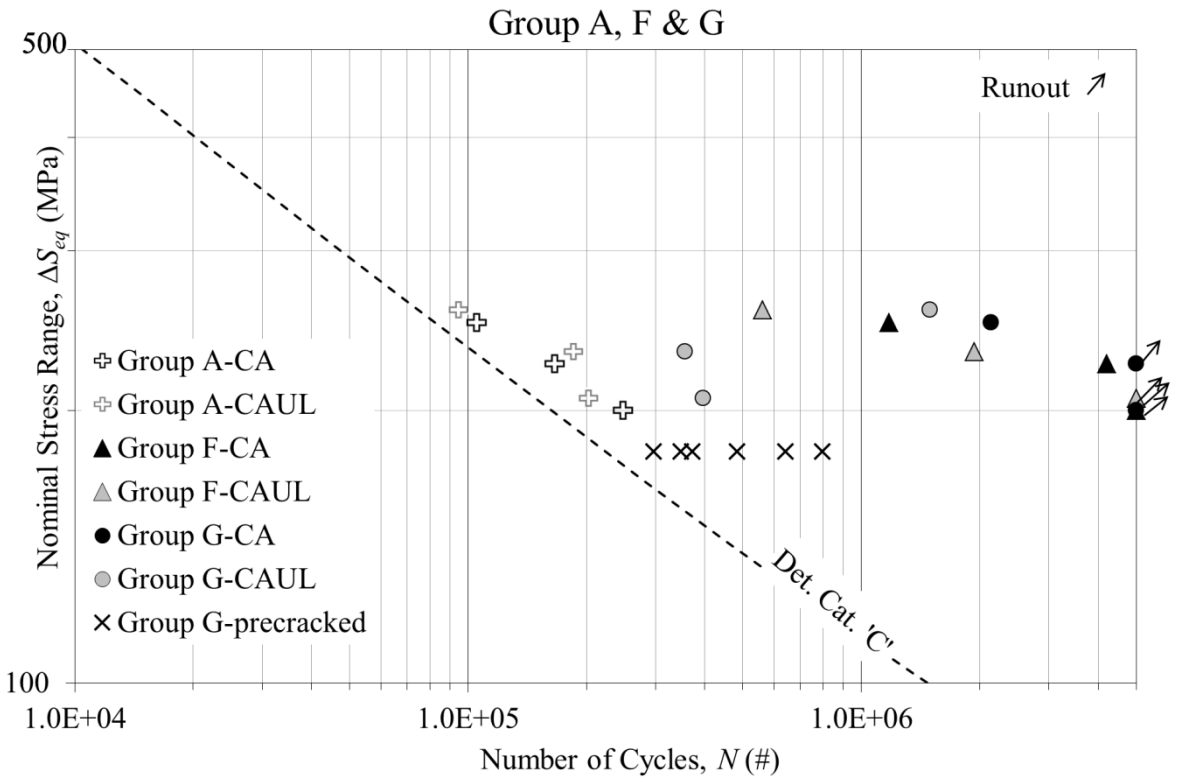

Figure 4.3: S-N curve Group A, F & G

Since Group G was pre-cracked, and then was treated and fatigue tested, it is shown separately in the figure at a stress range of 180 MPa. Group G had 2 run-outs, two specimens that had unexpectedly short lives and the other two specimen results fall on top of the Group F data. On average, the fatigue improvement factor of Group G (15.0) is very close to the one from Group E and F. However, the individual fatigue results show that the fatigue life increase for Group G is less reliable (i.e. there is more scatter in the results). This highlights the importance of detecting and removing existing cracks before applying UIT to structures such as bridges that have been in service for some time.

Figure 4.4 shows the S-N data for Groups A, B, C, D and F. This figure demonstrates how under-treating and over-treating the specimens affect their fatigue performance. Group B and Group C have one and three run-outs respectively. Group B and Group C have fatigue life increase factors of 16 and 19 respectively. The Group C data is more spread out compared to Group B.

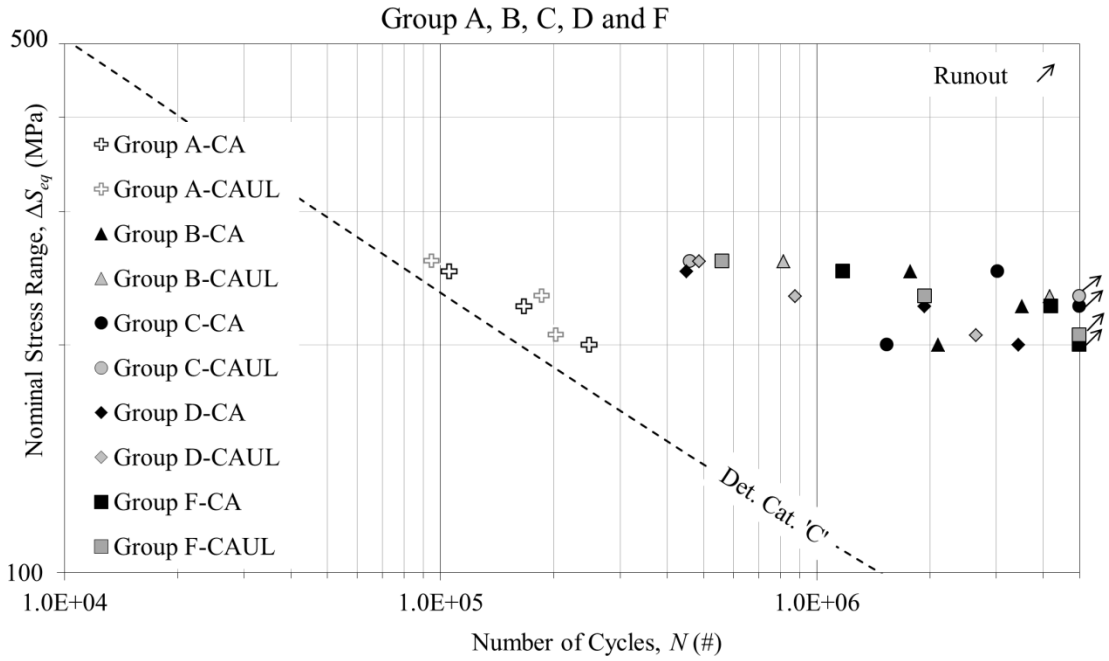

Figure 4.4: S-N curve Group A, B, C, D & F

The fatigue life increase factor for Group D (the robotically over-treated specimens) is only 8.8 on average, which is much lower than the other treatment cases.

In general, it can be seen that the fatigue lives of the treated specimens were slightly lower under CA-UL loading than under CA loading. It must be noted that except for Group D (the robotically over-treated specimens); all of the treated groups had at least one run-out. However, none of these run-outs were at a stress range of 250 MPa. UIT resulted in a substantial fatigue life increase. Even under-treating resulted in a significant fatigue life increase on average.

In the following series of figures, histograms of specimen ranking in terms of fatigue performance are plotted. Figure 4.5 shows the histogram for the CA loaded specimens.

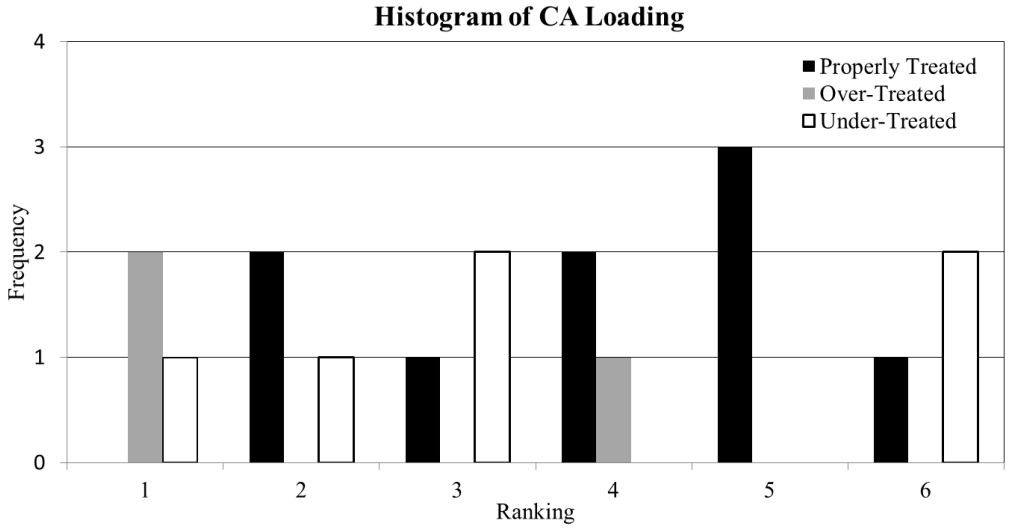

Figure 4.5: Histogram of CA Loading

The horizontal axis in this figure shows a ranking from one to six. One is considered the worst ranking which means the data point from that treatment category failed first, whereas, ranking 6 shows that the data point was the furthest from the detail category 'C' curve. The vertical axis shows the frequency. Properly treated specimens show up a maximum of three times in category 5. Properly treated specimens do not show up in ranking one. The under-treated specimens which are from Group B and C combined show up in almost all the rankings. However, over-treated specimens with CA loading do not even make it to the fifth or sixth ranking. Figure 4.6 shows a similar histogram for CA-UL loading.

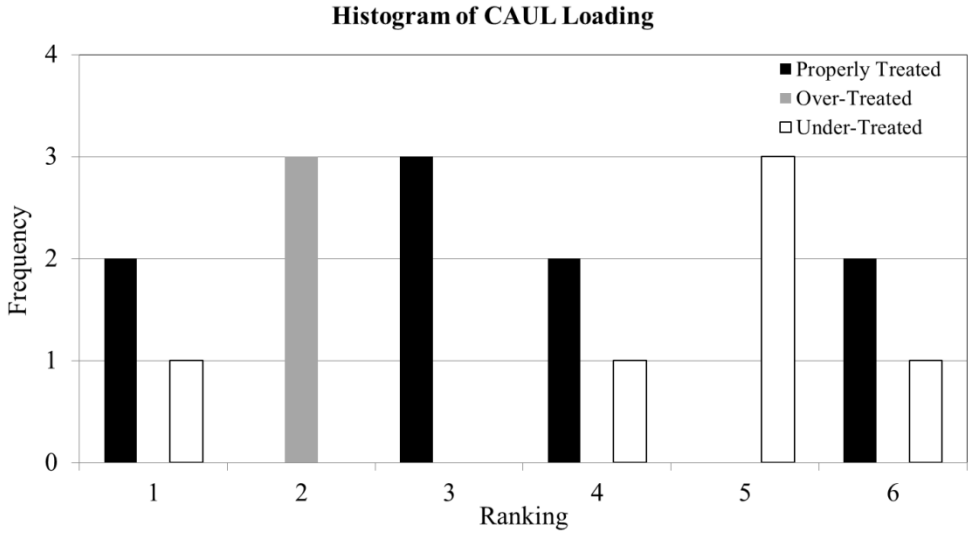

Figure 4.6: Histogram of CA-UL loading

Compared to Figure 4.5 where the various treatment cases are spread throughout the rankings, in this case, the grouping of the various treatment categories is much more evident. For example, ranking two, three, and five only have over-treated, properly treated, and under-treated specimens respectively. Properly treated specimens show up in all the rankings except two whereas, under-treated specimens show up in ranking one and then in the last three categories.

Figure 4.7 shows the histograms of CA and CA-UL loading combined.

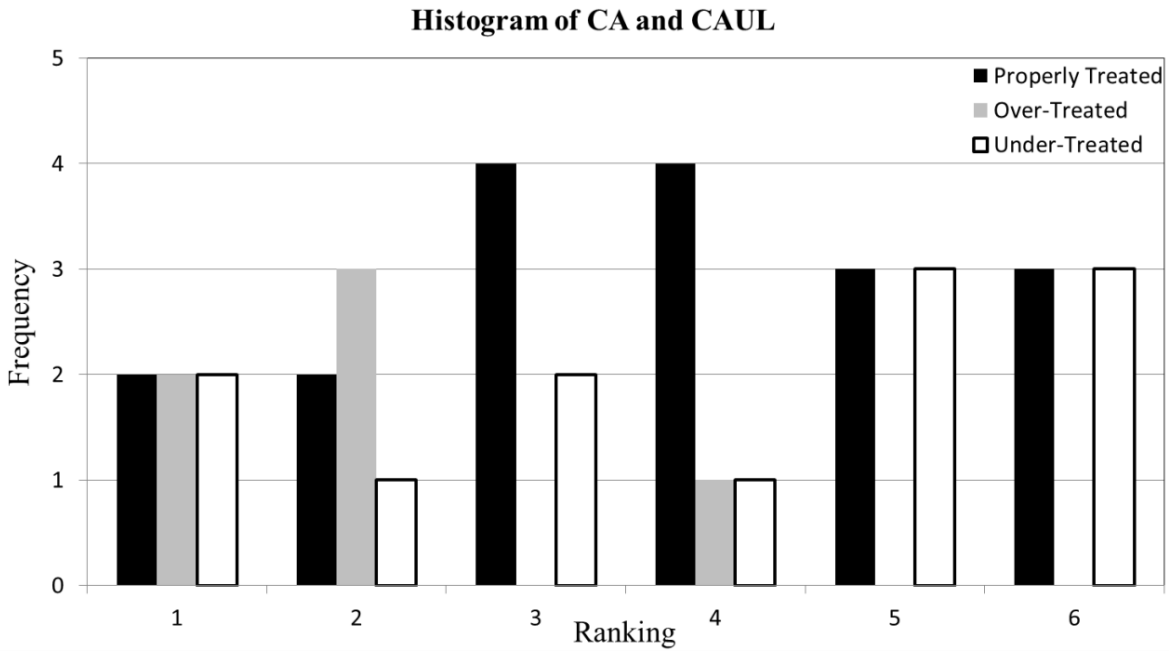

Figure 4.7: Histogram of CA and CA-UL loading

This figure gives an overall view of how the treated specimens are distributed. For example, the over-treated specimens fall on the left side of the histogram, whereas the properly and under-treated specimens appear to the right side. These results suggest that the over-treated specimens are not performing as well as under- and properly treated specimens.

It is difficult to draw strong conclusions about the effects of treatment quality on fatigue performance from the comparison of the average fatigue life increase factors and rankings presented in this section. For this reason, a statistical analysis of the S-N results is presented in Chapter 5, which makes it easier to compare the results of tests conducted under different loading conditions and to draw stronger conclusions about the effects of treatment quality on fatigue performance.

4.3 Crack Growth Observations

As mentioned in Section 3.6, the ACPD method was used to monitor the crack growth in all of the fatigue tests. Measurements were made at two locations on each of the four weld toes or at eight locations for each specimen using the TSC ACPD system and magnetic probes. Most of the ACPD data had considerable noise, which made it hard to compare the crack growth data of one specimen with another at the same level of loading. The results for CA-UL loading with 250 MPa stress range are shown here for illustration purposes. Figure 4.8 shows crack growth curves for Specimens A6 and F6.

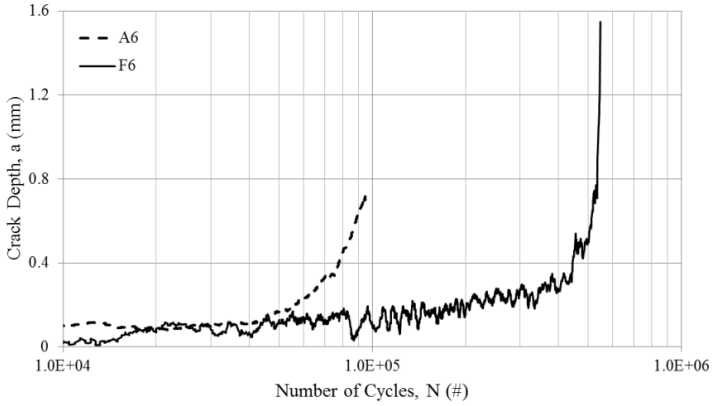

Figure 4.8: Crack growth curves for Specimens A6 and F6

Specimen A6 was untreated and hence had a much shorter life compared to the properly treated Specimen F6. Also, the crack in A6 has started propagating at an earlier stage compared to F6. All specimens were fatigue tested until they fractured. The fracture surfaces for Specimens A6 and F6 are shown in Figure 4.9. The top and bottom pictures in this figure represent both pieces of the same fractured specimen.

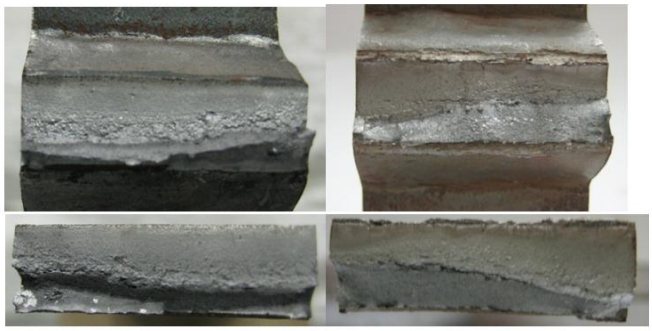

Figure 4.9: Fractured surface of Specimen A6 (left) & Specimen F6 (right)

Figure 4.10 shows similar crack growth results for the under-treated Specimens B6 and C6, and over-treated Specimen D6, each tested under CA-UL loading at 250 MPa.

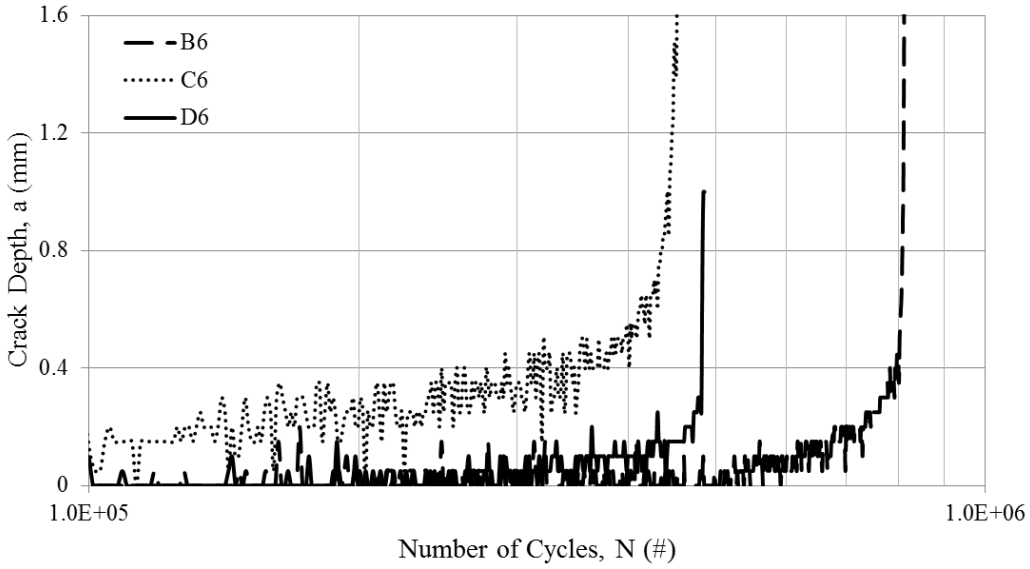

Figure 4.10: Crack growth curves of specimens B6, C6 and D6

As shown in this figure, Specimen C6 has a much shorter fatigue life than B6. This suggests that increasing the treatment speed results in a greater reduction in fatigue performance than reducing the treatment intensity. The crack growth curve for Specimen D6 falls between the other two. Figure 4.11 shows the fractured surfaces for Specimens B6, C6, and D6.

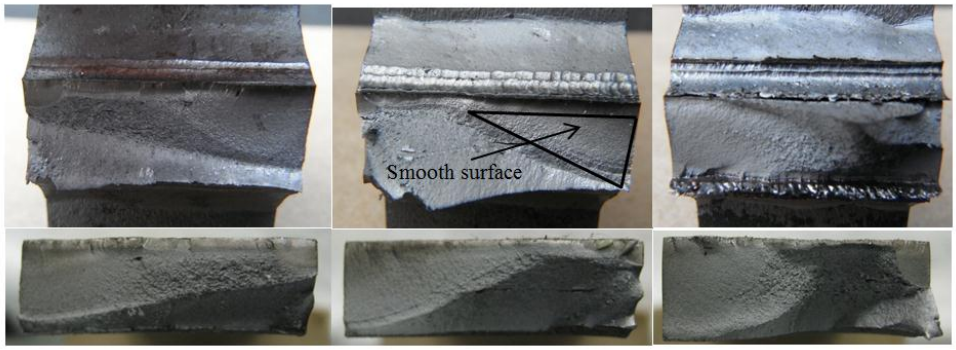

Figure 4.11: Fractured surface of untreated specimen B6 (left), C6 (middle) & D6 (right)

There are two stages to the fracture, which are apparent in this figure: fatigue crack growth, followed by ductile fracture. For example, Specimen C6 in this figure has a smooth surface on the top right triangular part due to fatigue crack growth. The remainder of the fracture surface, which is rough and highly deformed, corresponds with the subsequent ductile fracture. The

treated specimens broke at an angle of roughly 45° with respect to the load direction. Figure 4.12 shows fractured Specimens E2 and E3, tested under CA loading at 225 and 250 MPa.

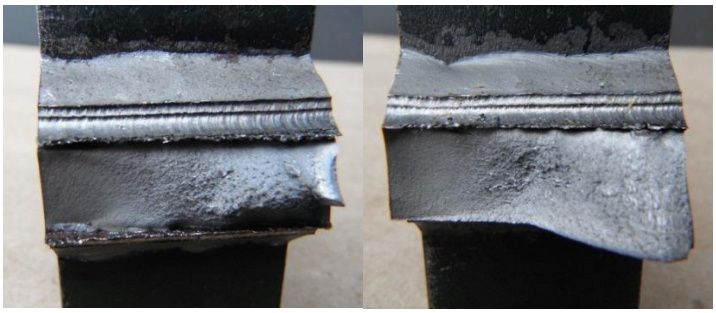

Figure 4.12: Fractured surface of specimen E2 (left) and E3 (right) at different loadings

As shown in this figure, Specimen E3 has a larger inclined ductile area than Specimen E2. In general, it can be seen in these fracture surfaces and those of the other test specimens that as the stress level increases, so does the area of the ductile fracture surface.

4.4 Weld Toe Geometry Measurements

To obtain the potential geometric parameters for quality control, weld toe geometry measurements such as the weld toe angle and radius before and after UIT application were obtained for each specimen. The sliced silicon impressions of the weld toe were placed under a microscope, and photographed. AutoCAD 2012 was then used to obtain measurements of the geometric parameters. Figure 4.13 shows impressions of the untreated and treaded weld toe WT-2 of Specimen B1 (reduced treatment intensity, CA loading at 200 MPa).

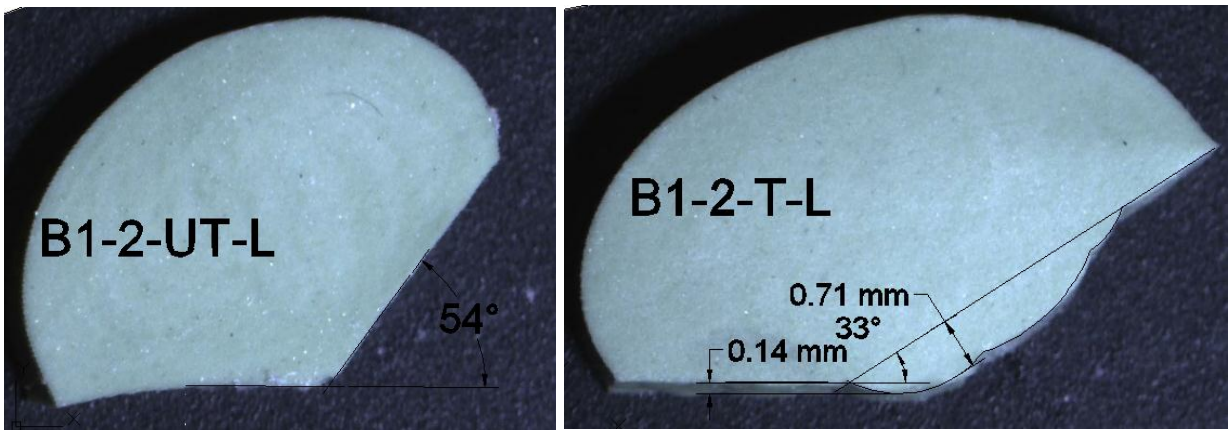

Figure 4.13: Untreated (left) and treated (right) Specimen B1 weld toe measurements

In this figure, the ‘B1-2-UT-L’ label indicates that the specimen ID and weld toe number are B1 and 2 respectively. UT means that the specimen was untreated and ‘L’ indicates the location of the base metal surface, which is on the left side. The weld toe angle for the untreated specimen was measured easily between the base line and the weld metal. Measuring this angle for the treated cases presented more of a challenge, in particular for the robotically treated specimens. The reason is that the tool was directed at the weld than the base metal and multiple grooves resulted due to the multiple treatment passes at various degrees. During the treatment, the force exerted on the tool pushes away the material at the weld toe and hence the local angle for the treated specimens changes. As shown in Figure 4.13, the untreated angle is 54° and the angle for the treated specimen is 33°. Due to flaking and multiple passes of the needles of the tool, most of the weld toes have multiple grooves, which result in multiple radii and indent depths.

The figure above demonstrates two ways of measuring indent depth. Usually indent depth measured by weld inspectors is the maximum perpendicular distance measured from a line following the surface of the base metal. For B1 this indent depth is 0.14 mm; however, measuring the indent depth from the weld metal side gives a higher depth of 0.71 mm. The reason is that the tool was directed more at the weld than the base metal. The untreated and treated angles were measured for 36 specimens and the results are shown in Table 4.4.

Table 4.4: Statistical results of local weld toe angle measurements

		Maximum angle	Minimum angle	Average	Standard Deviation
Weld toe angle (°)	Untreated	80	38	55.36	10.02
	Treated	60	28	38.06	7.21

The average weld toe angle for untreated and treated specimens are 55.36° and 38.06° respectively. The untreated specimens have a higher standard deviation than the treated specimens, which means that the measurements for treated specimens have less scatter. Figure 4.14 and Figure 4.15 show the distribution of untreated and treated weld toes respectively.

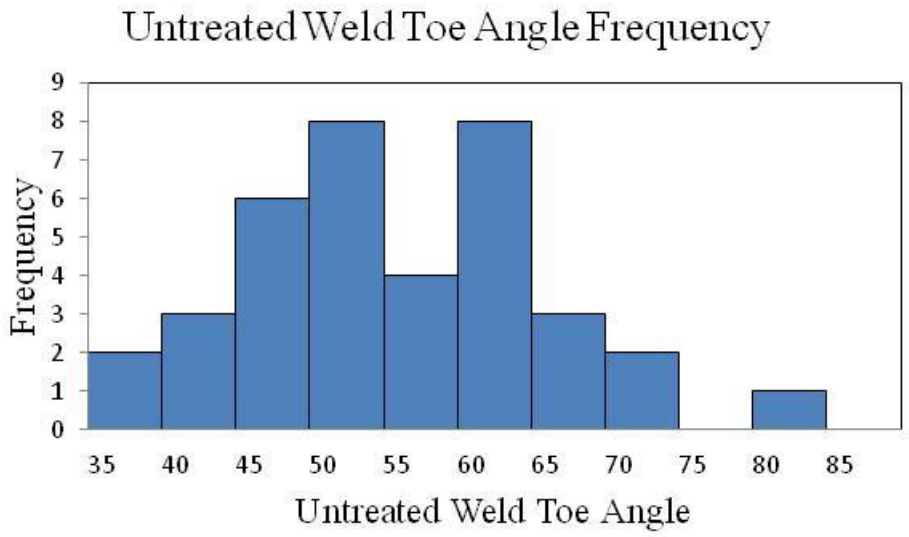

Figure 4.14: Distribution of untreated weld toe angles

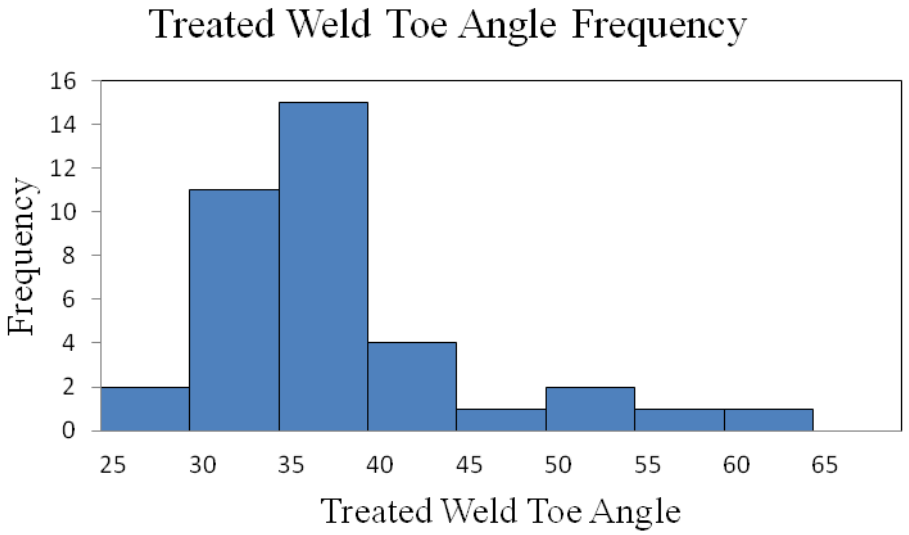

Figure 4.15: Distribution of treated weld toe angles

It can be seen from the histogram that the highest frequencies of angles are between 45-65° for the untreated weld toes. However, the distribution for the treated weld toe angles varies mostly from 30-40° with much less scatter compared to the distribution of untreated weld toe angle. In general, the treatment has flattened the weld toe angles by 17°.

The radii for the specimens were measured and are presented in Table 4.5. With the exception of the properly treated weld toes, it was very challenging to define a circle and measure the radius due to the rough shape of the weld toe. The radius corresponding with the greatest indent depth

on the base metal side was considered to be the most important one, because it corresponds with the normal location of crack initiation. Radii smaller than 0.1 mm were not measured.

Table 4.5: Statistical data for radius measurement of treated specimens

Radius Measurement			
Specimen ID	**Average radius (mm)**	**Standard Deviation**	**Maximum radius (mm)**
Group B	1.76	0.36	2.17
Group C	2.09	0.18	2.35
Group D	1.17	1.09	2.81
Group E	1.69	0.27	2.07
Group F	2.37	0.11	2.52
Group G	2.55	1.22	5.00

Most of the robotically treated specimens had multiple indents which created multiple arches with different radii measurements. Figure 4.16 shows Specimen B1 with multiple radii measurements.

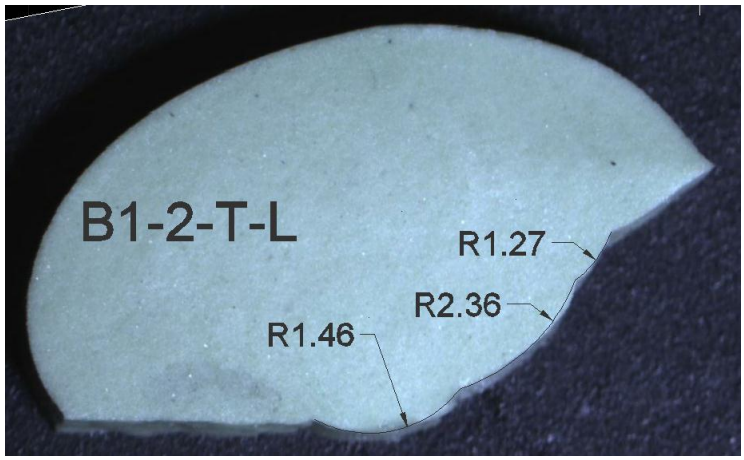

Figure 4.16: Specimen B1 radii measurements

Most of the groups have a high standard deviation. However, the maximum radius is approximately the same for all of them except the radius for Group G. Based on the statistical data shown in the table, it is concluded that the radius measurements are not a good geometric property to be taken into account for quality control of treated welds. Most of the robotically treated specimens had two indent depths. One was measured perpendicular from the base metal

and the other one which happened to be the larger indent depth was from the weld metal. Table 4.6 shows the indent depth from the weld and base metal.

Table 4.6: Indent depth from the weld metal and the base metal

Specimen ID	Indent depth from the weld toe (mm)	Indent depth from the base metal (mm)
B1-2	0.71	0.14
B2-3	0.63	0.18
B3-3	0.46	0.19
B4-1	0.79	0.18
B5-2	0.47	0.09
B6-1	0	0.15
C1-4	0.61	0.22
C2-3	0.38	0.22
C3-1	0.19	0.19
C4-2	0.31	0.16
C5-1	0.23	0.11
C6-3	0.49	0.07
D1-4	1.02	0.39
D2-2	1.30	0.20
D3-3	0.96	0.26
D4-1	1.20	0
D5-4	0.69	0.14
D6-1	1.43	0
E1-1	0.69	0.2
E2-1	0.61	0.03
E3-3	0.81	0.13
E4-1	0.00	1.1
E5-4	0.13	0.52
E6-3	0.92	0.17
F1-1	0.14	0.33
F2-4	0.20	0.2
F3-2	0.51	0.22
F4-4	0.17	0.37
F5-4	0.18	0.2
F6-1	0.32	0.27
G1-1	0.38	0.11
G2-2	0.45	0.17
G3-2	0.38	0.16
G4-1	0.37	0.32
G5-4	0.18	0.23
G6-2	0.36	0.29

Table 4.4 and Table 4.7 present the data for the base metal and weld metal indent depths respectively. Each table shows the average indent depth, standard deviation and the maximum indent depth of each treated group.

Table 4.7: Summarized base metal indent depth data

Base metal			
Specimen ID	**Average indent depth (mm)**	**Standard Deviation**	**Maximum indent depth (mm)**
Group B	0.16	0.04	0.19
Group C	0.16	0.06	0.22
Group D	0.17	0.15	0.39
Group E	0.36	0.40	1.10
Group F	0.27	0.07	0.37
Group G	0.21	0.08	0.32

Table 4.8: Summarized weld metal indent depth data

Weld metal			
Specimen ID	**Average indent depth (mm)**	**Standard Deviation**	**Maximum indent depth (mm)**
Group B	0.51	0.28	0.79
Group C	0.37	0.16	0.61
Group D	1.10	0.27	1.43
Group E	0.53	0.38	0.92
Group F	0.25	0.14	0.51
Group G	0.35	0.09	0.45

For the base metal indent depths, Group E has the highest standard deviation which shows a higher scatter compared to the rest of the groups. This high standard deviation corresponds to the maximum indent depth of 1.1 mm for Group E. The under-treated groups have an average indent depth of 0.16 mm. Since the results for the radii are very variable, radius measurements are not going to be used a quality control parameter.

4.5 Microhardness Results

The objective of the microhardness tests was to obtain the local material hardness properties at the weld toe of the as-received and treated specimens. This section presents the results of the microhardness measurements for Specimens A1 to G1. For all of the specimens, eleven indentations were made along the expected crack path. The indentations were done in the direction of the crack growth, which is shown in Figure 4.17.

Figure 4.17: Location and direction of microhardness measurements

These indentations started from 0.1 mm below the surface and then every 0.2 mm up to a depth of 2.1 mm. Each measurement set was repeated in three trials for each specimen. When the indents were placed under the microscope for diameter measurement, pictures were taken of each indent on the metal surface. Figure 4.18 shows all eleven indents for Specimen B2 with a 5X magnification zoom and the first four indents magnified by a 10X magnification zoom.

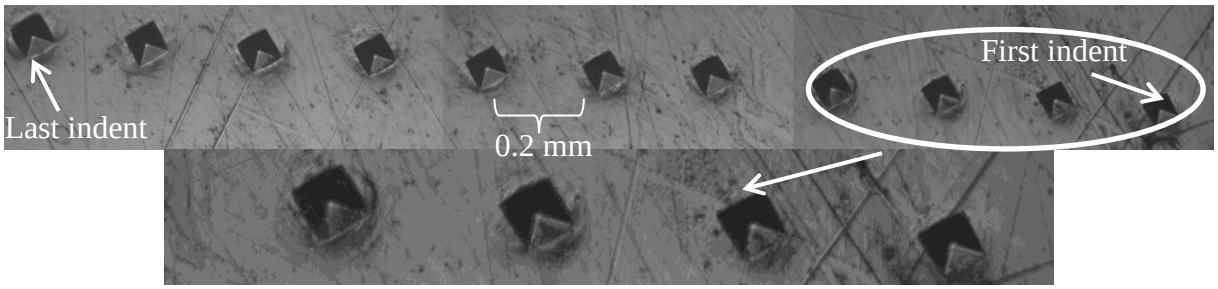

Figure 4.18: Indents of specimen B2

As shown in the bottom picture in Figure 4.18, the indents tend to get larger as their distance below the surface increases. Using a 20X magnification zoom, the diameters of each indent was measured. Figure 4.19 below shows two indents from Specimen B2 at depths 0.1 and 2.1 mm respectively. The diameter measurements from the first trial are shown in the figures.

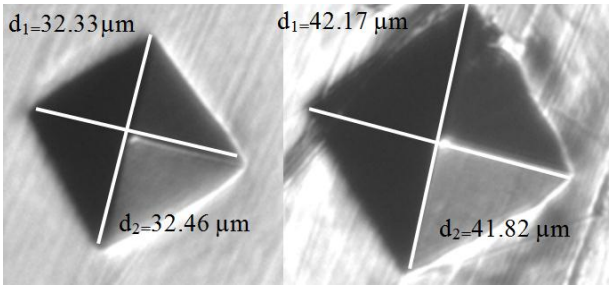

Figure 4.19: First location (left) and last location (right) of B2 Vickers indents

As seen in this figure, the indent at depth 0.1 mm has smaller diameter measurements than the indent at 2.1 mm. The larger the diameter, the lower the HV number will be. The reason for the hardness change is that near the surface the weld toe is treated using UIT and hardened by hard work. As mentioned in Section 3.8, the diameters were measured to calculate the HVN for each depth using Equation 3.2. Figure 4.20 shows the microhardness envelope for Specimen A2. The envelopes include the results of all three trials. The horizontal axis shows the HVN number and the vertical axis show the depth in mm below the weld toe surface.

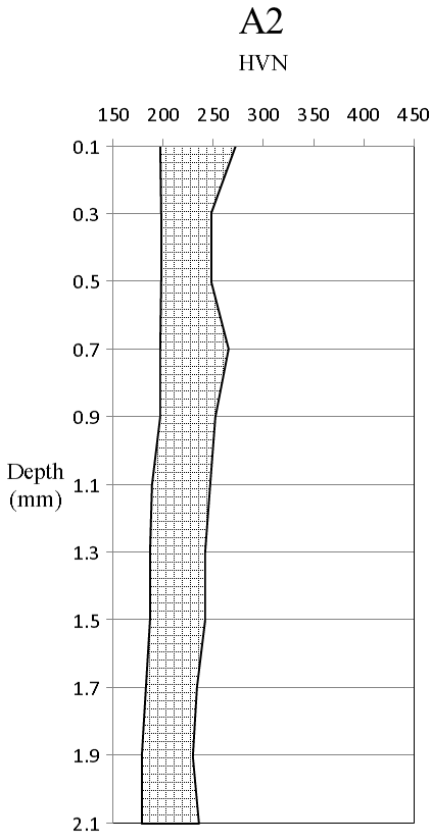

Figure 4.20: Microhardness envelope for Specimen A2

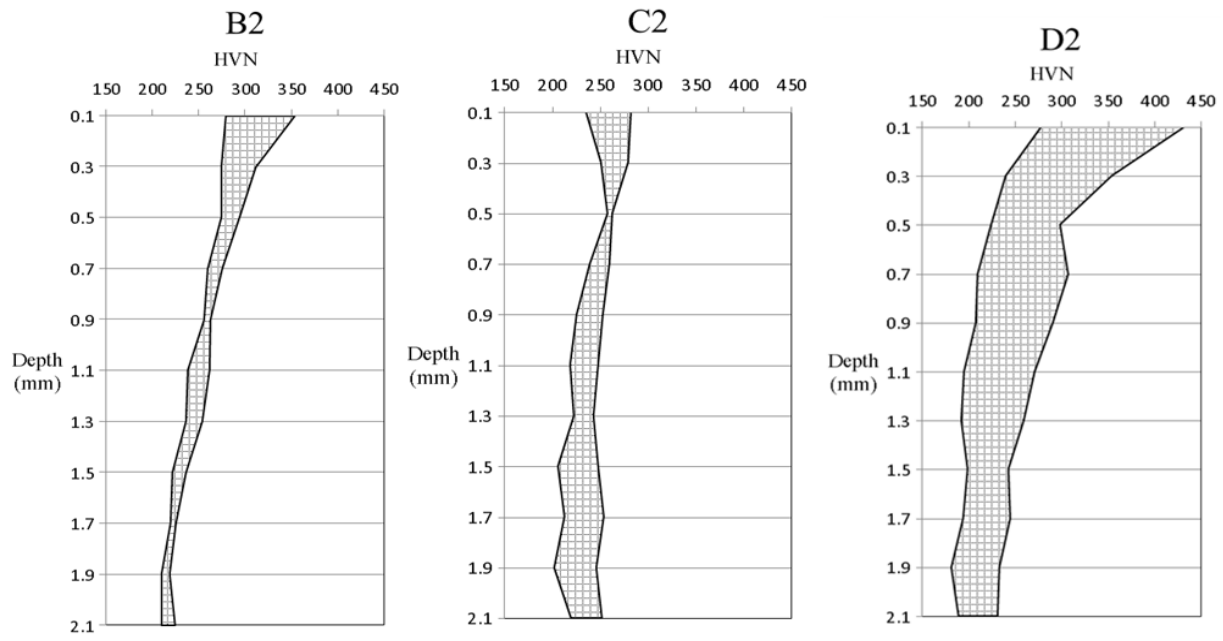

Figure 4.21: Microhardness measurements for Specimens B2, C2, and D2

As shown in these figures, the results for under-treated Specimens B2 and C2 have much less scatter than the over-treated specimen D2. The first HVN measurement at 0.1 mm is normally the highest in the treated specimens. The trend for all three specimens is that at 0.5 mm the HVN starts decreasing and at some points it becomes almost constant until depth 2.1 mm. The HVN of Specimen B2 at 0.1 mm varies from 279 to 354 whereas the HVN of Specimen C2 varies from 235 to 282. Specimen C2 covers a lower range which shows that increasing the treatment speed leads to greater reductions in the local hardness than reducing the treatment intensity. Specimen D2 has a much wider envelope where the HVN at the surface varies from 228 to 432. Figure 4.22 shows the microhardness measurements for the properly treated specimens: E2, F2 and G2.

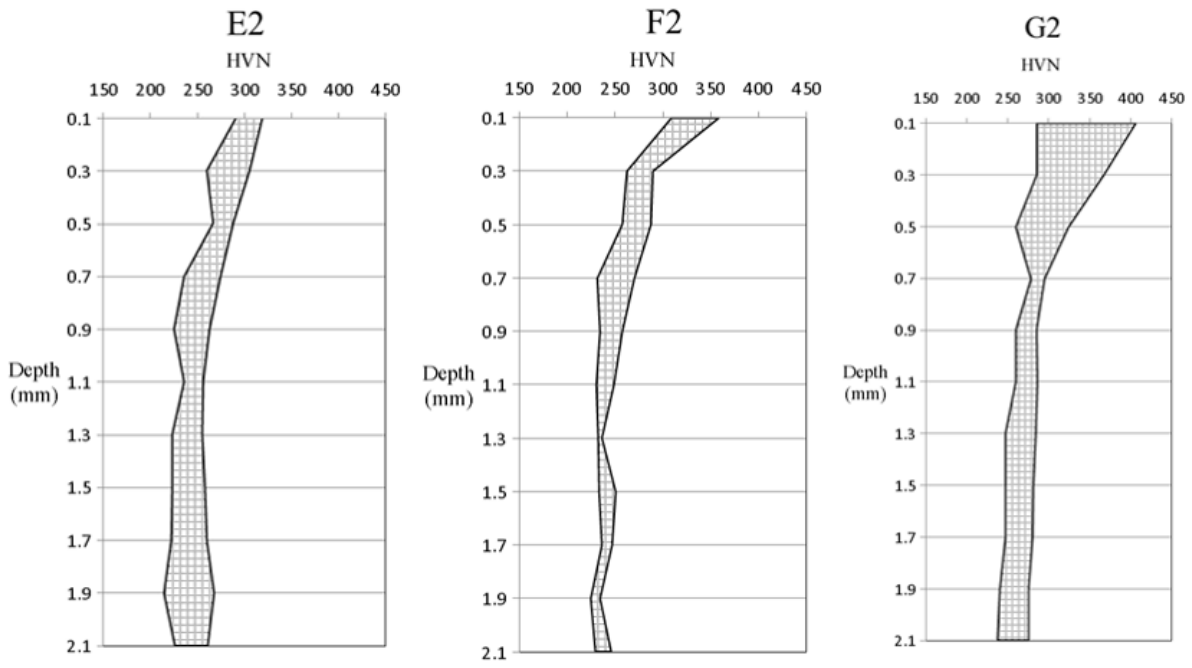

Figure 4.22: Microhardness measurements for specimens E2, F2 and G2

Specimen E2 was treated using a robot whereas F2 and G2 were treated manually. F2 has a much less scatter especially as the depth increases. The HVN varies from 290 to 319 at depth 0.1 mm and starts decreasing from this point. Specimen F2 has an HVN that varies from 310 to 360 at depth 0.1 mm. The HV numbers for specimens E2 and F2 are approximately the same. Hence it can be concluded that the microhardness measurements are the same for properly treated specimens that were treated manually or using a robot. Specimen G2 has an HVN that varies from 286 to 400 at depth 0.1 mm and starts decreasing to an average HVN of 300. For all three figures, the HVN decreases after 0.5 mm and the HVN stays consistent through the rest of the depths.

Figure 4.23 shows the image of the microstructure of the properly treated Specimen F2, and the over-treated Specimen D2.

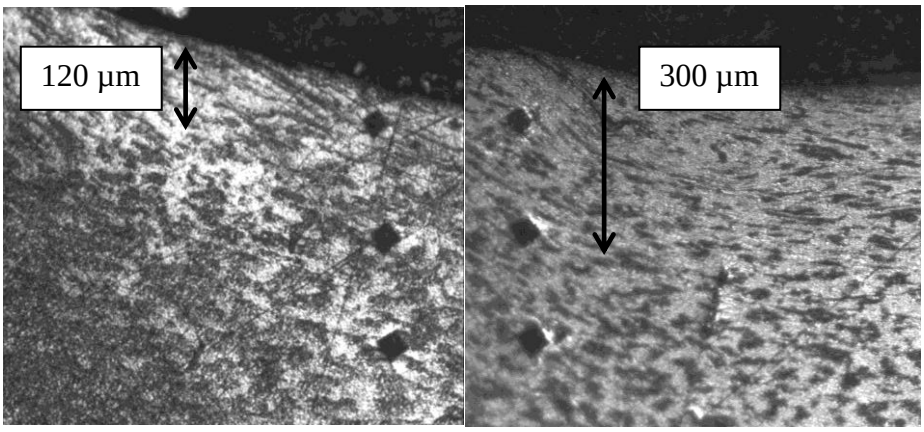

Figure 4.23: Microstructure of F2 (left) and D2 (Right)

The region near the surface shows the compressed grains. It can be seen that the compressed region of the over-treated specimen is more than twice that of the properly treated one. Microhardness measurements can be used to confirm the depth of material affected by the treatment. It should be noted, however, that hardness has no effect in crack propagation and Microhardness testing is not a good quality control method, since it is destructive.

4.6 Residual Stress Results

Residual stresses measurements for six specimens, one from each group (except Group G) were performed and the results are shown below in Table 4.9. The residual stress profiles of all six specimens are graphed in Figure 4.24. The positive and negative values represent tensile stresses and compressive stresses respectively.

Table 4.9: Residual stress measurements for specimens A1- F1

Depth (mm)	Residual stresses (MPa)					
	A1	B1	C1	D1	E4	F1
0.00	-416 ± 6	-109 ± 22	-91 ± 5	-131 ± 9	-169 ± 10	-540 ± 24
0.15	-121 ± 7	-400 ± 13	16 ± 4	-374 ± 18	-335 ± 5	-288 ± 11
0.30	-111 ± 7	-255 ± 14	-83 ± 7	-619 ± 23	-245 ± 7	-476 ± 9
0.60	-91 ± 8	-270 ± 5	-116 ± 9	-624 ± 25	-258 ± 2	-374 ± 7
1.20	-120 ± 6	-366 ± 13	-217 ± 16	-405 ± 7	-366 ± 9	-233 ± 7

The residual stress measurement results from the surface until 0.3 mm are highly unreliable. The reason for this is that the measurements were presented on tested specimens. An extra set of specimens should have been put aside just for residual stress measurements. However, this was not considered in the planning of the original test program. Based on the FE analysis presented in Chapter 5, it is estimated that the local stresses due to the fatigue loading at a stress range of 200 MPa exceeded the nominal yield strength of the material at depths less than approximately 0.3 mm. Thus, cyclic plasticity at these depths meant that the first few readings were influenced by the stress relaxation accompanying the plastic stress-strain cycling. Microhardness and residual stress measurements are both destructive methods. However, microhardness measurements are significantly cheaper than residual stress measurements.

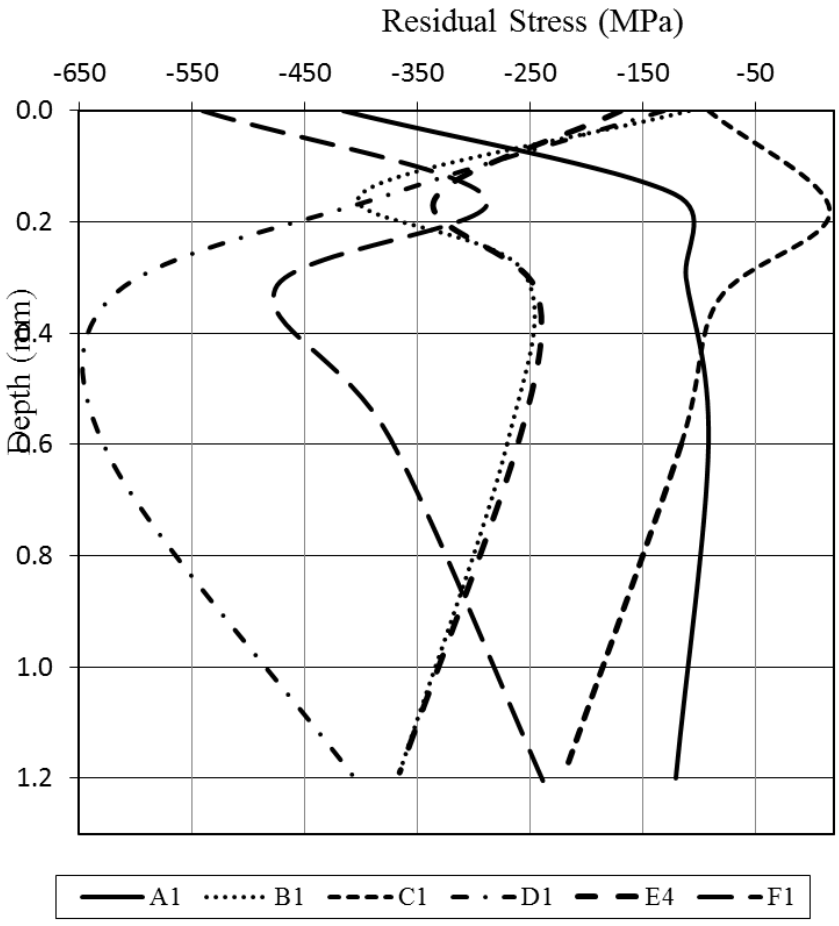

Figure 4.24: Residual stress profiles

Looking at the measurements for depths of 0.3 mm and greater in Figure 4.24, it is observed that the residual stresses are the highest (-619 MPa) for the over-treated Specimen D1. The next highest compressive residual stress level (-476 MPa) is seen for Specimen F1, which is the manually treated weld toe. The residual stress at the same depth (-245 MPa) is lower in magnitude for Specimen E4, which is the robotic "proper" treatment. The under-treated Specimens, B1 and C1, have the lowest residual stress levels. Specimen B1 with reduced treatment intensity has almost the same residual stress as E4, whereas Specimen C1 with increased treatment speed has significantly lower residual stress measurements, which approach those of the untreated Specimen A1. Based on these measurements, it can be concluded that UIT resulted in a significant change in the residual stress distribution through the specimen thickness. The highest (beneficial) compressive residual stresses are seen in the over-treated specimen, followed by the properly treated, under-treated, and untreated specimens.

5 Analysis of Fatigue Specimens and Test Results

5.1 Introduction

In this chapter, the analytical work conducted for this research project is summarized. In Section 5.2, a statistical analysis of the S-N results is presented and design and mean S-N curves for the various treatment cases are established. Section 5.3 describes the finite element analysis conducted to establish stress concentration factors along the crack path due to the applied cyclic loads. Sections 5.4 5.5 and 5.5 present and discuss the results of this finite element analysis. Section 5.6 attempts to relate the various measured geometric and metallurgical parameters to the observed fatigue performance of the treated weld specimens. Recommendations concerning the quality control of UIT are then made based on the results of this comparison.

5.2 Statistical Analysis of S-N Results

In order to establish design S-N curves for a specified survival probability, based on limited fatigue test data, a Gaussian log-normal distribution should be assumed according to (Hobbacher, 2005). Ten or more failed test specimen results (i.e. not run-outs) should be used if possible (Hobbacher, 2005). For analyzing the fatigue data from the tests, a regression model is used where *logN* is the dependent variable (Hobbacher, 2005). Characteristic values are calculated for *k* standard deviations of the dependent variable from the mean. These characteristic values should correspond with a 95% survival probability with a two-sided 75% confidence level of the mean, according to the International Institute of Welding (IIW) Recommendation (Hobbacher, 2005). Other standards, e.g. (AASHTO 2008), use design curves based on a 97.7% survival probability, which corresponds to two standard deviations below the mean.

For the establishment of S-N curves, stress ranges should be include at least two levels giving fatigue lives within the range of 10^5 to 10^6 cycles (Hobbacher, 2005). The stress range, ΔS, and number of cycles to failure, N, should be plotted on a $\log_{10}$ scale. Equation 5.1 defines the relationship between m, $logC$, $logN$, and $log\ \Delta S$:

$$logN = logC - m \cdot log\Delta S \qquad 5.1$$

Equation 5.2 defines the mean, $x_{m,}$ and standard deviation, Stdv, of l*ogC* where x_i = *logC*:

$$x_m = \frac{\sum x_i}{n} \; and \; Stdv = \sqrt{\frac{\sum (x_m - x_i)^2}{n-1}} \qquad 5.2$$

Equation 5.3 defines the characteristic value x_k:

$$x_k = x_m - k \cdot Stdv \qquad 5.3$$

Table 5.1 provides k values for various sample sizes, *n*, for use in Equation 5.3.

Table 5.1: K values used for corresponding n value

n	10	15	20	25	30	40	50	100
k	2.7	2.4	2.3	2.2	2.15	2.05	2.0	1.9

Design and mean curves were produced using these equations. Due to the limited test data available, four cases were considered for this analysis. In Case I, run-out data were included and the slope, *m*, was fixed at 3.0, as is often assumed for steel. Case II is similar to Case I except that the run-outs are removed. Case III includes run-outs and a variable m. Case IV does not include the run-out data but does assume a variable m. Figure 5.1 and Figure 5.2 show the mean (50% survival probability) and design (95% survival probability) curves for Case I.

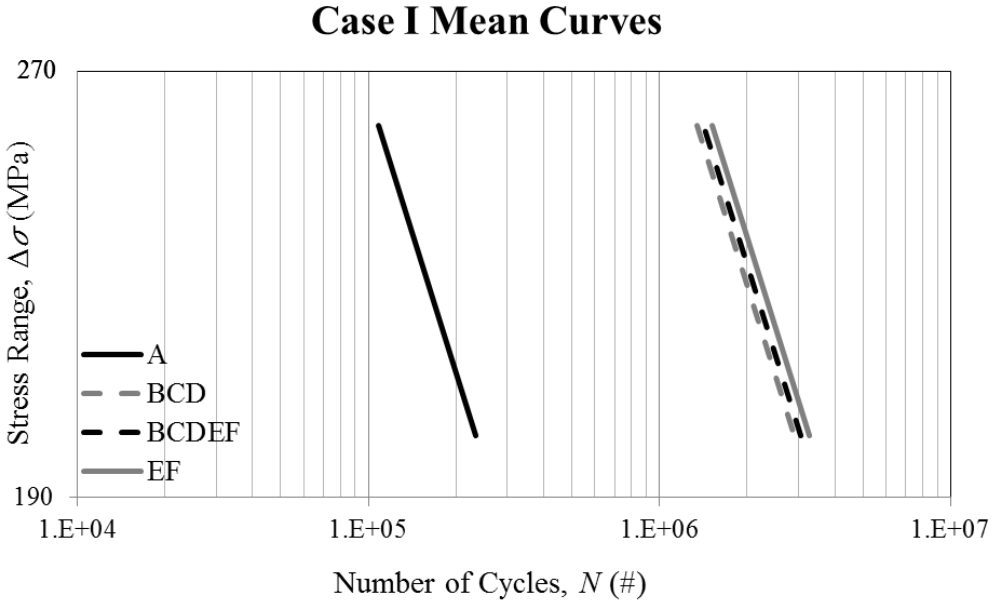

Figure 5.1: Case I mean curves

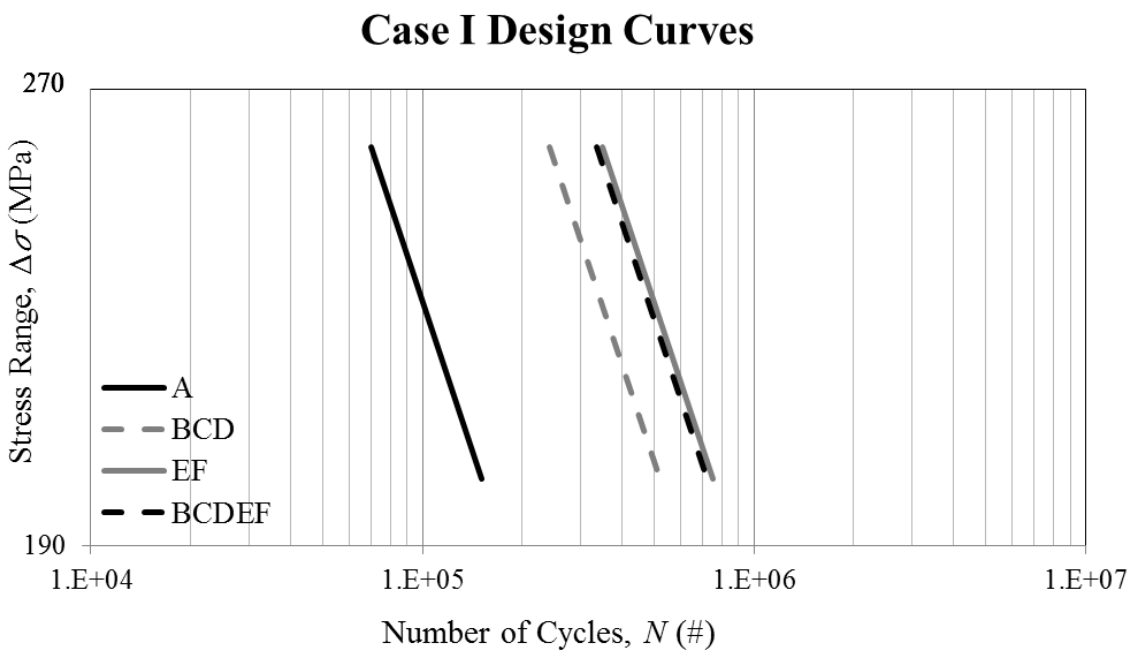

Figure 5.2: Case I design curves

In this figure, the test specimens are grouped together in several ways. Group A is the untreated group. Groups E and F were both properly treated. The data for these two groups are combined increase the sample size. Groups B, C, and D are all improperly treated (i.e. over- or under-treated). The EF curves in these figures can be associated with "high quality" or "quality controlled" treatment. The BCD curves can be associated with treatment that has not been performed properly, within the ranges investigated in this study. The BCDEF curves can be associated with treatment of unknown quality, within the same investigated ranges.

Group A has the lowest fatigue life in all the cases for the mean and design curves. Group BCD is always to the right of Group A by a considerable margin. Looking at the mean curves for the various groups of treatment cases, it can be seen that they are all very close together. However, the EF curve is the highest, the BCDEF curve is next, and the lowest is the BCD curve. Looking at the design curves, Group EF and BCDEF are very close to each other, although the EF curve is slightly higher. The BCD curve is considerably lower than both, although it is still significantly higher than the Group A curve. The fact that the design curves are more spread out than the mean curves is an indication that although the mean life doesn't change much between the various treatment cases, the scatter in the results is higher when the treatment quality is not "proper" or when the quality of the treatment is not controlled.

Figure 5.3 and Figure 5.4 and show similar mean and design curves for Case II.

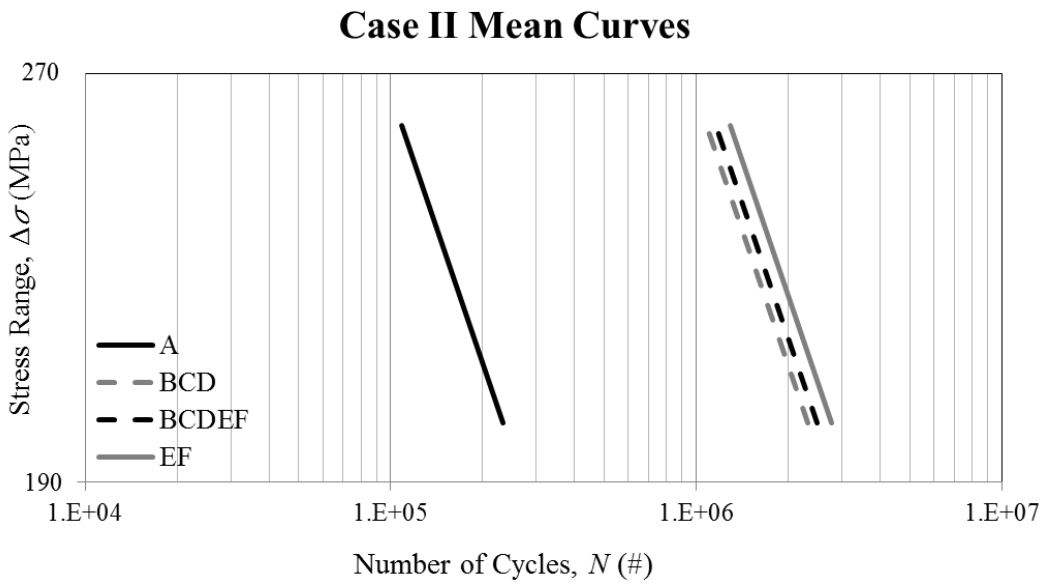

Figure 5.3: Case II mean curves

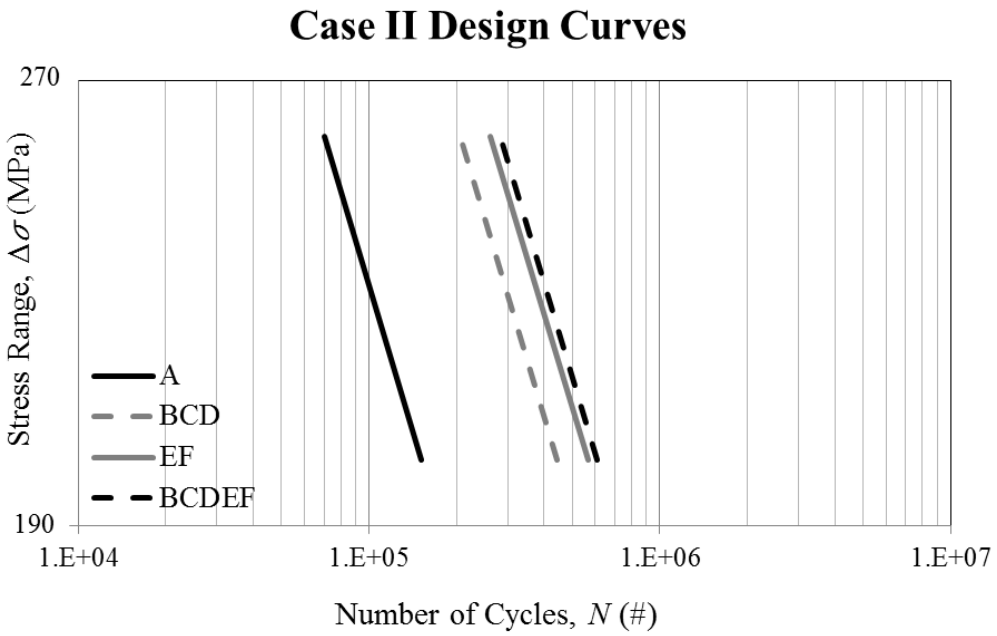

Figure 5.4: Case II design curves

Figure 5.5 and Figure 5.6 show similar mean and design curves for Case III.

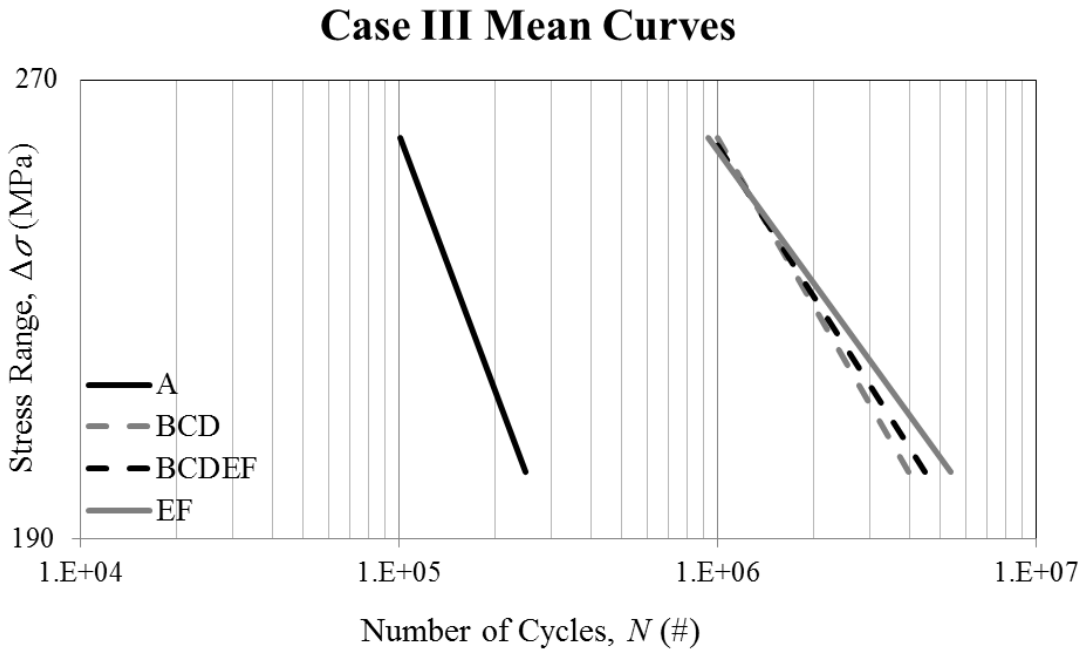

Figure 5.5: Case III mean curves

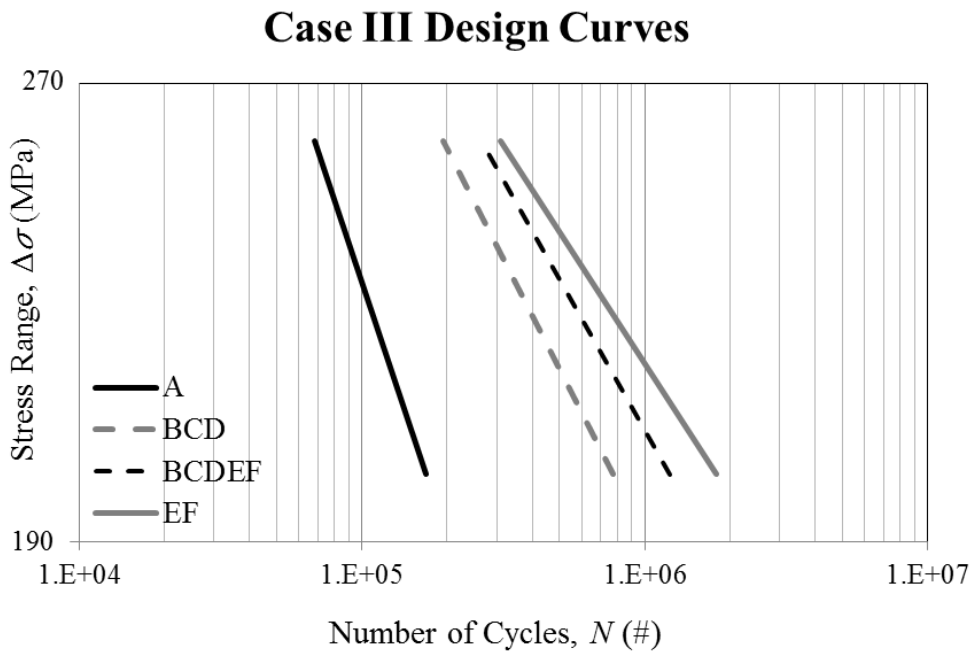

Figure 5.6: Case III design curves

Figure 5.7 and Figure 5.8 and show similar mean and design for Case IV.

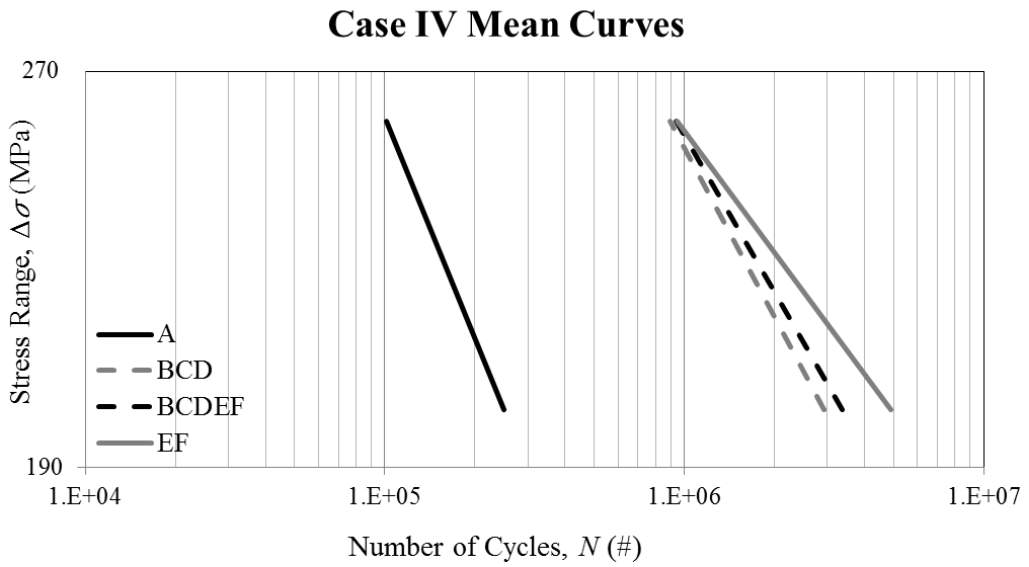

Figure 5.7: Case IV mean curves

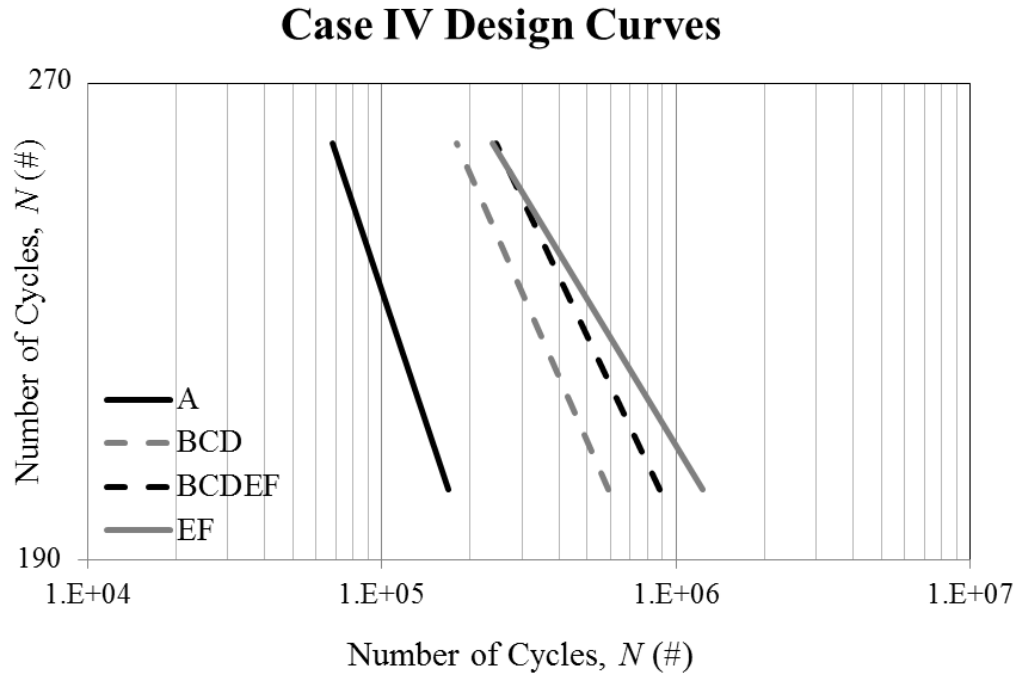

Figure 5.8: Case IV design curves

Comparing the different cases, the same general trends can be seen as for Case I, in terms of the ranking of the treatment curves and increase in scatter when the treatment quality is either unknown or known to be not "proper". Thus, it can be concluded that the decisions of whether or

not to fix the S-N curve slope and whether or not to include run-outs in the statistical analysis have little or no impact on these general trends, as described for Case I.

In order to quantify the benefit of treatment for the various levels of treatment quality, comparisons of fatigue life were made for a stress range of 200 MPa. Table 5.2 and Table 5.3 show the percent increase in fatigue life, based on the mean and design curves respectively.

Table 5.2: Percent increase in fatigue lives for mean curves

	% increase in fatigue life		
Mean	**BCD**	**BCDEF**	**EF**
Case I	1147%	1206%	1300%
Case II	895%	967%	1090%
Case III	1489%	1694%	2052%
Case IV	1071%	1249%	1853%
Average	1150%	1279%	1574%

All of the comparisons are made with respect to the Curve A (as-welded) fatigue life. For example, in Case I, there is an 1147% increase in fatigue life predicted using the BCD curve compared to Curve A. The best improvement is seen for Case IV and Curve EF, with a percent increase of 1853% compared to Curve A. The averages for each curve show that Curves EF, BCDEF and BCD had the highest to lowest percent increase in the fatigue life respectively.

Table 5.3: Percent increase in fatigue lives for design curves

	% increase in fatigue life		
Design	**BCD**	**BCDEF**	**EF**
Case I	244%	380%	399%
Case II	194%	304%	274%
Case III	361%	628%	962%
Case IV	250%	424%	629%
Average	262%	434%	566%

The percent increases in fatigue life predicted using the design curves are much lower than those based on the mean curves. However, the same trend is observed in terms of the ranking of each curve, where the high quality curve (EF) results in the highest fatigue life increase and Curve BCD has the lowest percent increase in fatigue life.

In order to further analyze the fatigue performance results and to prove that there is a significant difference between the fatigue lives of untreated and treated specimens; t-test analysis is

performed. The t-distribution is a bell-shaped and symmetric distribution with a zero mean value, which is widely used in statistics (Walpole & Myers, 1998). This distribution is used for sample sizes less than thirty and its equations are derived from a normal population (Walpole & Myers, 1998). The t-distribution can be used to compare data and to determine whether the means of two data sets are significantly different. For this analysis, a two-sided test is chosen to analyze whether two sets of data are significantly different or not (Walpole & Myers, 1998). The objective is to prove that the UIT has had a significant effect on fatigue lives of specimens. For this analysis, a null and an alternative hypothesis are presented below:

H_o: $\mu_{1=}\mu_2$

H_a: $\mu_{1\neq}\mu_2$

The null hypothesis is stating that the mean of data set one is the same as the mean of data set two and the means are assumed to belong to the same population, which means that there is no significant difference between the mean results of the two analyses with 95% confidence (α = 0.05). The alternative hypothesis is stating that the means of the samples are from two different populations and there is a significant difference between the mean results of the two analyses with 95% confidence (α = 0.05). In order to perform the t-test analysis, the following equation is used to calculate a parameter, *M*, which is independent of the stress range. A slope (*m*) of 3 is used to calculate *M*:

$$\log_{10} M = m \log_{10} \Delta S + \log_{10} N \qquad 5.4$$

The mean and standard deviation of *M* is calculated for each group. The calculated t-value (t-cal) is then calculated by using equation 5.5.

$$t = \frac{\mu_1 - \mu_2}{\sqrt{\frac{S_1^2}{n_1} + \frac{S_2^2}{n_2}}} \qquad 5.5$$

where μ_1 and μ_2 are the means of the first and second samples, S_1 and S_2 are the variances of the first and second samples, and n_1 and n_2 are the sizes of the data sets for each sample. Figure 5.9 shows the graph of *M* vs. ΔS which illustrates that *M* is independent of ΔS.

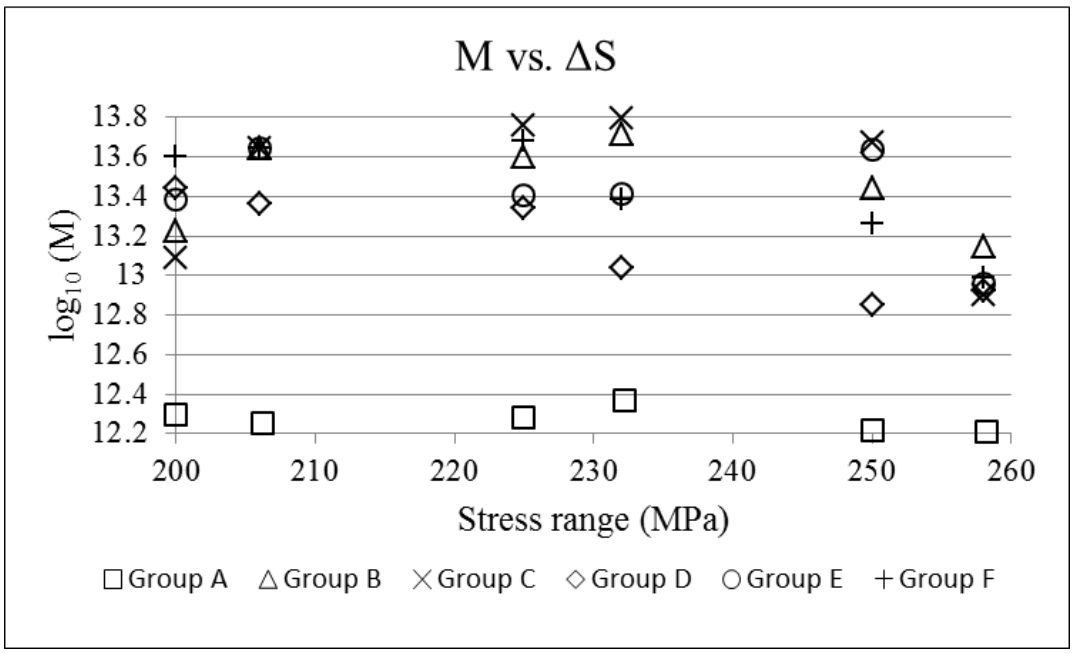

Figure 5.9: M vs. ΔS

The t-cal is compared to the critical t value (t-table) from the statistical tables based on the number of degrees of freedom (number of samples-1). If t-cal < t-table, then the null hypothesis is accepted. Otherwise, the alternative hypothesis is accepted. Using cumulative density functions, the probability whether two samples are likely to have come from the same population is calculated.

Table 5.4 shows the t-distribution results for different groups based on a 95% confidence. The first column shows the names of the groups that were compared. The second group shows the probability that the sample data belong to the same population. The third column indicates the probability that the sample data belong to a different population and that the results are significantly different. The third column is simply the difference between 100% and the percentage indicated in column two. The null hypothesis is accepted if the probability of the first column is more than 5% which means that there is more than 5% chance that there was no significant improvement. Otherwise, the null hypothesis is rejected. First, the untreated Group A is compared to the rest of the groups. The results show that there is a significant difference between the performances of the treated and untreated groups. Under-treating the specimens by reducing the treatment intensity (Group B) or increasing the treatment speed (Group C) showed

similar results. Regardless of the investigated level of treatment quality, UIT has a significant influence on the performance of the specimens.

Table 5.4: t-distribution results

	Probability that the samples are from the same population	Probability that the samples are **NOT** from the same population
A vs. B	2.594 E-07%	100%
A vs. C	1.757 E-05%	100%
A vs. D	8.019 E-06%	100%
A vs. E	6.709 E-07%	100%
A vs. F	1.273 E-06%	100%
A vs. EF	6.670 E-09%	100%
A vs. BCD	1.757 E-05%	100%
A vs. BCDEF	6.174 E-11%	100%
E vs. F	90%	10%
E vs. B	70%	30%
E vs. C	72%	28%
E vs. D	12%	88%
EF vs. BCD	65%	35%

Comparing the high quality group (EF), the low quality group (BCD) and the unknown quality group (BCDEF) with the untreated group still shows that the null hypothesis is rejected and the alternative hypothesis is accepted. The t-test analysis shows that there is a 90% chance that the data from Groups E and F are from the same distribution. This shows that manually or robotically treating the specimens will likely produce the same results. Comparing Group E to B and C shows that there is at least a 70% chance that they are from the same distribution. This percentage is much lower for Group D (only 12%). Comparing the high quality group (EF) to the low quality group (BCD) shows that there is a 65 % chance that they are from the same distribution. In conclusion, based on the t-test analysis, it is proven that the UIT significantly influenced the performance of weld details regardless of the treatment type.

5.3 Finite Element Model Description

The finite element (FE) method was used in this research project to predict stress concentration factors (SCFs) along the crack path for the various treatment cases. In this context, the SCF is defined as the local elastic stress divided by the nominal, remotely applied stress. The nominal stress is taken as the applied load divided by the cross section area of the loaded plate. The nominal specimen and weld toe geometry dimensions were used to create the finite element model. Figure 5.10 shows the weld toe of a typical properly treated specimen.

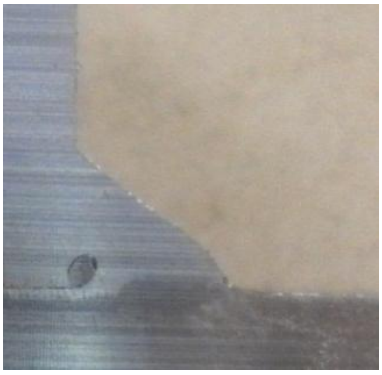

Figure 5.10: Weld toe of specimen F1

The ABAQUS CAE Version 6.11 software was used to perform the FE analysis. Sixteen specimens were chosen (A1-G1, B3, B5, C3, C5, D4, D6, E3, E6, F4 and F6) for modelling. The purpose of the FE analysis was to illustrate the possible effects of variations in the indent geometry on the local elastic stresses. To perform the FE analysis, a 2D plane strain model was chosen and the material properties were assumed to be homogenous and linear elastic. Values of 200,000 MPa and 0.3 were assigned as the Young's modulus (E) and Poisson's ratio (μ) respectively. The untreated specimen geometry was modelled first. The boundary conditions were then assigned, along with a unit pressure at the edge of the loaded plate. Figure 5.11 illustrates the nominal geometry that was used as a starting point for building all of the specimen models.

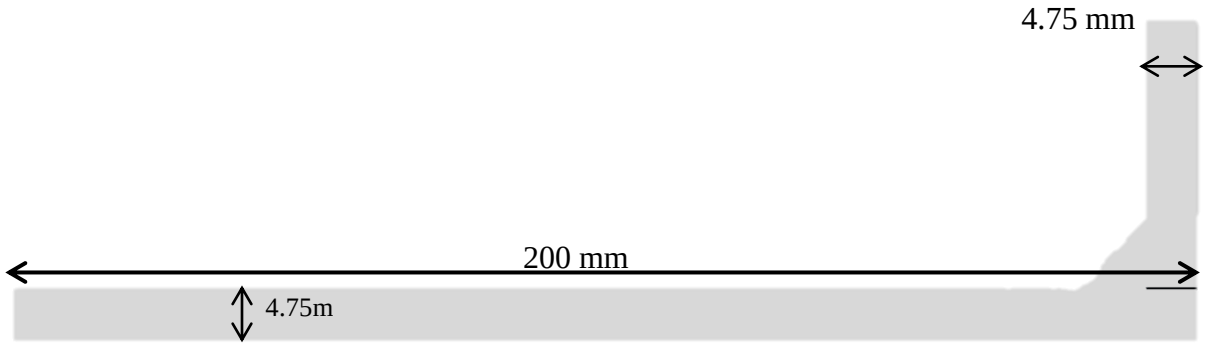

Figure 5.11: Geometry of specimens in ABAQUS

The basic model was then modified by superimposing a tracing of the weld toe from the corresponding impression photograph to the base model (untreated). Figure 5.12 shows weld toe WT-1 impression for Specimen F1 and an outline of the corresponding FE model.

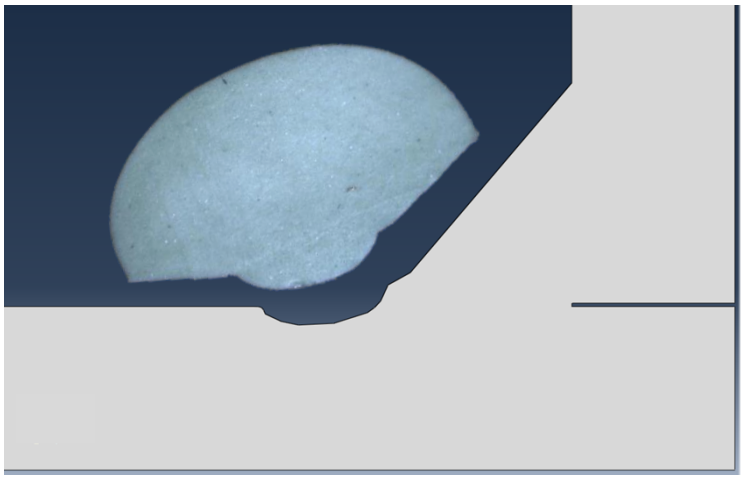

Figure 5.12: F1 weld toe 1 impression and the modified model

The straight line on the right side of the figure represents the gap between the loaded plate and the transverse stiffener. The model was then seeded to facilitate the automatic meshing process. The entire model was seeded with 1 mm node spacing, except at the weld toe, where a much smaller node spacing of 0.02 mm was prescribed. The smaller elements were used at the weld toe to provide more accurate results. Biased seeding in between the two regions was used to ensure that the meshing did not result in excessively elongated elements. The meshed model of F1 is shown below in Figure 5.13. The upper picture shows the magnified meshed weld toe.

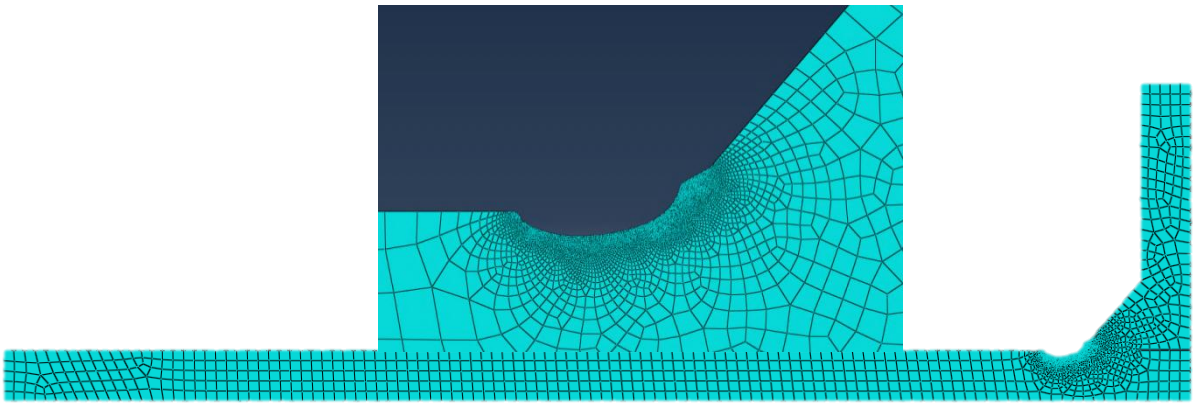

Figure 5.13: Meshed model of specimen F1

5.4 Finite Element Analysis

The specimens were analyzed after meshing to obtain the stress concentration factors (SCFs) at the weld toe. Table 5.5 presents the stress concentration factor for different specimens. The stress concentration factor was calculated for one untreated specimen from each group except Group G. Because Group F and Group G specimens were properly treated, similar results were expected for the Group G specimen. In addition to calculating the SCF for untreated specimens, the SCF for three treated specimens for each group was calculated. In order to obtain the SCF for different flange thicknesses that are used in the girders of bridges (9.5, 19 and 38 mm), one specimen from Group B, D and E were chosen for additional finite element analysis. The specimen ID is placed before the SCF in brackets.

Table 5.5: Peak stress concentration factors

	Untreated Specimen	Impression 1	Impression 2	Impression 3	Thickness: 9.5 mm	Thickness: 19 mm	Thickness: 38 mm	Average of impression 1,2 &3
Group A	(A1) 2.76							
Group B	(B1) 2.73	(B1) 2.15	(B3) 1.96	(B5) 1.96	(B3) 2.13	(B3) 2.18	(B3) 2.17	2.02
Group C	(C1) 2.37	(C1) 2.03	(C3) 1.87	(C5) 2.20				2.03
Group D	(D1) 2.67	(D1) 2.68	(D4) 2.86	(D6) 3.14	(D6) 3.31	(D6) 3.37	(D6) 3.37	2.82
Group E	(E1) 3.49	(E1) 1.95	(E3) 2.06	(E6) 2.25	(E3) 2.28	(E3) 2.33	(E3) 2.32	2.09
Group F	(F1) 3.89	(F1) 1.86	(F4) 2.29	(F6) 2.21				2.12
Group G		(G1) 2.13						

The last column of the table shows the average of the SCF of the three impressions for Group B to Group F. It is seen that the highest peak SCF is associated with the over-treated weld (D1). The lowest SCF is for under-treated Groups B and C. The properly treated Groups (E and F) fall in between the under- and over-treated Groups.

Figure 5.14 to Figure 5.20 present contour plots of the longitudinal stress, S11, for Specimens A1 to G1. The legend in each figure shows the SCF at the different locations. The highest number in this legend is the peak SCF, which generally occurs at the surface.

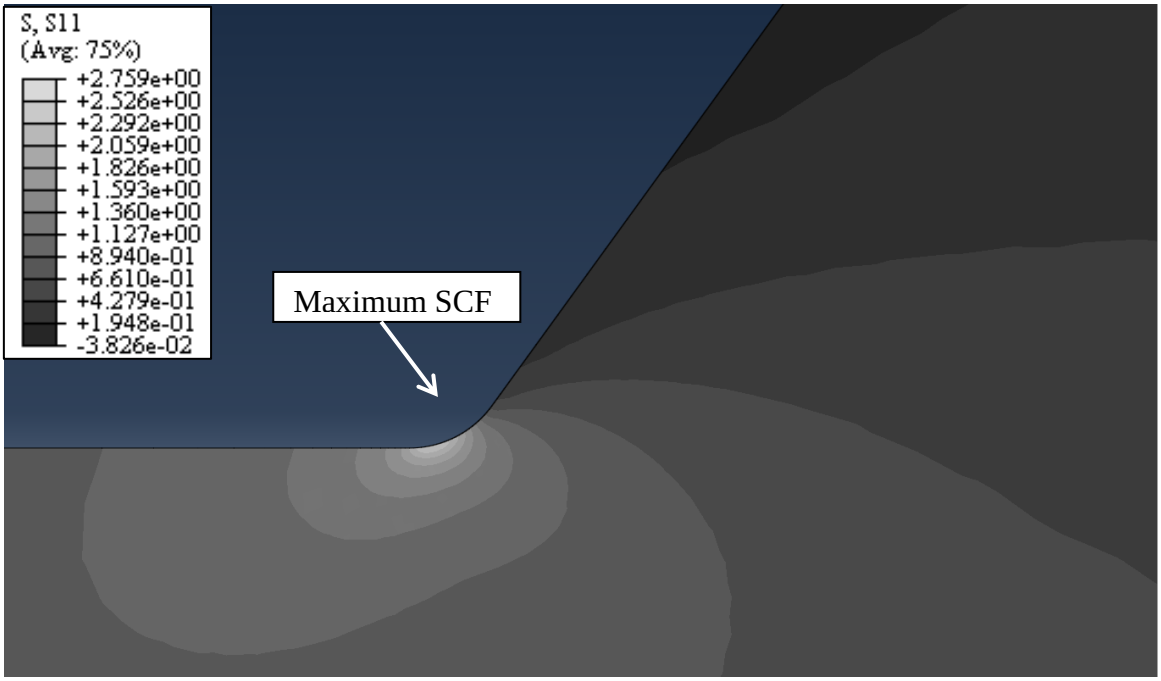

Figure 5.14: FE model and SCF contours for Specimen A1

For specimen A1, a radius of 0.5 mm was assumed at the weld toe, this is a typical average value for as-received welds, as reported in the literature. Table 5.5 summarizes the peak stress concentration factors for each specimen type.

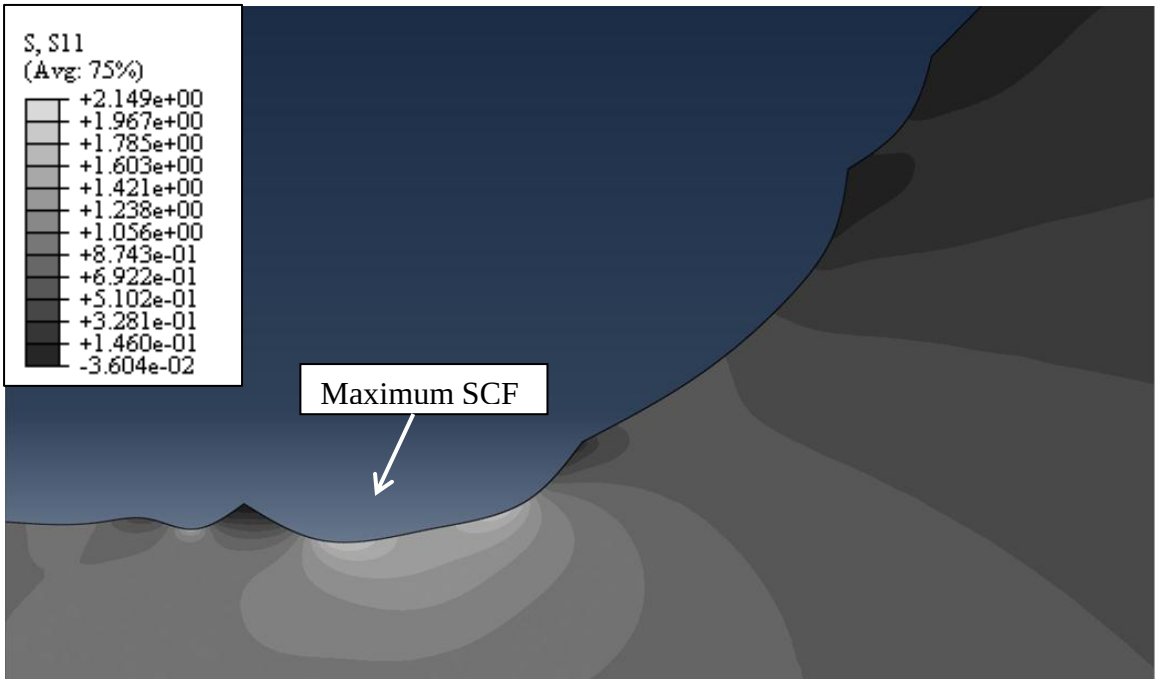

Figure 5.15: FE model and SCF contours for Specimen B1

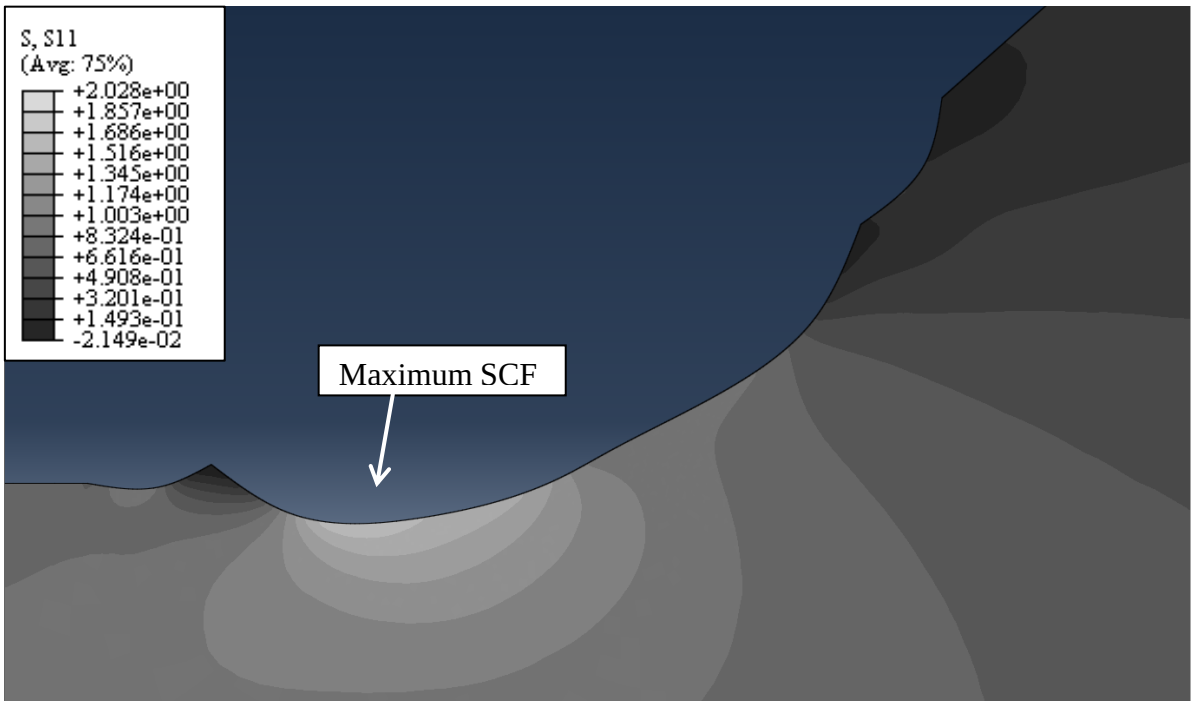

Figure 5.16: FE model and SCF contours for Specimen C1

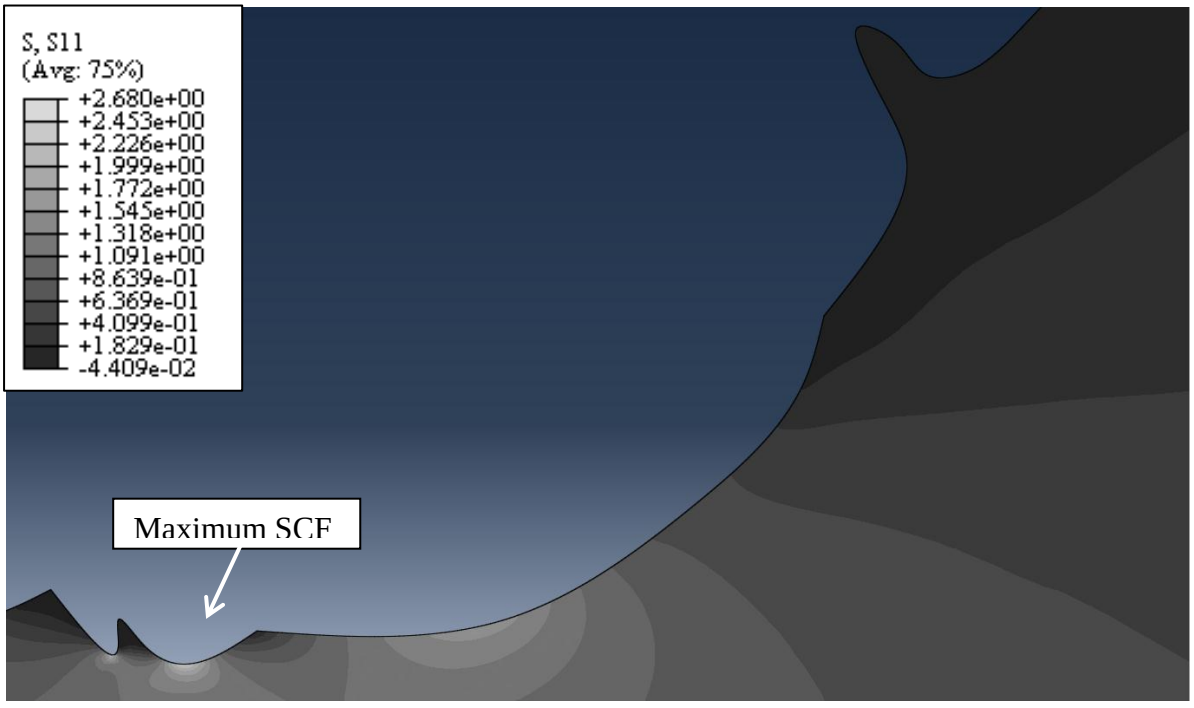

Figure 5.17: FE model and SCF contours for Specimen D1

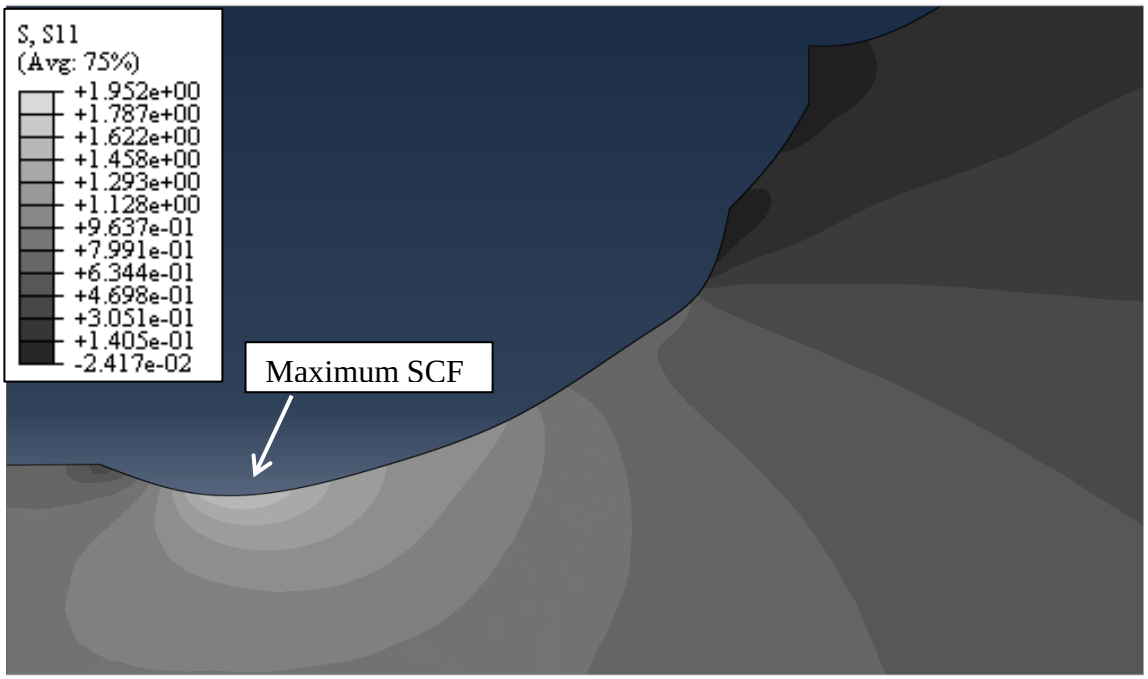

Figure 5.18: FE model and SCF contours for Specimen E1

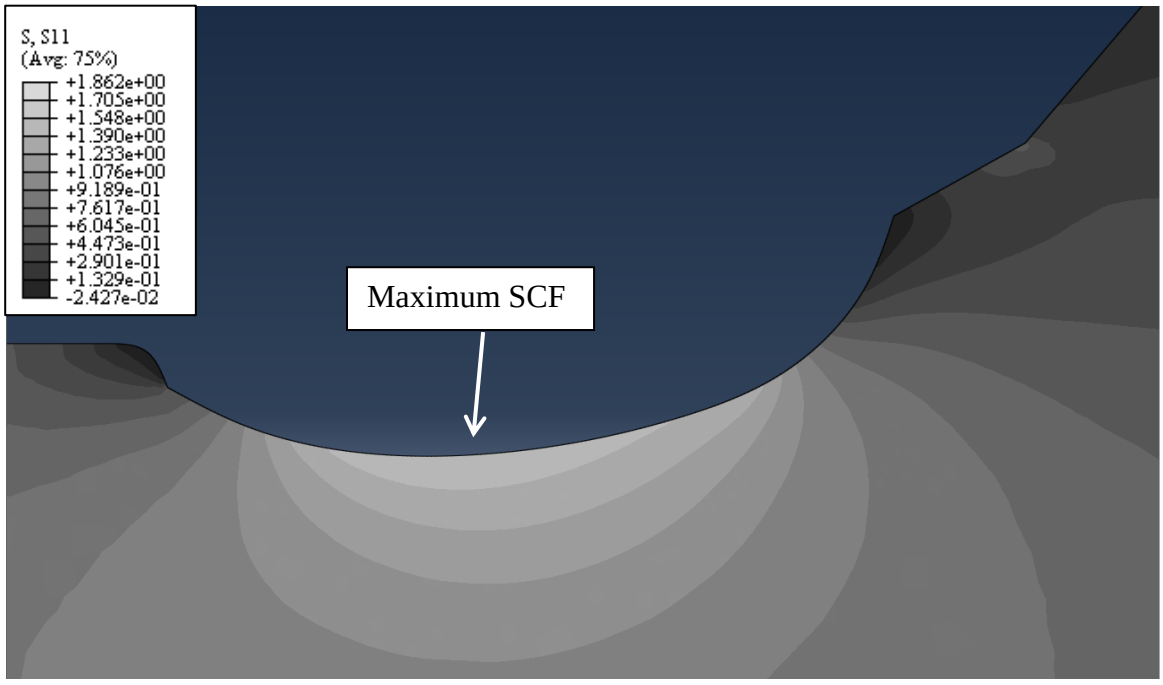

Figure 5.19: FE model and SCF contours for Specimen F1

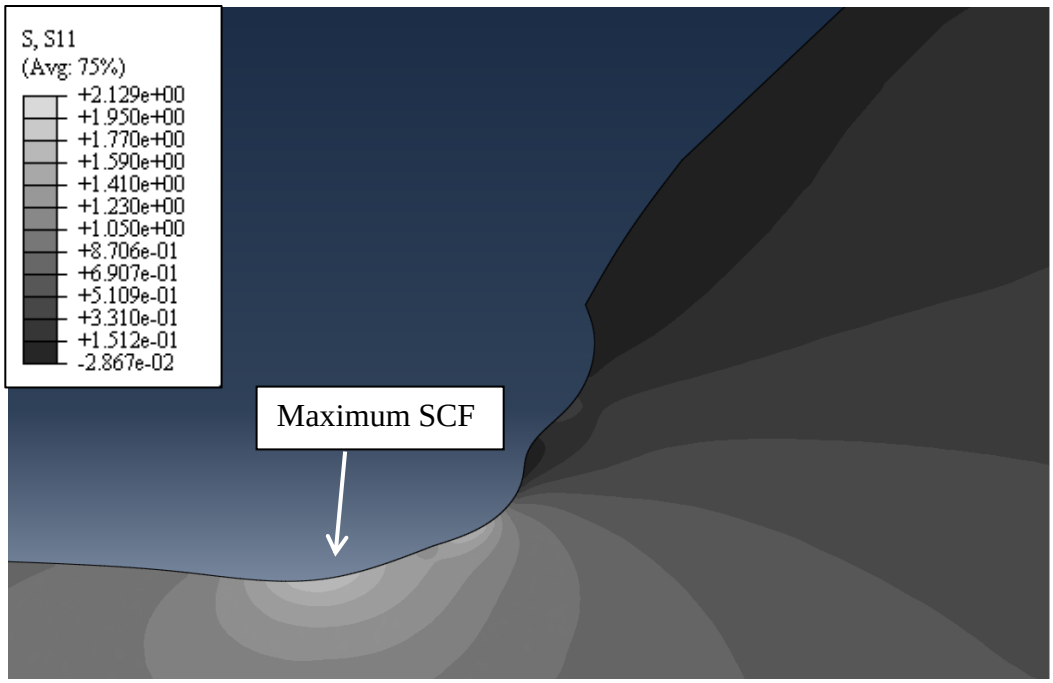

Figure 5.20: FE model and SCF contours for Specimen G1

5.5 Stress Distributions Along The Crack Path

The results in Table 5.5 only show the highest (peak) stress concentration for each specimen. In order to obtain the elastic stress distribution along the crack path, it was assumed that the crack initiated from the point where there is maximum stress and propagated through the base metal along a path running perpendicular to the loading direction. Data points were exported indicating the location and SCF level wherever the crack path crossed an element boundary. Figure 5.21 shows a comparison of the resulting SCF distributions for Specimens A1 and F1.

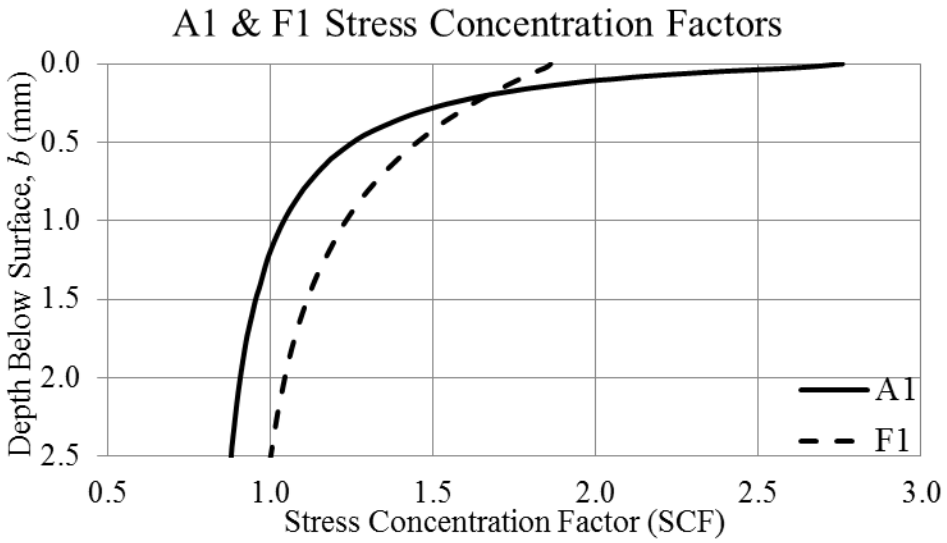

Figure 5.21: SCF result of specimen A1 and F1

The maximum stress concentration factors are 2.76 and 1.86 for the untreated and properly treated weld toes respectively. Specimen A1 is untreated and F1 is properly treated. This figure shows that the UIT application results in a significant reduction in the SCF of up to 67% at the surface of the weld toe. Figure 5.22 shows a similar comparison, with an SCF curve for Specimen E1 added.

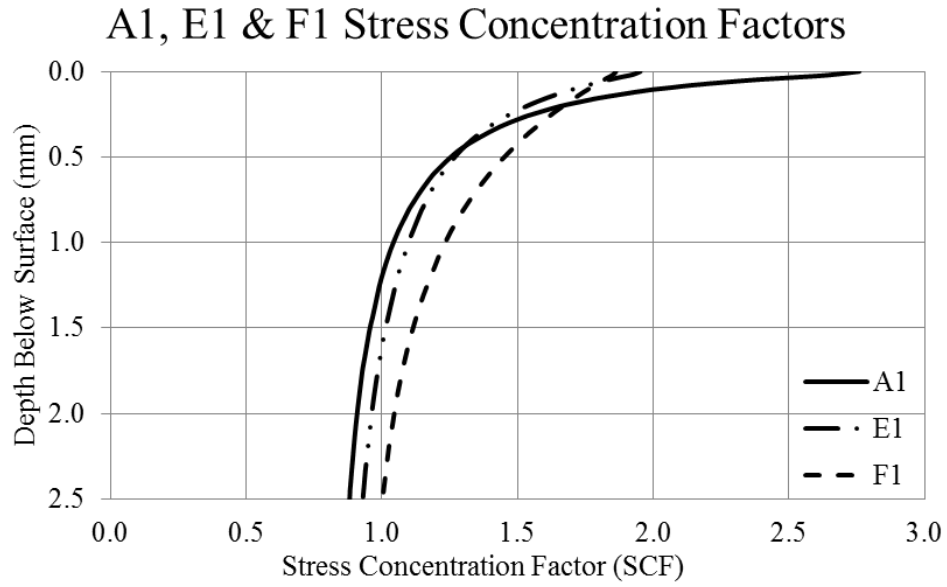

Figure 5.22: SCF results for untreated specimen vs. properly treated specimens

The maximum SCF for E1 is 1.95, which is very close to the peak SCF for F1. This illustrates that using a robot or a manually treating the specimens have a similar effect on SCF. This SCF is significantly less than the one for untreated specimens.

Figure 5.23 shows the SCF of pre-cracked specimen G1 compared to A1 and properly treated Specimen F1.

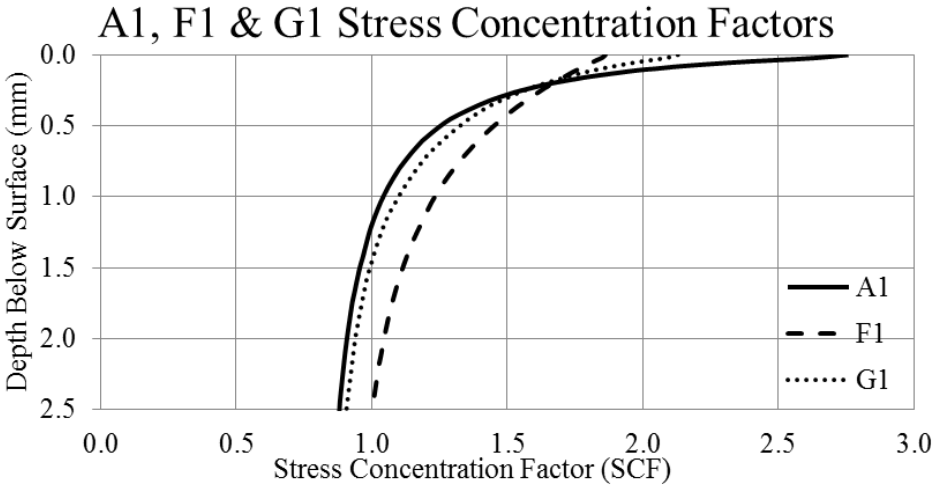

Figure 5.23: SCF results for pre-cracked specimen (G1) vs. untreated specimen (A1) and properly treated (F1) specimen

Specimen G1 has an SCF of 2.13 which is slightly higher than the SCF of Specimen F1 but significantly lower than Specimen A1. This result suggests that if the structure is treated prior to any cracking, better results will be achieved. Figure 5.24 shows the stress concentration factor results for Specimens B1 and C1, which were under-treated, and Specimen D1, which was over-treated.

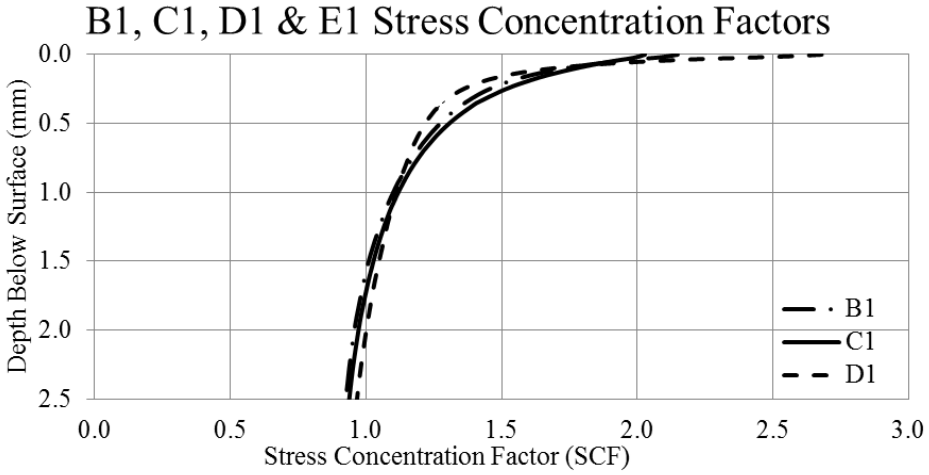

Figure 5.24: SCF results for under- and over- treated specimens

As shown in this figure, the SCF distributions for all three specimens almost overlap after 1 mm of depth. However, the maximum SCF for each of them is different. The under-treated Specimens B1 and C1 have SCFs of 2.15 and 2.03 respectively. These two stress concentration factors are really close to each other, which means that reducing the treatment intensity or increasing the treatment speed do not result in very different stress concentration factors. The over-treated specimen; however, has a significantly higher SCF of 2.68. This value is almost as high as the SCF of untreated Specimen A1. This high value is due to removal of material from the weld toe of Specimen D1 and plastically deforming the weld toe. Figure 5.25, Figure 5.26 and Figure 5.27 show the SCF for an under-, over- and properly treated (B3, D6 and E3).

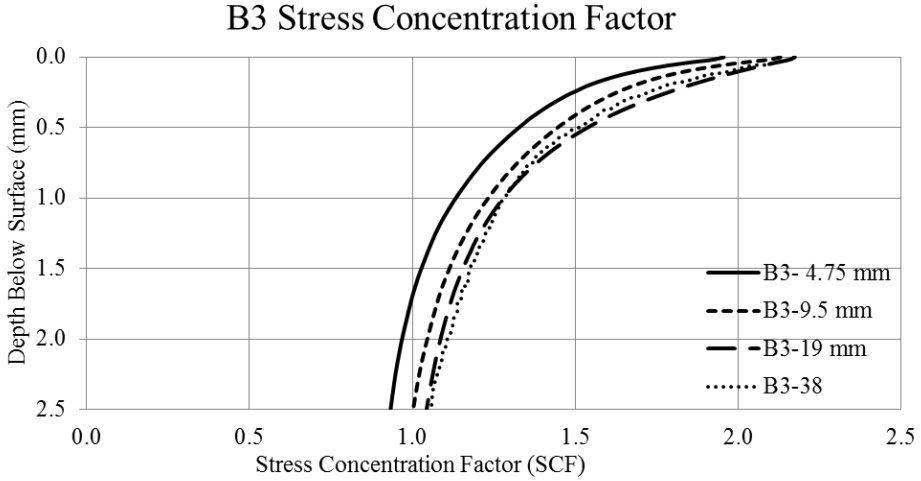

Figure 5.25: B3 SCF results for various thicknesses

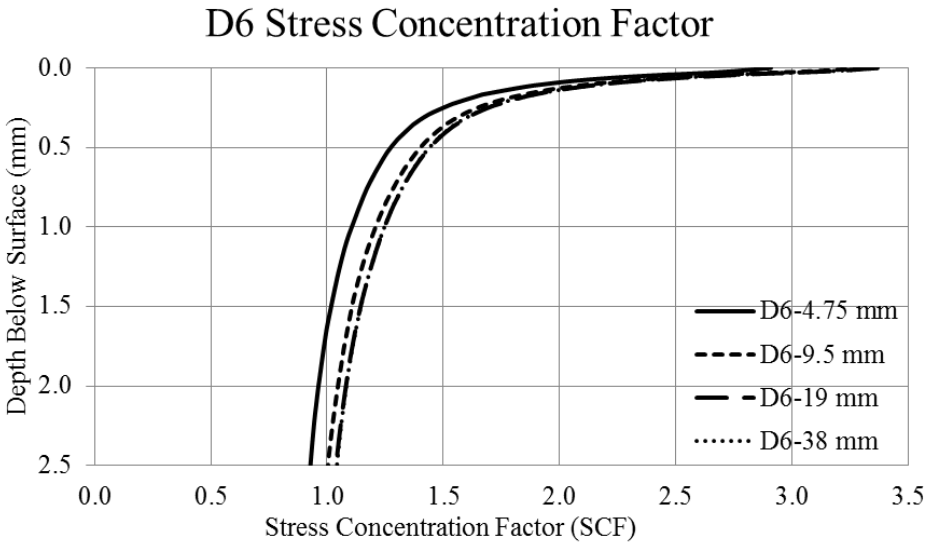

Figure 5.26: D6 SCF results for various thicknesses

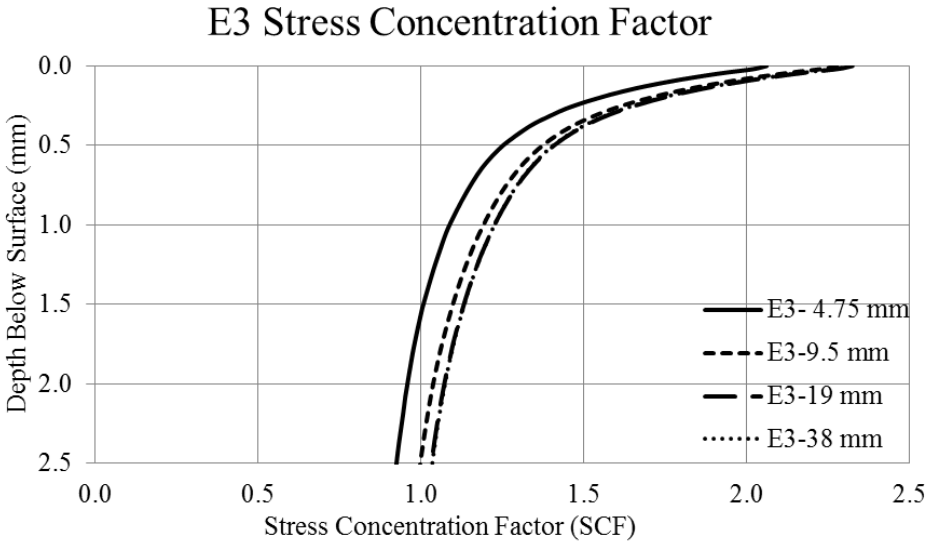

Figure 5.27: E3 SCF results for various thicknesses

All of the figures follow the same trend in which the SCF for the 4.75 mm thickness has the lowest SCF followed by the SCF from 9.5 mm thickness. The SCF for 19 and 38 mm almost completely overlap for specimen D6 and E3. The two SCFs are slightly off for B3. It can be concluded that the SCF becomes the same after the thickness increases 19 mm. Also, all four curves in the figures follow the same path.

5.6 Quality Control Recommendations for UIT

Two parameters that could be very useful for the quality control of UIT, due to the ease with which they can be obtained and the strong correlation that they appear to have with treatment quality, are the indent depths from the base metal and the weld metal. Figure 5.28 shows the base metal indent depth measurements in millimetres for all the treated groups.

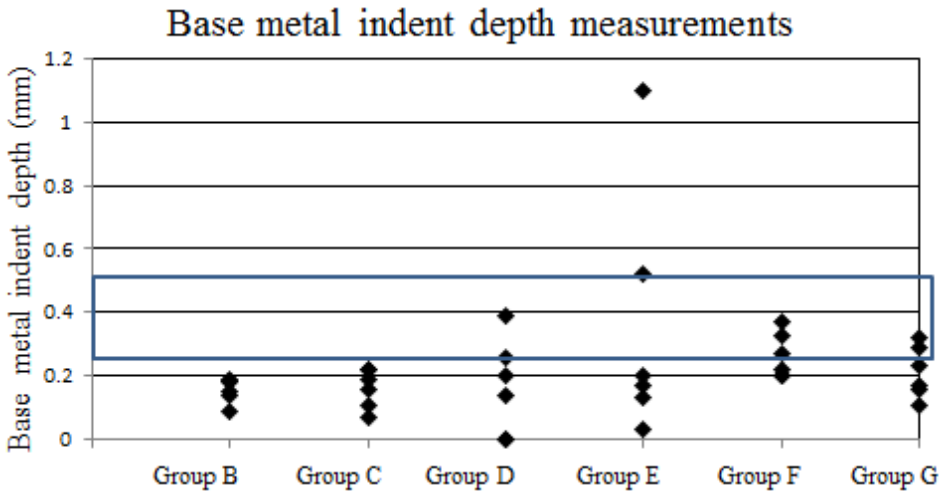

Figure 5.28: Base metal indent depth measurements for treated groups

The horizontal axis in this figure shows the treated group names, and the vertical axis shows the base metal indent depth. The rectangle in each graph covers the minimum and maximum area for indent depths of properly treated specimens recommended by AASHTO (2008), which is 0.25-0.5 mm. As mentioned in Chapter 4, it appears that for the robotic treatment, the tool was directed to a much larger degree towards the weld, rather than towards the base metal. Hence, the indent depths for the base metal were lower than expected for the robotically treated Groups. However, Group F and G fall within or close to the identified standard range. Figure 5.31 shows the weld metal indent depth measurements for all the treated groups.

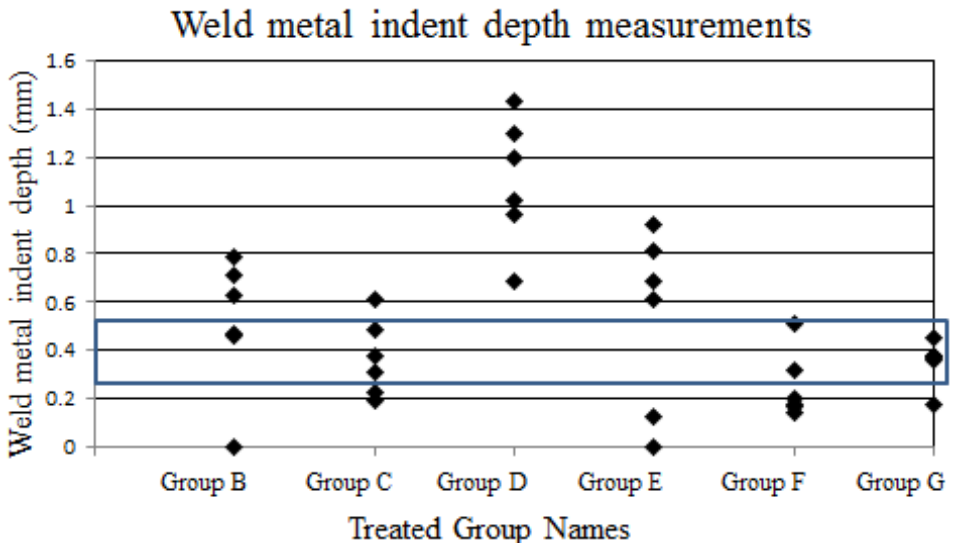

Figure 5.29: Weld metal indent depth measurements for treated groups

In this figure, it is observed that the indent depths for the Group D specimens, which were over-treated, fall well above the maximum boundary. Group B and E have a higher scatter compared to the rest of the groups. The data for Group F and G are within or close to the identified standard range. The Group E data show considerable scatter and fall outside of this range. Figure 5.30 shows the average indent depth measurements for all the treated groups.

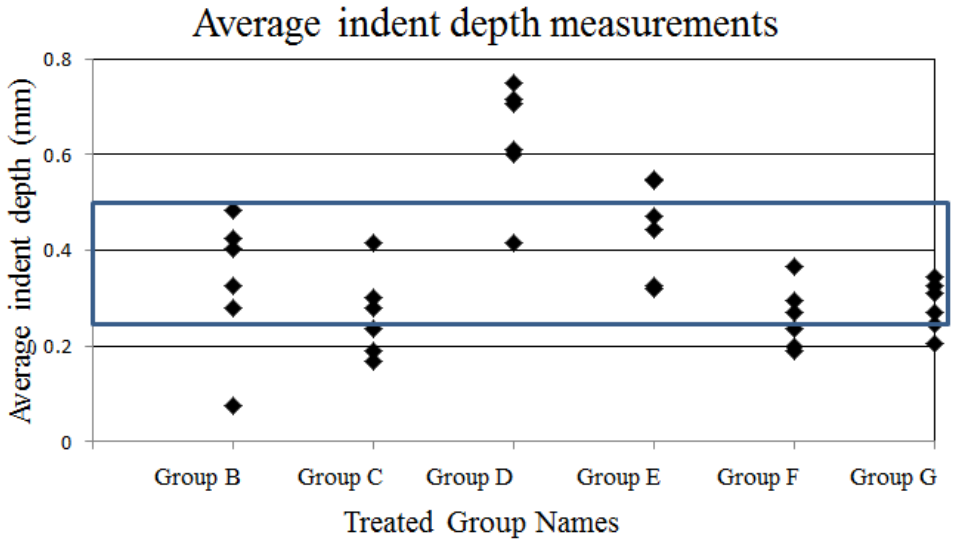

Figure 5.30: Average metal indent depth measurements for treated groups

The average of the weld metal and base metal indent depths for each group were taken and presented in Figure 5.30. It can be observed immediately that more of the data in this figure do

fall within the AAHTO envelope. Group D data still fall mostly above the maximum boundary. Groups B, C, F, and G have the most data within the standard range. Figure 5.31 shows the maximum indent depth measurements for all the treated groups.

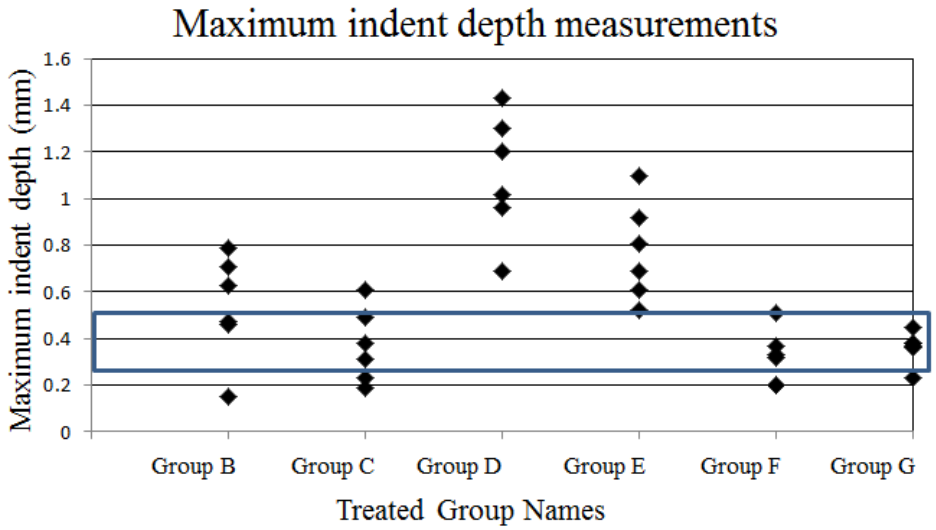

Figure 5.31: Maximum metal indent depth measurements for treated groups

In this figure, Group C and both of the manually properly treated groups (F and G) data mostly fall within the standard range. However, Group D and E data fall above the maximum boundary. There is a very good correlation between the indent depth and the treatment level for the robotically treated specimens (Groups B, C, D, and E). If the standard range is ignored, the properly treated data fall in between the under-treated data and the over-treated data.

Based on these results, it is concluded that measuring the indent depth is a good parameter for quality control specially for identifying over-treatment. Since the data for the under-treated specimens are very similar to the data for the manually properly treated specimens, it is recommended to perform a precise and accurate visual inspection of the weld toe in addition to the indent depth measurements, to identify if a weld has been under-treated. In addition, it is noted that these quality control recommendations are not intended to replace the recommendations of the manufacturer and standards on controlling the treatment inputs. In other words, the treatment has to be performed by a trained person who is aware of all the standards, input parameters and variables mentioned in Sections 2.8.3.1 and 2.9.2.3.

6 Conclusions and Recommendations

In this chapter, the main conclusions of the research presented in the previous chapters are summarized in Section 6.1. In Section 6.2, recommendations for the quality control of UIT are summarized. In Section 6.3, future research needs are identified.

6.1 Conclusions

- Fatigue tests were conducted on welded steel specimens subjected to UIT at various load levels and levels of treatment quality, including: properly, under- and over-treatment. The results from Section 4.2 and the t-test analysis from Section 5.2 show that UIT resulted in a significant increase in the fatigue life of the welded steel specimens, regardless of the simulated level of treatment "quality". Manually or robotically treating the specimens resulted in a similar performance in terms of increasing the fatigue life. There is a 90% probability that the manually and robotically treated specimens are from the same population, according to the t-test analysis. On average, the fatigue lives of the treated specimens were slightly lower under CA-UL than under CA loading.
- The statistical analyses of the S-N data in Section 5.2 illustrate that the simulated level of treatment quality had little impact on the mean S-N curve. Treatment quality did have an impact, however, on the design (95% survival probability) S-N curves, with the curve associated with "proper treatment" slightly higher than the curves for poor or unknown treatment quality.
- The results from Section 4.5 and 4.6 indicate that the local near-surface microhardness and compressive residual stresses are greatest for the over-treated specimens, followed by the properly treated and then the under-treated specimens. UIT resulted in a significant change in the residual stress distribution through the specimen thickness. Increasing the treatment speed results in a greater reduction in the surface microhardness and compressive residual stresses than decreasing the treatment intensity.
- Finite element analyses from Section 5.4 show that the change in weld toe geometry due to UIT can cause a significant decrease in the stress concentration factor near the surface of the treated weld toe. The stress concentration factors were lowest for the properly treated specimens and slightly higher for the under-treated specimens. For the over-

treated specimens, the stress concentration factors were nearly as high as for untreated welds. In general, under-treating the specimens by decreasing the treatment intensity will lead to a lower stress concentration factor than reducing the treatment speed. Over-treating a specimen will produce a stress concentration factor that can be as high as the untreated stress concentration factor. The FEA also showed that as the flange (plate) thickness increases, the SCF increases as well, up to a flange thickness of 19 mm, beyond which there is no substantial change in the SCF up to a thickness of 38 mm.

- The analysis from Section 5.6 shows that indent depth measurements from the base metal side, commonly used for quality control, may not identify over-treatment on their own, if the UIT tool is directed primarily at the weld metal. Indent depth measurements from both the weld and the base metal side, obtained by measurement of weld toe impressions offer a good alternative means for identifying over-treatment. For identifying under-treatment, indent depth measurements should be used in conjunction with visual inspection for traces of the original weld toe.

6.2 Quality Control Recommendations

Based on the experiments done and results obtained in this research study, the following recommendations are made, with regards to the quality control of UIT:

- The current recommendations for the qualitative visual inspection of welds treated by UIT would have likely been successful in identifying the under- and over-treated weld specimens fabricated for the current study.
- For identifying over-treatment, indent depth measurements from both the weld and base metal sides, obtained by measurement of weld toe impressions, are recommended.
- For identifying under-treatment, indent depth measurements should be used in conjunction with visual inspection for traces of the original weld toe.
- Through-thickness microhardness and residual stress measurements are not practical for application to actual bridge structures, since they require destruction of the weld. The use of these methods on sample specimens is recommended, however, for the evaluation of new UIT methods or procedures, prior to their implementation on bridges.

6.3 Recommendations for Future Research

The following is a list of recommended areas for future research:

- Residual stress measurements are already planned on a UIT-retrofitted weld that has not been fatigue tested, in order to observe the effects of UIT on the residual stress distributions prior to cyclic loading.
- Additional FE analyses of actual weld toe geometries obtained from impressions are needed to assess scatter in the SCFs for the various levels of treatment quality.
- Variable amplitude (VA) loading fatigue tests are recommended, simulating actual in-service loading conditions for bridge welds retrofitted by UIT.
- Fracture mechanics analysis of bridge welds retrofitted by UIT should be performed using for input/validation the residual stress data, SCF distributions, S-N data, and crack growth data obtained as a result of the current research project.
- Probabilistic fracture mechanics analysis of bridge welds retrofitted by UIT is another recommended area of future study.

References

AASHTO. (2004). American association of state highway and transportation officials: LFRD bridge design specifications. (2nd ed.). Washington, D.C.

AASHTO. (2008). American association of state highway and transportation officials: LFRD bridge design specifications. (4th ed.). Washington, D.C.

Albrecht, P., Artley-Dean, M., & Bergman, L. A. (1982). Foreword to fatigue and fracture reliability: A state-of-the-art review. *Journal of Structural Engineering, 108*(American Society of Civil Engineers (ASCE)), 1-21.

Applied Ultrasonics. (2006). *Esonix UIT.application guide: Post weld treatment for fatigue enhancement carbon steel welded structures.* Alabama, USA.

ASTM E384-10. (2010). Standard test method for knoop and vickers hardness of materials.*American Society for Testing and Materials*

ASTM E-8. (2004). Standard test methods for tension testing of metallic materials. () American Society for Testing and Materials.

Bannantine, J. A., Comer, J. J., & Handrock, J. L. (1990). *Fundamentals of metal fatigue analysis*. The United States of America: Prentice Hall.

Canadian Standards Association (CSA). (2006). *Canadian highway bridge design code CAN/CSA-S6-06.*

Costa Borges, L. A. (2008). *Size effects in the fatigue behaviour of tubular bridge joints.* EPFL, Lausanne, Switzerland. *Thesis No. 4142.*

Council of the Federation. (2005). Looking to the future: A plan for investing in canada's transportation system. Retrieved from http://www.councilofthefederation.ca/pdfs/NTS_Booklet.pdf

Crosley, P. B., & Ripling, E. J. (1990). *Acceptance criteria for steel bridge welds*. Washington, D.C: American Association of State Highway and Transportation Officials.; United States.National Cooperative Highway Research Program Report (NCHRP 335).

Dechaumphai, P., & Phongthanapanich, S. (2009). *Easy finite element method : With software*. Oxford, U.K.: Alpha Science International.

Desai, C. S., & Abel, J. F. (1971). *Introduction to the finite element method; a numerical method for engineering analysis*. New York: Van Nostrand Reinhold.

Fisher, J. W. (1984). *Fatigue and fracture in steel bridges : Case studies*. New York: Wiley.

G.A.L. Gage Company. (2012). *G.A.L. gage - weld measuring gauges- adjustable.* Retrieved June/25, 2012,

Ghahremani, K. (2010). *Predicting the effectiveness of post-weld treatments applied under load.* (Master of Applied Science, University of Waterloo). 129.

Ghahremani, K., & Walbridge, S. (2011). Fatigue testing and analysis of peened highway bridge welds under in-service variable amplitude loading conditions. *International Journal of Fatigue,* (300-312.)

Gurney, T. R. (1971). In Welding Institute. (Ed.), *Fatigue of welded structures*. Cambridge Eng. Welding Institute, c1971.

Haagensen, P. J., & Maddox, S. J. (2001). *IIW recommendations on post weld improvement of steel and aluminium structures.* (No. XIII-1815-0).

Haagensen, P. J., Statnikov, E. S., & Lopez-Martinez, L. (1998). Introductory fatigue tests on welded joints in high strength steel and aluminium improved by various methods including ultrasonic impact treatment (UIT). *International Institute of Welding, DOC.XIII-1748-98*

Hobbacher, A. (2005). *Recommendations for fatigue design of welded joints and component* (No. XIII-1965-03/XV-1127-03).International Institute of Welding.

Kirkhope, K. J., Bell, R., Caron, L., Basu, R. I., & Ma, K. (1999). Weld detail fatigue life improvement techniques. part 2: Application to ship structures. *Marine Structures, 12*(7-8), 477-496.

Klippstein, K. H., & Schilling, C. G. (1989). Pilot study on the constant and variable amplitude behavior of transverse stiffener welds. *Journal of Constructional Steel Research, 12*(3-4), 229-252.

Kuhn, B., Lukic, M., Nussbaumer, A., Gunther, H., Helmerich, R., Herion, S., Bucak, O. (2008). Assessment of existing steel structures: Recommendations for estimation of remaining fatigue life., 595-607.

Kulak, G. L., & Smith, I. F. C. (1993). *Analysis and design of fabricated steel structures for fatigue: A primer for civil engineers.* (No. 190).University of Alberta, Department of Civil Engineering.

Lihavainen, V., & Marquis, G. (2000). Estimation of fatigue life improvement for ultrasonic impact treated welded joints. *Lappeenranta University of Technology,*

Lopez-Martinez, L., & Korsgren, P. (1993). Characterization of initial defect distribution and weld geometry in welded fatigue test specimens. *Fatigue under spectrum loading and in corrosive environments* (pp. 3-21). UK: Warley.

Lugg, M. C. (2008). TSC inspection systems.

Maddox, S. J. (2000). Fatigue design rules for welded structures. *TWI, Cambridge, UK,* , 102-109.

McClung, R. C. (1994). Finite elment analysis of specimen geometry effects on fatigue crack closure. *Fatigue & Fracture of Engineering Materials & Structures, 17*(8), 861-872.

Nyborg, E., Moffatt, P., Cavaco, J., & Nyborg, D. (2006). Ultrasonic impact treatment for life extension of bridges with crack and crack susceptible welded details. *IAMBAS-06, Port.*

Pepper, D. W., & Heinrich, J. C. (2006). *Finite element method : Basic concepts and applications* (2nd ed ed.). New York: Taylor & Francis.

Pineault, J. A., Belassel, M., & Brauss, M. E. (2002). X-ray diffraction residual stress measurement in failure analysis. *ASM International, 11*, 484-497.

Proto. Manufacturing Ltd. (2011). *X-ray diffraction residual stress measurement: An introduction.*Automated Residual Stress Analysis.

Roensch, S. (2008). Finite element analysis: Introduction. *American Society of Mechanical Engineers (ASME).*

Roy, S., & Fisher, J. W. (2005). Enhancing fatigue strength by ultrasonic impact treatment. *ATLSS Engineering Research Center, 5*(Lehigh University).

Roy, S., & Fisher, J. W. (2006). Modified AASHTO design S-N curves for post-weld treated welded details. *2:4,* , 207-222.

Rugg, K. (2008). *National aeronautics and space administration.* Retrieved 06/13, 2012, from http://www.aeronautics.nasa.gov/contributions/

Schneider, C. R. A., & Maddox, S. J. (2003). *Best practice guide on statistical analysis of fatigue data.* (No. IIW-XIII-WG1-114-03). Granta Park, Great Abington, Cambridge, UK: International Institute of Welding.

Schutz, W. (1996). A history of fatigue.*54*, 263-300.

Smith, I. F. C., & Hirt, M. (1985). A review of fatigue strength improvement methods. *Canadian Journal of Civil Engineering, 12*, 166-183.

Statnikov, S. (1999). Guide for application of ultrasonic impact treatment improving fatigue life of weldd structures. *International Institute of Welding, IIW/IIS - Document XIII - 1757 - 99.*

Stephens, R. L., Fatemi, A., Stephens, R. R., & Fuchs, H. O. (2001). *Metal fatigue in engineering* (2nd ed.). USA & Canada: Wiley-Interscience.

The Office of the Auditor General of Ontario. (2009). *Bridge inspection and maintenance.* Ministry of Ontario. Retrieved from http://www.auditor.on.ca/en/reports_en/en09/302en09.pdf

Tilly, G. P., Jackson, P. A., & Maddox, S. J. (2010). Fatigue strengthening of welds in light rail structures., 147-152.

Tinsley Oden, J. (1990). Historical comments on finite element, 152-166.

Vilhauer, B., Bennett, C. R., Matamoros, A. B., & Rolfe, S. T. (2012). Fatigue behavior of welded coverplates treated with ultrasonic impact treatment and bolting. *Engineering Structures, 34*, 163-172.

Walbridge, S. (2005). *A probabilistic study of fatigue in post-weld treated tubular bridge structures.* École Polytechnique Fédérale de Lausanne).

Walker, M., Van Berkel, S., & Walbridge, S. (2008). Needle peening to improve the fatigue performance of existing steel bridge welds. *CSCE Conference.*

Walpole, R. E., & Myers, R. H.,joint author. (1998). *Probability and statistics for engineers and scientists* (6th ed. - ed.). New York: London: Macmillan; Collier Macmillan.

Welding Technology Institute of Australia. (2006). Introduction to fatigue of welded steel structures and post-weld improvement techniques.

Ye, N., & Moan, T. (2008). Improving fatigue life for aluminium cruciform joints by weld toe grinding. *Fatigue & Fracture of Engineering Materials & Structures, 31*(2), 152-163.

Zienkiewicz, O. C., & Taylor, R. L. (2005). *Finite element method* (6th ed ed.). Oxford ; Burlington, MA: Elsevier Butterworth-Heinemann.

Zoubir Louni. (2007). Aging highway bridges. *National Research Council Canada, 48*, 1-3. Retrieved from http://www.nrc-cnrc.gc.ca/obj/irc/doc/pubs/nrcc49239/nrcc49239.pdf